

**MAPPING AND MONITORING WETLAND ENVIRONMENT BY
ANALYSIS OF DIFFERENT SATELLITE IMAGES AND FIELD
SPECTROSCOPY**

**Ph.D. Thesis by
Filiz BEKTAŞ BALÇIK**

Department : Geodesy and Photogrammetry Engineering

Programme : Geomatic Engineering

MARCH 2010

**MAPPING AND MONITORING WETLAND ENVIRONMENT BY
ANALYSIS OF DIFFERENT SATELLITE IMAGES AND FIELD
SPECTROSCOPY**

**Ph.D. Thesis by
Filiz BEKTAŞ BALÇIK
(501032602)**

**Date of submission : 08 January 2010
Date of defence examination: 16 March 2010**

**Supervisor (Chairman) : Assis. Prof. Dr. Çiğdem GÖKSEL (ITU)
Members of the Examining Committee : Prof. Dr. Filiz SUNAR (ITU)
Prof. Dr. Cumali KINACI (ITU)
Assis. Prof. Dr. Hayriye EŞBAH TUNÇAY (ITU)
Assis. Prof. Dr. Füsun BALIK ŞANLI (YTU)**

MARCH 2010

İSTANBUL TEKNİK ÜNİVERSİTESİ ★ FEN BİLİMLERİ ENSTİTÜSÜ

**SULAK ALAN ÇEVRESİNİN FARKLI UYDU GÖRÜNTÜLERİ VE ARAZİ
SPEKTROSKOPİSİ İLE İZLENMENSİ VE HARİTALANMASI**

**DOKTORA TEZİ
Filiz BEKTAŞ BALÇIK
(501032602)**

Tezin Enstitüye Verildiği Tarih : 08 Ocak 2010

Tezin Savunulduğu Tarih : 16 Mart 2010

**Tez Danışmanı : Yrd. Doç. Dr. Çiğdem GÖKSEL (İTÜ)
Diğer Jüri Üyeleri : Prof. Dr. Filiz SUNAR (İTÜ)
Prof. Dr. Cumali KINACI (İTÜ)
Yrd. Doç. Dr. Hayriye EŞBAH TUNÇAY (İTÜ)
Yrd. Doç. Dr. Füsun BALIK ŞANLI (YTÜ)**

MART 2010

FOREWORD

Gratitude is owed to many individuals who have helped me in one way or another over the past six years, often without knowing they were doing so.

My deepest appreciation goes to my advisor Ass. Prof. Çigdem GÖKSEL, for her advice, commitment, encouragement, and mentorship. She thought me how to make my own choices at decisive points along the way to be an independent scientist.

I am very grateful to Prof. Andrew K. Skidmore for his supportive and thoughtful suggestions during the period of my study at ITC. I would like to thank him for giving me the opportunity to work for his project, where I gained great knowledge and experience about hyperspectral remote sensing. My special thanks go to Prof. Filiz Sunar for her criticism and enthusiasm during the period of this work.

I wish to thank several friends who worked closely with me during the two year period of my study at the Netherlands. Claudia Pittiglio, Tyas Maturi Basuki, Laura Dente, Mariella Yveness, Ha Naguyen, Nicky Knox, many thanks for your wonderful friendship. Special thanks goes to Dr. Ahmet Özgür Doğru for his friendship, wonderful support and presence. I would like to thank to my colleague Prof. Necla Ulugtekin, for her presence in my life.

Many people at Terkos Lake ISKI helped and supported me when it came to logistics issues. I deeply appreciate their valuable support during my field work at Terkos. ITU Institute of Science and Technology and Civil Engineering Faculty supported this work. I would like to thank HUYGENS-NUFFIC for supporting me as a Ph.D Scholar in the Netherlands.

I extend my gratitude to my father, mother and brother who gave me tremendous support and deserve much more than a simple ‘thank you’. I owe them a lot and will be grateful to them all my life.

Finally, to my son, Mert Rüzgar, thank you for bringing so much happiness and joy into my life.

Last but not least, to my husband, Hakan, I say thank you for your presence, support and encouragement. I am sincerely grateful to you for your patience, appreciation, trust and most of all for your love.

March 2010

Filiz BEKTAŞ BALÇIK
Geodesy and Photogrammetry
Engineer, M. Sc.

TABLE OF CONTENTS

	<u>Page</u>
FOREWORD	v
TABLE OF CONTENTS	vii
ABBREVIATIONS	xi
LIST OF TABLES	xiii
LIST OF FIGURES	xv
SUMMARY	xvii
ÖZET	xxi
1. INTRODUCTION	1
2. WETLAND SYSTEMS	7
2.1 Definitions of Wetlands.....	7
2.2 The Global and Regional Distribution of Wetlands	9
2.3 Wetlands of Turkey	10
2.4 Wetland Ecosystem Benefits: The Functions and Values of Wetlands	13
2.5 Major Threats to Wetlands	13
2.6 Wetland Loss and Degradation	14
3. REMOTE SENSING OF WETLANDS	17
3.1 Introduction	17
3.2 Remote Sensing Research in Wetland Ecosystems.....	18
3.3 Conventional Approaches to Wetland Ecosystems.....	20
3.4 Field Spectroscopy	22
4. REMOTE SENSING, FIELD SPECTROSCOPY AND GEOSTATISTICS. 27	
4.1 Image Processing.....	27
4.1.1 Radiometric and Atmospheric Correction	27
4.1.1.1 Dark Object Subtraction (DOS)/Haze Removal.....	31
4.1.1.2 Scene-to-scene normalization/ Invariant Object Method / Pseudo Invariant Feature (PIF)	31
4.1.1.3 FLAASH.....	32
4.1.2 Geometric Correction	33
4.1.3 Hyperion EO-1 Hyperspectral Data Pre-processing.....	35
4.1.3.1 Band Selection	35
4.1.3.2 Bad Band Selection	36
4.1.3.3 Bad Line Detection and Correction	36
4.1.3.4 Minimum Noise Fraction (MNF)	37
4.1.4 Classification	37
4.1.4.1 Selection of Appropriate Band Combinations.....	37
4.1.4.2 Spectral Separability Analysis.....	38
4.1.4.3 Unsupervised Classification	39
4.1.4.4 Supervised Classification	39
4.1.4.5 Hybrid Classification.....	40
4.1.4.6 Spectral Angle Mapper (SAM) classification	40

4.1.4.7 The Coordination of Information on the Environment (CORINE) Land Cover Data Set	41
4.1.4.8 Accuracy Assessment	43
4.2 Land Cover Change Detection	45
4.2.1 Principal Component Analysis Based Change Detection	46
4.2.2 Change Vector Analysis	47
4.2.2.1 Tasseled Cap Transformation	50
4.2.2.2 Gram Schmidt Orthogonalization Technique and TCT parameters Extraction	51
4.2.3 Semivariogram and spatial profile analysis	53
4.3 Field Spectroscopy	55
5. STUDY AREA, DATA and CASE STUDY	107
5.1 Study Area	57
5.2 Remote Sensing Data	61
5.3 Field Spectroscopy Data	64
5.4 Meteorological Data	66
5.5 Digital Image Pre-Processing of Satellite Data Set	66
5.5.1 Radiometric and Atmospheric Correction	66
5.5.2 Geometric Correction	67
5.5.3 Radiometric Normalization	68
5.5.4 Hyperion Pre-processing	69
5.5.4.1 Band Selection	69
5.5.4.2 Bad Detection Element	71
5.5.4.3 Bad Line Detection and Correction	71
5.5.4.4 FLAASH Atmospheric Correction	72
5.5.4.5 Minimum Noise Fraction Transformation	72
5.6 Classification of Satellite Data	73
5.6.1 Classification of Multispectral Satellite Data	74
5.6.2 Unsupervised Classification	77
5.6.3 Supervised Classification	79
5.7 Change Detection	80
5.7.1 Principal Component Analysis Based Change Detection	80
5.7.1.1 Change-information extraction and labelling using Hybrid classification	81
5.7.1.2 Spatial Profiles and Semivariogram	84
5.7.2 Tasseled Cap Transformation	86
5.7.2.1 Change Vector Analysis	87
5.7.2.2 Classification Accuracy Assessment	92
5.8 Field Spectroscopy	94
5.8.1 Processing of field spectroscopy data	95
5.9 Classification of Hyperion EO-1 Hyperspectral Data	97
5.9.1 Supervised and Spectral Angle Mapper (SAM) Classification	97
5.9.2 Spectrally Segmented PCA Classification of Hyperion EO-1 data	102
6. RESULTS AND CONCLUSIONS	107
6.1 Preprocessing Results	107
6.2 Change Detection Results	108
6.3 Field Spectroscopy Results	111
6.4 Hyperspectral Classification Results	112
6.5 Conclusion	113
REFERENCES	117

APPENDICES	133
CURRICULUM VITA	139

ABBREVIATIONS

ANOVA	: Analysis of Variance
ASD	: Analytical Spectral Devices
ATCOR	: Atmospheric Correction and Haze Reduction
AVHRR	: Advanced Very High Resolution Radiometer
BIL	: Band Interleaved by Line
CC	: Correlation Coefficient
CORINE	: Coordination of Information on the Environment
DEM	: Digital Elevation Model
DN	: Digital Number
DOS	: Dark Object Subtraction
ED	: Euclidian Distance
EO	: Earth Observing
EO-1	: Earth Observation
EU	: European Union
ERGAS	: Erreur relative globale adimensionnelle de synthèse
FLAASH	: Fast Line-of-Sight Atmospheric Analysis of Spectral Hypercubes
FOV	: Field of View
GCP	: Ground Control Points
GIS	: Geographic Information Systems
GPS	: Global Positioning System
GST	: Gram Schmidt Transform
HDF	: Hierarchical Data Format
HPF	: High Pass Filter
IHS	: Intensity Hue Saturation
ISODATA	: Iterative Self- Organizing Data Analysis
JM	: Jefferies-Matusita distance
LIDAR	: Light detection and ranging
LMM	: Local Mean Matching
LMVM	: Local Mean Variance Matching
LULC	: Land Use Land Cover
mCVA	: Modified Change Vector Analysis
ML	: Maximum Likelihood
MNF	: Minimum Noise Fraction
MMTG	: Mineral Mapping Technology Group
MODTRAN	: MODerate spectral resolution atmospheric TRANSmittance
MS	: Multispectral
NASA	: National Aeronautics and Space Administration
NDVI	: Normalized Difference Vegetation Index
OIF	: Optimum Index Factor
PAN	: Panchromatic
PCA	: Principal Component Analysis
PIF	: Pseudo Invariant Feature
RAMSAR	: The Convention on Wetlands of International Importance

RASE	: Relative average spectral error
RFM	: Rational function model
RGB	: Red-Green-Blue
RMSE	: Root Mean Square Error
SAM	: Spectral Angle Mapper
SAR	: Synthetic Aperture Radar
SMAC	: Simplified Method for the Atmospheric Correction
SNR	: Signal to Noise Ratio
SPOT	: Satellite pour l'Observation de la Terre
SWIR	: Short Wave Infrared
TCT	: Tasseled Cap Transformation
TD	: Transformed divergence
TOA	: Top of Atmosphere
TWPCR	: Turkish Water Pollution Control Federation
USGS	: U.S. Geological Survey
UTM	: Universal Transfer Mercator
VNIR	: Visible Near Infrared
WT	: Wavelet Transform

LIST OF TABLES

	<u>Page</u>
Table 2.1: Wetland definitions.....	8
Table 2.2: Estimated area of wetlands in each of the regions of the world recognized under the Ramsar Wetlands Convention.....	9
Table 2.3: Wetland functions and values.....	13
Table 3.1: Wavelengths of importance for vegetation studies and their role.....	23
Table 4.1: Offset and bias parameters for SPOT sensors.....	29
Table 4.2: Solar spectral irradiances for SPOT images.....	30
Table 4.3: Hyperion EO-1 bands.....	36
Table 4.4: The CORINE land cover nomenclature.....	42
Table 5.1: Population growth of Turkey and İstanbul.....	57
Table 5.2: The characteristics of the satellite data used.....	62
Table 5.3: Hyperion EO-1 detailed sensor characteristics.....	63
Table 5.4: Meteorological information on image acquisition date.....	66
Table 5.5: Geometric correction information.....	68
Table 5.6: Linear regression analysis between 2003 and 2007 image by using PIF.....	69
Table 5.7: Selected bands from Hyperion based on spectrum region.....	70
Table 5.8: The schema of the CORINE land use and land cover classes.....	74
Table 5.9: Correlations and standard deviations between bands of 2003 data.....	74
Table 5.10: Correlations and standard deviations between bands of 2007 data.....	75
Table 5.11: OIF values of band combinations.....	75
Table 5.12: Transformed divergence matrix (2003 SPOT 4).....	76
Table 5.13: Transformed divergence matrix (2007 SPOT 5).....	76
Table 5.14: Statistical results of supervised classification.....	80
Table 5.15: LULC conversion matrix.....	83
Table 5.16: Range, nugget, and sill values for selected transect.....	86
Table 5.17: Tasselled cap coefficients for SPOT 5 data at satellite reflectance.....	87
Table 5.18: Change classes of raw differences in TCT components derived from the sign of the change.....	88
Table 5.19: Landscape dynamic classes and their corresponding area in the Terkos.....	92
Table 5.20: Table overall accuracy and Kappa statistics result.....	93
Table 5.21: <i>Typha Latifolia</i> and other wetland species in Terkos.....	96
Table 5.22: Overall accuracy and Kappa statistics using different band combinations and MNF transformation.....	102
Table 5.23: Four –group segmentation for spectrally segmented PCA.....	104
Table 5.24: Overall accuracy and Kappa statistics.....	106
Table A.1: Results of classification and change detection methods.....	137

LIST OF FIGURES

	<u>Page</u>
Figure 2.1 : Distribution of wetlands.	10
Figure 2.2 : Distribution of Turkish wetlands.....	11
Figure 3.1 : Spectral signatures for photosynthetically and non- photosynthetically active vegetation recorded using a handheld spectroradiometer	22
Figure 4.1 : Scene-to-scene normalization.....	32
Figure 4.2 : Basic processing flow used in FLAASH.....	33
Figure 4.3 : Transforming coordinates from one system (map) to another one (image).....	34
Figure 4.4 : The confusion matrix and some common measures of classification accuracy that may be derived from it.....	44
Figure 4.5 : Change vector directions represented by (a) shift sector coding and (b) angle grouping	49
Figure 4.6 : Geometric representation of a change vector and its corresponding polar coordinates along the planes formed by the three Tasseled Cap Transforms: brightness (x), greenness (y), and wetness (z).	50
Figure 4.7 : A semivariogram	54
Figure 4.8 : Selected test sites for field study	55
Figure 5.1 : Surface water resources basins in the province of Istanbul.....	58
Figure 5.2 : Location of Istanbul and Terkos Water Basin.....	59
Figure 5.3 : Wetland vegetation types in Lake Terkos.	60
Figure 5.4 : Mean and the spectral variability of the canopy reflectance spectra of sample plots in Terkos Water Basin, Istanbul.	65
Figure 5.5 : Typical field sites showing the wetland vegetation layer with water....	65
Figure 5.6 : 2003 dated SPOT data (4,3,2) a) Original data b) Geometrically corrected data.	68
Figure 5.7 : Selected and unselected 242 bands of Hyperion EO-1 data.....	70
Figure 5.8 : Differences between columns a) Bad column in Hyperion EO-1 image b) Corrected bad column in image.....	71
Figure 5.9 : Striping problem and after correction applied by MMTG-A.	72
Figure 5.10 : First three components of the MNF.	73
Figure 5.11 : Unsupervised classification of absolute protected area a) 1991 dated SPOT 2 and b) 2007 dated SPOT 5.....	77
Figure 5.12 : ISODATA Unsupervised classification a) 2003 dated unsupervised image b) 2007 dated unsupervised image.	78
Figure 5.13 : Maximum likelihood supervised classification a) 2003 dated b) 2007 dated.	79
Figure 5.14 : Methodology of the PCA based change detection.	80
Figure 5.15 : Principal components of stacked eight SPOT bands.....	81
Figure 5.16 : LULC change detection by PCA and hybrid classification.....	83

Figure 5.17 : Spatial profile analyze a) Location of the transect b) the transect view from 2003 dated SPOT 4 b) the transect view from 2007 dated SPOT 5.	84
Figure 5.18 : Semivariograms of Transect, Left side: 2003 SPOT image, right side: 2007 SPOT image.	85
Figure 5.19 : Difference images produced by TCT a) Brightness, b) greenness and c) wetness.	87
Figure 5.20 : Graphical model script of the extended change vector analysis algorithm for SPOT 4 XS 2003 and SPOT 5 XS 2007 data.	89
Figure 5.21 : Change vector magnitude representing the intensity of change between a pixel's brightness, greenness, and wetness in 2003 and 2007.	90
Figure 5.22 : Changed and no-changed area.	90
Figure 5.23 : Direction images produced by CVA.	91
Figure 5.24 : Landscape dynamic in the Terkos derived.	92
Figure 5.25 : Sample vegetation reflectance spectra from Terkos Wetlands.	94
Figure 5.26 : Distribution of the field collected reflectance data.	94
Figure 5.27 : Spectral Profile a) Mean b) Smoothed Mean.	95
Figure 5.28 : Selected transect and test site.	98
Figure 5.29 : Hyperion data classification with Maximum Likelihood.	99
Figure 5.30 : Hyperion data classification with Spectral Angle Mapper.	100
Figure 5.31 : Input data. a) MNF transformed data (colour composite of MNFbands 1–3), b) results of SAM algorithm using c) 1–10 MNF bands.	101
Figure 5.32 : General procedure of spectrally segmented PCA.	103
Figure 5.33 : PCA segmented and PCA all Hyperion Classification a) ML and b) SAM c) ML d) SAM.	105
Figure A.1 : Methodology of the study	134
Figure A.2 : NDVI images a) 2003 dated SPOT 4 b) 2007 dated SPOT 5.....	135
Figure A.3 : Hyperion EO-1 NDVI image (band-30 (650 nm) and band-50 (854 nm))	136

MAPPING AND MONITORING WETLAND ENVIRONMENT BY ANALYSIS OF DIFFERENT SATELLITE IMAGES AND FIELD SPECTROSCOPY

SUMMARY

This study examines various remote sensing methods, which can be applied to find out the performance in detecting land cover changes and the wetland vegetation by using satellite images that contain different spectral and spatial resolution, with in the case study of “Terkos Basin Wetland”. The feasibility of structuring a basic guide was searched for sustainable conservation and management of natural lands by supporting performances of processed images with field collected reflectance values.

Wetlands are the most important ecosystem of the earth because of the biological diversity, natural functions and financial values they have. Cutting reed beds, drainage for agricultural activities, supplying drinking water, and constructing buildings are the main reasons for wetland loss and degradation. Turkey signed RAMSAR Agreement in 1994 in order to prioritize the preservation of wetlands and to take necessary measures in sustaining biological diversity of wetland ecosystems. In Turkey, as well as in the whole world, accurate and reliable data and data processing methods are needed to preserve, manage and monitor wetlands. The technology that enables production of multi-purpose maps via data support and continuous monitoring of these lands is required. Remote sensing technology is considered as a powerful and useful tool that enables providing accurate and temporal digital data and images of wetlands in different bands.

In the present work, Terkos Basin within the borders of Istanbul has been selected as the study area. After 1980, İstanbul has experienced rapid population growth, industrialization and a consequent increase in settlements as well as changes in land cover. Terkos Basin that supplies approximately 30% of drinking water needed in İstanbul is an important vegetation area; it has been entitled ‘under preservation’ on accounts of being a nature preservation area, natural site area and wild life preservation area according to the international criteria.

In this thesis, in order to analyze performances of remote sensing data, land cover types in Terkos Basin have been studied via field collected reflectance values and remotely sensed images of SPOT 4, SPOT 5 MS, SPOT 5 PAN, and Hyperion EO-1.

During the first phase of application, 1991 dated SPOT XS, 2003 dated SPOT 4, 2007 dated SPOT 5 MS and PAN images which have medium and high spatial resolution have been preprocessed. These images radiometrically and atmospherically corrected. Consequently, deterioration effects originating from atmospheric particles and systematic distortions were eliminated. In the present study, “spectral band center shift” that emerges due to calibration errors between detectors and “radiometric errors” of 2007 dated Hyperion EO-1 data have been corrected by using MMTG-A (CSIRO Mineral Mapping and Technologies Group) module operating with ENVI program. In this context, too noisy bands in Hyperion

image, non-calibrated bands with zero value were eliminated through preprocessing steps. Each image was geometrically corrected in order to define images under a common coordinate system and correct pixel relative location distortions. In this study, Tasseled Cap Transformation (TCT) coefficients were produced for SPOT 5 data by using “Gram-Schmidt method”. Images of brightness, greenness and wetness were obtained by using these coefficients. TCT images that were produced via 2003 dated SPOT4 and 2007 dated SPOT5 satellite data were used in “Change Vector Analysis” (CVA) to detect emerging land cover changes in Terkos Basin. For the change vector analysis, three TCT difference images, one change vector magnitude image, three vector direction images; and one final landscape dynamic image depicting the most changed landscapes were produced. Threshold value was determined for the change detection determination by using statistical calculations and the analyst’s expertise. In this phase as a secondary method, “Principle Component Analysis (PCA) based change detection method” was applied. Results of the above stated methods were compared to examine the performance of the methods for change detection. In PCA based change detection method, 2003 and 2007 dated satellite images were stacked hence a new eight-band image was formed. PCA was applied on this new image and a hybrid classification was obtained by using the first three components with info of great importance. In this hybrid method, firstly unsupervised classification was applied and two categories were prepared as “an image change is present” and “an image change is not present”. Masking was applied to select “an image change is present” category and supervised classification method was followed. Through both methods, it has been shown that detection of change is possible for heterogeneous natural lands. The accuracy assessment results showed that better change detection results can be obtained by “PCA based change detection” method. Semivariogram and spatial profile analyses were applied alongside the test area near Lake Terkos. Accuracy of change detection results was supported by obtained results. At the end of change detection analyses it was found that changes in study area are rather limited because a certain part of the region is under protection by international criteria. It was detected that present changes have an orientation from agricultural lands to settlements and/or open lands, a decrease in wetlands, an increase in the area of roads and associated land, a transformation from forestry lands to sparsely vegetated lands and forestation of some open lands.

In the second part of the study, Hyperion EO-1 image was tested by MNF (Minimum Noise Fraction) and PCA (Principle Component Analysis) transformations. Original image and transformed images were classified through supervised method and Spectral Angle Mapper (SAM) method. Hyperion image was classified under four main spectral groups namely; visible, near infrared, short wave infrared I, short wave infrared II. PCA transformation was applied on each group and by using the components with the greatest information a new eight-band image was produced then supervised and SAM methods were applied. MNF transformation was applied on Hyperion data and based on Eigen values first three and first ten components were selected. SAM classification was conducted on these images. Obtained classified images were compared with respect to accuracy assessment results. For the accuracy assessment SPOT 5 MS image with high spatial resolution was produced by using image fusion techniques such as IHS (Intensity-Hue-Saturation), Brovey, Multiplicative, HPF (High Pass Filter), PCA (Principal Component Analysis), LMM (Local Mean Matching), LMVM (Local Mean Variance Matching), mIHS (Modified Intensity-Hue-Saturation) and Wavelet. Obtained results were compared with respect to visual and statistical aspects. Fused image with the best result has been used in

present study to detect accuracy assessment and classification. At the end of this phase, it was concluded that wetland vegetation cover is distinguishable from other green lands by using Hyperion.

In the final phase, field collected reflectance values obtained via ASD Field Spec-Pro spectroradiometer were preprocessed. To eliminate noise effect Savitsky-Golay filter was used. Field collected reflectance values that have different wetland flora types have been compared by statistical Analysis of Variance (ANOVA) method and reflectance differences between vegetation types have been put forward through calculations.

In this study, different remote sensing data and their land cover classification and land cover change detection performances were compared. In line with these results methods were searched to obtain vital information on land cover for the protection and management wetlands. Land cover categories obtained in this study have been arranged according to CORINE legend. Consequently, a footer guide was prepared that shows which images and on which scale information can be produced based on CORINE levels and which methods can be efficiently used for complex natural areas.

SULAKALANLARIN VE ÇEVRESİNİN FARKLI UYDU GÖRÜNTÜLERİ VE ARAZİ SPEKTROSKOPİSİ İLE İZLENMESİ VE HARİTALANMASI

ÖZET

Bu çalışmada farklı spektral ve mekansal çözünürlükte uydu görüntülerinin “Terkos Havzası Sulak Alanı” örneğinde; arazi örtüsünde meydana gelen değişimleri ve sulak alan bitki türlerinin belirlenmesinde kullanılabilirlikleri için uygulanabilecek uzaktan algılama yöntemleri ele alınmıştır. Kullanılan yöntemler ile elde edilen yeni işlenmiş görüntülerin performanslarının yersel yansıtım değerleri kullanılarak desteklenmesi ile doğal alanların sürdürülebilir korunma ve yönetimi için uzaktan algılama verilerine dayalı bir altlık rehberin oluşturulması imkanı araştırılmıştır.

Sulak alanlar sahip olduğu biyolojik çeşitlilik, doğal işlevleri ve ekonomik değerleriyle yeryüzünün en önemli ekosistemleridir. Sazlıkların kesilmesi, tarım amaçlı kurutmalar, sanayi kirliliği, içme suyu amaçlı kullanımlar ve yapılaşmalar sulak alanların giderek tükenmesine yol açmıştır. Türkiye sulak alanların korunmasına birincil öncelik sağlanması, sulak alan ekosistemlerindeki biyolojik çeşitliliğin sürdürülmesi yönünde gerekli önlemlerin alınması için, 1994 yılında RAMSAR sözleşmesini imzalamıştır. Gerek ülkemizde gerek dünyamızda sulak alanların korunması, yönetilmesi ve geliştirilmesi için doğru ve güvenilir verilere ve veri elde etme yöntemlerine gereksinim duyulmaktadır. Veri desteği ile çok amaçlı haritaların üretilmesi ve bu alanların sürekli izlenmesini sağlayacak teknolojilerin kullanımı gerekmektedir. Uzaktan algılama teknolojisi sulak alanların farklı bantlarda görüntülerinin elde edilebildiği, doğru, tekrarlanabilen ve zamansal sayısal verinin elde edilmesine olanak sağlayan güçlü ve yararlı bir araç olarak tanımlanmaktadır.

Bu çalışmada, özellikle 1980 yılı sonrasında hızlı nüfus artışı, sanayileşme ve buna bağlı olarak yerleşim alan artışı ve farklı arazi örtüsü değişimlerinin gözlemlendiği İstanbul ili sınırları içerisinde yer alan Terkos Havzası çalışma bölgesi olarak seçilmiştir. İstanbul nüfusunun içme suyu ihtiyacının yaklaşık olarak % 30’ unu sağlayan Terkos Havzası uluslararası ölçütlere göre önemli bitki alanı olarak tanımlanmış ve tabiatı koruma alanı, doğal sit alanı ve yaban hayatı koruma sahası ilan edilerek koruma altına alınmıştır.

Bu tez çalışmasında, Terkos Havzası’na ait arazi örtüsü tipleri farklı özelliklere sahip uzaktan algılama verilerinin performanslarını analiz etmek amacı ile SPOT 4, SPOT 5 MS ve SPOT 5 PAN, Hyperion EO-1 ve yersel yansıtım değerleri kullanılmıştır.

Uygulamanın ilk aşamasında, orta ve yüksek mekansal çözünürlüğe sahip 1991 tarihli SPOT XS, 2003 tarihli SPOT 4, 2007 tarihli SPOT 5 MS ve PAN görüntüleri elde edilmiş ve görüntüler radyometrik ve atmosferik olarak düzeltilerek atmosferik parçacıklardan kaynaklanan bozulma etkileri ve sistematik hatalar eleminde edilmiştir. Bu çalışmada, 2007 tarihli Hiperspektral Hyperion EO-1 görüntüsündeki şerit tarama, detektörler arasındaki kalibrasyon hataları sonucunda oluşan “spektral bant merkez kayıklıkları” ve “radyometrik hatalar” ENVI programı ile çalışmakta olan MMTG-A (CSIRO Mineral Mapping and Technologies Group) modülü kullanılarak

giderilmiştir. Hyperion görüntüsündeki çok gürültülü bantlar ve sıfır değerine sahip kalibre edilmemiş bantlar ön işleme adımları ile elimine edilmiştir. Görüntüleri ortak bir koordinat sisteminde tanımlamak ve piksel bağıl konum hatalarını düzeltmek amacıyla her bir görüntü geometrik olarak düzeltilmiştir.

Çalışmada, yeni bir yaklaşım olarak SPOT uydu görüntüleri için Tasseled Cap Transformation (TCT) katsayıları “Gram-Schmidt yöntemi” kullanılarak üretilmiştir. Bu katsayılar kullanılarak çalışma bölgesine ait parlaklık, yeşillik ve nemlilik görüntüleri elde edilmiştir. 2003 tarihli SPOT4 ve 2007 tarihli SPOT5 uydu verileri ile üretilen TCT görüntüleri, Terkos Havzası’nda ortaya çıkan arazi örtüsü değişimlerinin tespit edilmesi için “Değişim Vektör Analizi” (DVA) (Change Vector Analysis CVA) yönteminde kullanılmıştır. Bu aşamada, ikinci yöntem olarak “Ana Bileşen Dönüşümü (ABD) (Principle Component Analysis PCA) tabanlı değişim yöntemi” kullanılmıştır. Her iki yöntemle elde edilen sonuçlar karşılaştırılmıştır. “Ana bileşen dönüşüm tabanlı değişim tespiti yöntemi”nde 2003 ve 2007 tarihli uydu görüntüleri birleştirilmiş (stacking) ve sekiz bantlı yeni bir görüntü oluşturulmuştur. Bu yeni görüntüye ABD uygulanmış ve en fazla bilgi içeren ilk üç bileşen kullanılarak hibrid bir sınıflandırma gerçekleştirilmiştir. Bu hibrid yöntemde ilk olarak kontrolsüz sınıflandırma uygulanmış ve “görüntü değişimi var” ve “görüntü değişimi yok” olmak üzere iki kategori belirlenmiştir. “Görüntü değişimi var” sınıflarından örnekleme alanları seçilmiş ve kontrollü sınıflandırma yöntemi uygulanmıştır. Her iki yöntem ile heterojen yapıdaki doğal alanlar için değişim tespitinin mümkün olduğu gösterilmiş ve doğruluk değerlendirmesi sonucunda ABD tabanlı değişim tespiti yönteminin daha iyi sonuç verdiği gözlemlenmiştir. Terkos Gölü civarında seçilen test bölgesinde semivariogram ve mekansal profil analizleri gerçekleştirilmiştir. Sonuçlar ile değişim alanlarının doğruluğu desteklenmiştir. Yapılan değişim analizleri sonucunda, çalışma bölgesindeki değişimlerin oldukça sınırlı olduğu belirlenmiştir. Çünkü bölgenin bir kısmı uluslar arası kriterlere göre koruma altına alınmıştır. Mevcut değişimlerin ise tarım alanlarının yerleşim alanlarına ve/veya açık alanlara dönüşümü yönünde olduğu, göl etrafındaki sulak alanların azaldığı, yol ve sanat yapılarının arttığı, bazı ormanlık alanların açık alan ve seyrek bitkilik alanlara dönüştürüldüğü ve bazı açık alanların ağaçlandırıldığı saptanmıştır.

Çalışmanın ikinci aşamasında, Hyperion EO-1 görüntüsü MNF (Minimum Noise Fraction) ve PCA (Principle Component Analysis) dönüşümleri ile test edilmiştir. Orijinal görüntü ve dönüşüm uygulanmış görüntüler kontrollü ve Spektral Angle Mapper (SAM) yöntemleri ile sınıflandırılmıştır. Hyperion görüntüsü görünür, yakın kızıl ötesi, kısa dalga kızıl ötesi I ve kısa dalga kızıl ötesi II olmak üzere dört ana spektral gruba ayrılmıştır. Her bir gruba PCA dönüşümü uygulanmıştır ve en çok bilgiye sahip bileşenlerden sekiz bantlı yeni bir görüntü elde edilmiştir ve buna kontrollü ve SAM yöntemleri uygulanmıştır. MNF dönüşümü uygulanan görüntüye ilk üç bileşen ve ilk on bileşen için SAM uygulanmıştır. Elde edilen sınıflandırılmış görüntüler doğruluk değerlendirmesi sonuçlarına göre karşılaştırılmıştır. Doğruluk değerlendirmesinde kullanılmak üzere yeni SPOT 5 MS görüntüsü dokuz farklı görüntü birleştirme algoritması kullanılarak üretilmiştir. Görüntülerin birleştirilmesi için IHS (Intensity-Hue-Saturation), Brovey, Multiplicative, HPF (High Pass Filter-Yüksek Geçirgenlikli Filtre), PCA (Principal Component Analysis- Ana Bileşen Dönüşümü), LMM (Local Mean Matching), LMVM (Local Mean Variance Matching), mIHS (Modified Intensity-Hue-Saturation) ve Wavelet görüntü birleştirme yöntemleri kullanılmış ve elde edilen sonuçlar görsel ve istatistik açıdan

karşılaştırılmıştır. En iyi sonuca sahip birleştirilmiş görüntü yer gerçeği verisi olarak çalışmada sınıflandırma ve doğruluk değerlendirmesi aşamasında kullanılmıştır. Bu aşama sonucunda Hyperion ile sulak alan bitki örtüsünün diğer yeşil alanlardan ayırt edilebildiği sonucuna varılmış ve orta mekansal çözünürlüğe sahip olmasına rağmen yüksek spektral çözünürlük ile bitki örtüsü sınıfları arasında karışmanın olmadığı ortaya konmuştur.

Son aşamada, ASD Field Spec-Pro spektrometresi ile elde edilen yersel yansıtım değerleri ön işleme adımlarından geçirilmiştir. Gürültü etkisinin giderilmesi için Savitsky-Golay filtresi uygulanmıştır. Farklı sulak alan bitki türlerinin sahip olduğu yansıtım değerleri istatistik ANOVA yöntemi ile karşılaştırılmış ve bitki türleri arasında yansıtım farklılıkları hesaplamalar ile ortaya konmuştur.

Bu çalışmada, farklı uzaktan algılama verileri ve bunların arazi örtüsü sınıflandırma ve arazi örtüsü değişimi tespiti performansları karşılaştırılmıştır. Bu sonuçlara göre sulak alanların yönetimi ve korunması için vazgeçilmez arazi ve bitki örtüsü bilgilerinin elde edilmesi yöntemleri araştırılmıştır. Tüm çalışmada elde edilen arazi örtüsü kategorileri CORINE lejantına göre düzenlenmiştir. Böylece, rehber olarak kullanılabilir hangi görüntüler ile CORINE seviyelerine göre hangi ölçekte bilgi üretilebileceğini ve hangi yöntemlerin verimli şekilde kullanılabilirliğini gösteren bir altlık çalışma gerçekleştirilmiştir.

1. INTRODUCTION

Remote sensing technologies have been utilized in multidisciplinary applications by many scientists. Remotely sensed data is the major source of spatial information on the earth's surface cover and constitution (Curran, 1994; Schmidt and Skidmore, 2003). Satellite images provide economic, accurate and updated information of earth surface characteristics in a very short collection time for rapid analysis. Remote sensing technology accommodates accurate and reliable information as base input of many research subjects with different spatial, spectral and temporal resolution. Remotely sensed data derived land cover information have huge importance in order to monitor, manage, understand and protect natural resources. With the help of this important information, it is possible to determine land cover change and impacts on sensitive areas. Many applications, such as sustainable management, monitoring and mapping natural resources, determination of land use/cover changes in a different scale from local to global, delineate human induced effect on environment can be conducted by using remote sensing technology (Bektas Balcik and Goksel, 2005, Dogru et al, 2006, Dogru et al, 2008; Bektas Balcik et al, 2009). One potential use of remote sensing is in wetland assessment and management. Remote sensing in this field has focused on the spectral and spatial properties of vegetation and the surrounding landscape.

Wetlands are some of the most productive and wide spread ecosystems in the world. These areas are valuable for sustaining wildlife habitat, carbon sequestration, flood water management, shoreline erosion protection and water quality improvement, as well as having aesthetic and recreational opportunities and educational benefits to humans (Mitsch and Gosselink, 2000a). Increased awareness of wetland functions and benefits has shifted wetlands to the forefront of conservation science (Hoffstetter, 1983) putting efforts to inventories and monitor wetland ecosystems. All around the world, wetlands have come under natural and human threats from subsiding or sinking land to draining or filling for new development such as urbanization or agricultural activities.

The ability of human's to alter the natural environment has been noted one of the greatest concerns for global environmental change. The global population is approximately 7 billion and the human population continues to grow at a rate of 1.14% (or about 75 million people) per year (U.S. Census Bureau, 2009). As the world population rapidly increases, humans are increasingly disturbing natural resources, ecosystems and the environment. As a result, the world is facing serious water quality problems, deforestation, desertification, soil erosion, degradation of land productivity, and the disappearance of biodiversity and sensitive regions such as wetland (URL-1). This is prompting the urgent need to monitor and determine the changes due to humans. Many scientists have been studying on developing new methods for detecting and mapping global or regional change of natural areas such as wetlands.

In order to conserve ecological balance of the world, wetlands have to be managed, monitored and conserved. The management of these environments, especially in response to human activities, requires information on the quality and quantity of the vegetation. For this aim, different disciplines work together; accurate, detailed and reliable maps of sensitive regions have to be produced and new methods have to be developed in order to monitor these areas, constantly. There are many advantages in using remote sensing technology rather than conventional ground-survey techniques for wetland applications. Remote sensing provides a method of feasible and practical data acquisition for wetlands that frequently occur in rugged and inaccessible terrain, and for monitoring seasonal or directional changes in wetlands. Analysis and inventory of remotely sensed data is a cost effective method for mapping wetlands especially vegetation across large geographic areas (Butera, 1983). Several different types of remotely sensed data have been evaluated for use in wetland application especially identification and mapping of wetlands, including aerial photographs, airborne video imagery and many spaceborn and airborne imagery.

There have been developed various image-aided change detection and mapping methods. However, there is still a long way to go for accurate and reliable change detection and mapping.

The wetlands of Turkiye are important as natural ecosystem remnants offering wildlife habitat, biodiversity and tourist destinations, as well as functioning as important nutrient cycling capacity for maintaining water quality (Ozesmi and Bauer,

2002). The management of these environments, especially in response to human activities, requires information on the quality and quantity of vegetation, which produce a food source and habitat for wild life. Long term threats to these wetlands include agricultural activities, urbanization, and climate change.

Field wetland determinations require observation of the three wetland parameters: hydric soils, hydrology, and hydrophytic vegetation. Identification of vegetation is very important component of wetland management and protection. Vegetation is a fundamental element of earth's surface and has a major influence on the exchange of energy between the atmosphere and earth's surface (Bacour et al., 2002).

This research evaluates the potential of using different satellite remote sensing data from multispectral to hyperspectral to map wetland vegetation and land cover categories surrounded wetlands, by looking at the reflectance spectra at canopy level of wetland vegetation in the Terkos Water Basin. Hyperspectral remotely sensed data were integrated with the field based reflectance spectra to improve the accuracy of land cover maps especially for wetland vegetation. In this study, different methods were analyzed for land cover change detection to derive more accurate information for complex natural areas.

Land cover and land use (LCLU) change detection were determined by using different change detection techniques, such as modified Change Vector Analysis (mCVA) and Principle Component Analysis (PCA) based classification. As a novel application, Tasseled Cap Transformation (TCT) components were derived for Istanbul SPOT 5 data by using Gram-Schmidt Transformation (GST) for Change Vector Analysis. Results illustrated that PCA based method performance is better than mCVA for complex natural areas.

Different image fusion algorithms were applied to SPOT 5 MS and SPOT 5 PAN data to produce more accurate and detailed wetland vegetation map of the test areas in the study region. Fused image was used as a base map for the hyperspectral image classification with the field collected spectra data.

Hyperspectral Hyperion EO-1 data were used to provide a significant enhancement of spectral measurement capabilities with 220 bands over conventional remote sensor systems. With this feature, the identification and discrimination capabilities and classification accuracies were analysed for vegetation types and land cover types.

PCA transformation method was applied to Hyperion data for different spectrum range. Therefore, supervised and SAM (Spectral Angle Mapper) classification methods were applied original and transformed data for tested spectrum ranges.

Two different test sites were selected from the east side of the Terkos Lake for field reflectance collection from wetland vegetation samples. Analytical Spectral Devices (ASD) FieldSpec Pro spectroradiometers used for collecting reflectance data. The data collected simultaneously with satellite images to define different reflectance values of each sample in different portion of electromagnetic spectrum. Collected data were processed to integrate with the hyperspectral data. This ability used to enhance for vegetation discrimination and land cover classification.

CORINE (Coordination of Information on the Environment) land cover schema was adopted in this study. Different remotely sensed data evaluated according to CORINE legend level for heterogenous natural areas.

The objectives of the study were pursued in the following sequence:

1. Determine Terkos Lake area change between the years of 1991 and 2007 by using SPOT data,
2. Determine LCLU change between the years of 2003 and 2007 in the Terkos basin by using mCVA and PCA based change detection methods, with the help of SPOT 5 and SPOT 4 data
3. Examine the performance of TCT components for multispectral data analysis for complex natural areas
4. Use image processing and geostatistics to determine change detection
5. Examine the performance of PCA transformation for hyperspectral data analysis
6. Examine the performance of SAM and supervised classification for original and transformed hyperspectral data
7. Determine data with high spectral resolution has better results than the data with high spatial resolution
8. Produce more accurate wetland map by integrating field collected data and remotely sensed data

9. Determine use of remote sensing in evaluating environmental impacts on wetlands
10. Different type of sensors, and their use, will be considered for determining vegetation cover and vegetation composition change, encroaching land development with the help of field spectroscopy
11. Analyse the results based on CORINE legend levels for complex natural areas

In this research, remote sensing technology and different types of satellite images were used. SPOT 2, SPOT 4 and SPOT 5 images were conducted to derive past and present land cover data of the Terkos Water basin based on PCA, and mCVA, to determine LCLU change. Current and past land cover data were produced based on CORINE Scheme. Several image-processing techniques were conducted to remove atmospheric, radiometric and geometric distortions available in the images. TCT was applied to produce greenness, brightness and wetness map for CVA. TCT coefficients were derived by using GST with the help of image classification. PCA was applied to extract useful information from multispectral data. These transformed data used in the hybrid classification to investigate land cover and land use change in the Terkos water basin area. Results of hybrid classification (unsupervised and supervised classification) were supported with semivariograms and spatial profiles to derive the accurate land cover of the study area especially for the wetland regions. Classification accuracy assessment was applied to determine the land cover/use change detection results. Moreover, mCVA was introduced to SPOT 5 and SPOT 4 data set with TCT to derive LULC change information. In mCVA process, a change magnitude image and three change direction images were produced. For the land cover change detection magnitude and direction images were used. At the end, the performance of two transformation based change detection methods was analysed by using error matrix. Different image fusion techniques were applied to SPOT 5 MS and PAN data to produce more reliable and detailed base data for test regions. The resultant fused data were compared by using different statistical methods such as CC (Correlation Coefficient), RMSE (Root Mean Square Error), SAM (Spectral Angle Mapper), RASE (Relative average spectral error) and ERGAS (Erreur Relative Globale Adimensionnelle de Synthèse). The best resultant fused data was used in the Hyperion image processing as an ancillary data for Spectral Angle Mapper and supervised classification. In this stage, PCA performance was investigated for

hyperspectral Hyperion EO-1 data for different spectral band intervals such as visible, near infrared and shortwave infrared. Therefore, MNF transformation method was applied to hyperspectral image. Hyperion data was pre-processed by using Mineral Mapping Technology Group (MMGT) program. To determine the relationship between satellite data and field spectroradiometer data, first of all, remotely sensed data digital numbers were converted reflectance value to have compatible data with the collected field reflectance data. Field data, collected in near-real time to coincide with satellite sensor overpass especially with Hyperion and SPOT 5, were used to (1) quantify and model the wetland vegetation with the help of field spectra measurements; and (2) characterize wetland land use/land cover (LULC) classes. Field collected reflectance data were processed in order to minimize noise effect. Statistical method was applied to determine the spectral differences between wetland vegetation species in the selected test site of the Terkos Lake. Details of conducted image and data processing techniques are presented in following chapters.

Overall results illustrated that different kinds of images can be used to derive past and present land cover of the concerned region. Implementing different land cover change analysis methods showed that it is possible to use medium spatial resolution data for heterogeneous natural areas but mixed pixel problem must be taken into consideration. Evaluating different classification and transformation methods separately and together gave the chance to analyze the performances of these methods for complex regions by using spaceborn hyperspectral data. Analysis showed that PCA gave better results than MNF transformation for the land cover classification in Terkos Basin. Spectral segmentation process improved the classification accuracy of Hyperion hyperspectral data. These results can be used to produce a base guideline for the Turkish wetlands research and management activities in the future studies.

2. WETLAND SYSTEMS

Wetlands are some of the most productive and widespread ecosystems in the world. These areas are valuable for the sustainability of various kinds of animals and plants, some of which are endemic, and perform vital ecosystem services, including floodwater management, shoreline erosion protection, carbon sequestration and water quality improvement & protection, as well as providing food, water, grazing for livestock, materials for building, transport, aesthetic, recreational, and educational benefits to human beings (Mitsch, and Gosselink, 2000b). Wetlands are faced with serious threats of degradation or loss from increasing human pressure caused by population expansion, conflicting demand upon wetland resources and improperly planned development activities in wetland sites such as building construction and cultivation. Increased awareness of wetland functions and benefits has shifted wetlands to the forefront of the conservation sciences, spurring efforts to keep inventories and monitor wetland ecosystems.

2.1 Definitions of Wetlands

Wetland encompasses a wide variety of habitats, from tropical mangroves to arctic peatlands. There have been different definitions of wetlands. These are widely varied, ranging from ecological to legal definitions to those based on wetland function (Cronk and Fennessy, 2001). Scientists are interested in those definitions that facilitate wetland classification, inventory and research, while managers and regulators are concerned with laws and regulations designed to protect and prevent or control wetlands (Mitsch and Gosselink, 2000b).

Dugan (1993) mentioned that there are more than 50 definitions of wetlands in use all around the world. Some of the more popular wetland definitions are shown in Table 2.1.

Table 2.1: Wetland definitions.

Group	Definition
Ramsar Convention on Wetlands of International Importance, 1971	<ul style="list-style-type: none"> • Wetlands are defined as; "areas of marsh, fen, peatland or water, whether natural or artificial, permanent or temporary, with water that is static or flowing, fresh, brackish or salt, including areas of marine water the depth of which at low tide does not exceed six meters".
United States Fish and Wildlife Service (Cowardin, 1979)	<ul style="list-style-type: none"> • Wetlands are lands transitional between terrestrial and aquatic systems where the water table is usually at or near the surface or the land is covered by shallow water. For the purposes of classification, wetlands must have one or more of the following three attributes: <ol style="list-style-type: none"> 1) At least periodically, the land supports hydrophytes 2) The substrate is predominantly undrained hydric soil. 3) The substrate is non-soil and is saturated with water or covered by shallow water at some time during the growing season.
(Canadian Wildlife Service, Environment Canada. 1996).	<ul style="list-style-type: none"> • Land that is saturated for a long enough period to promote wetland or aquatic processes as indicated by poorly drained soils, hydrophytic vegetation, and various kinds of biological activity which are adapted to a wet environment. (Federal Policy on Wetland Conservation – Implementation Guide for Federal Land Managers, Wildlife Conservation Branch, Canadian Wildlife Service, Environment Canada. 1996).

2.2 The Global and Regional Distribution of Wetlands

Wetlands are found on every continent except Antarctica, and in all climates, from subarctic to the tropics. Estimates of the total global wetland resources base range between 4 to 6% (7 to 8 million km²) of the Earth's surface (Mitsch and Gosselink, 2000b). Wetlands are extremely diverse as a result of regional and local differences in climate, topography, hydrology, geology, vegetation composition, water chemistry, soils and other factors, such as human disturbance (Mitsch and Gosselink, 2000b; Sipple, 2002; Jollineau, 2003). Wetlands occur in a variety of geomorphological compositions including river deltas, coastal lagoons, river floodplains, inland lakes, and inland depressions (Dugan, 1990; Jollineau, 2003). Estimated area of The Convention on Wetlands of International Importance (RAMSAR) wetlands is given in Table 2.2 based on Finlayson and Davidson (1999).

Table 2.2: Estimated area of wetlands in each of the regions of the world recognized under the Ramsar Wetlands Convention (Finlayson and Davidson 1999).

Region	Million km ²	Estimated area of wetlands
		Percentage of global estimated area
Africa	1.21	9.5
Asia	2.04	16.0
Eastern Europe	2.29	17.9
Western Europe	0.29	2.3
Neotropics	4.15	32.5
North America	2.42	19.0
Oceania	0.36	2.8
Global (total)	12.76	100

Global distributions of wetlands are given in Figure 2.1 based on the Global wetlands map (a reclassification of the FAO-UNESCO Soil Map of the World that produced in 1997) (URL-2). The major wetland regions of the world are found in: North America (e.g., the wetlands of Great Lake basin, and the Florida Everglades), South America (e.g., the Pantanal), Europe (e.g., the Rhine River Delta), Africa (e.g., the Okavango Delta), Australia (e.g., the billabons of the Eastern Australia), and Asia (e.g., the Southeast Asian river deltas) (Mitsch and Gosselink, 2000a).

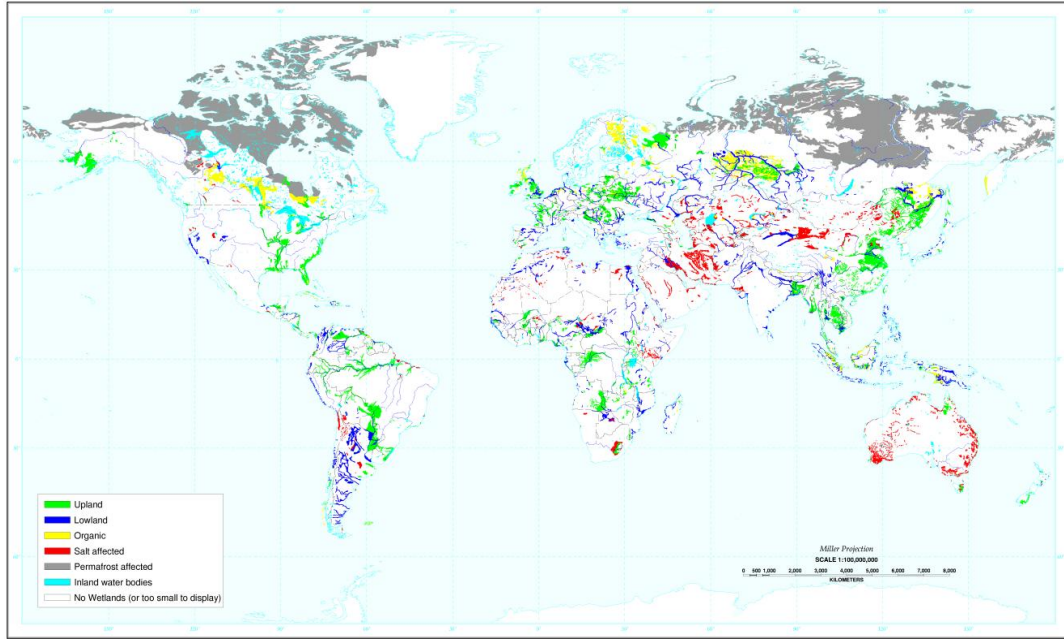


Figure 2.1 : Distribution of wetlands (URL-2).

2.3 Wetlands of Turkey

According to RAMSAR there are 81 sites designated as Wetlands of International Importance in Turkey, with a surface area of approximately 1.292 546 million hectares (ha).

Turkey acceded to RAMSAR in 1994 and, at the stage of accession, had its 5 wetlands (Lake Manyas, Lake Seyfe, Lake Burdur, Sultan Reedbed and Göksu Delta) recorded in the Convention List (RAMSAR convention, 2002). In 1998, the whole of Lake Manyas (Bird) and Lake Burdur, already included in the Convention List in part, and Gediz Delta, Akyatan Lagoon, Lake Uluabat and Kızılırmak Delta were also included in the Convention List. At present, there are 12 wetlands covered by RAMSAR, extending over a total area of 206,830 hectares. Following assessments made in consideration of international criteria, there are 200 areas determined to be wetlands of international importance. 76 of them are belonging to important bird area, 4 of them are included as important fish area and 16 of them can describe as important bird and fish area and 18 of these 81 places were accepted as class “A” wetland in Figure 2.2 (Atlas Dergisi, 2006). In 13 of these areas, the “Bird Sanctuaries Project” has been started.

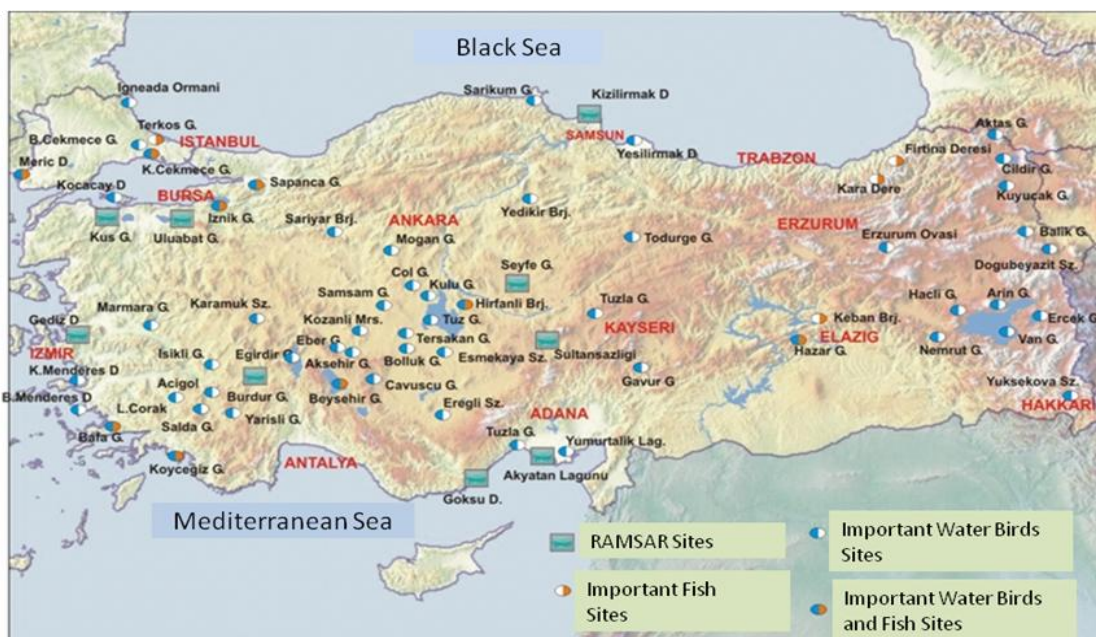


Figure 2.2 : Distribution of Turkish wetlands (Atlas Dergisi, 2006).

With its rivers and lakes covering an area of about 10,000 km², Turkey has very important inland water resources to maintain biological diversity. There exist 132 mammals, 457 birds and around 105 reptile species in Turkey. The two of the four important bird immigration routes in Palearctic region (between West Palearctic and Africa) pass over Turkey. In Turkey, there are 7 drainage basins including 26 river basins, and the ground waters are estimated at 94 billion m³. The average annual rainfall is about 640 mm, roughly one third of which reaches water reserves and thus contributes to the maintenance of wetlands.

Generally, the wetlands are rich in vegetation, but they are behind the continental habitats in terms of species diversity. In Turkey's wetlands, plants such as the cattail (*Typha* sp.), the reed (*Phragmites* sp.), the rush (*Schoenoplectus* sp.), and the reed mace (*Juncus* sp.) form large communities. In addition, there are also plants that cover the water surface such as the water lily (*Nymphae* sp.) and underwater plants that grow in shallow lakes such as the duck grass (*Phodophyllum* sp.), the duck lentil (*Wolffi* a sp.), the water lentil (*Lemna* sp.) and *Ceratophyllum* sp., *Myriophyllum* sp. and *Potamogeton* sp.

The Red Book of Turkey's Plants collects the flora of Turkey's wetlands under two categories: in-water flora and coastalmarsh flora (The National Biological Diversity Strategy and Action Plan, 2007).

Located on bird migration routes, Turkey is a key country for many bird species. The wetlands are a home to a considerable number of 460 bird species, which choose Turkey as their permanent or temporary habitat. For example, the Dalmatian Pelikan, marbled teal, cormorant, Audouin's gull, white-headed duck, slender-billed curlew, bittern, white-fronted goose, red-necked goose, and ferruginous duck, which are globally recognized as being under threat in Europe, breed in Turkey. Out of the world's entire white-headed duck population, around 70% winter in Turkey. The purple gallinule (*Porphyro porphyro*), which is found only in certain areas in the Mediterranean Region and is gradually decreasing in number, breeds in the Göksu Delta, in particular. The Lake Manyas is both a breeding area for the cormorant (*Phalacrocorax carbo*), pygmy cormorant (*Phalacrocorax pygmeus*), Dalmation Pelikan (*Pelecanus crispus*), night heron (*Nycticorax nycticorax*), squacco heron (*Ardeola ralloides*), little egret (*Egretta garzetta*), and spoonbill (*Platalea leucorodia*) species and a wintering area for the white-headed duck (*Oxyura leucocephala*), Dalmation Pelikan (*Pelecanus crispus*), and pygmy cormorant (*Phalacrocorax pygmeus*) species. The Lake Bafa is both a wintering area for the little grebe (*Tachybaptus rufi collis*), great crested grebe (*Podiceps cristatus*), black-necked grebe (*Podiceps nigricollis*), cormorant (*Phalacrocorax carbo*), pygmy cormorant (*Phalacrocorax pygmeus*), Dalmatian Pelikan (*Pelecanus crispus*), gadwall (*Anas streperg*), pochard (*Aythya ferina*), and coot (*Fulica atra*) and breeding area for the bald eagle (*Haliaeetus albicilla*), pratincole (*Glareola pratincola*), and spur-winged plover (*Vanellus spinosus*) (The National Biological Diversity Strategy and Action Plan, 2007).

Turkey's wetlands contain mainly the following fish species: trout, pike, carp, *Clarias lazera*, mullet, rudd, pike-perch, and perch. The common otter (*Lutra lutra*), which is found in many of Turkey's wetlands, is under the threat of extinction and put under conservation in the entire Europe (The National Biological Diversity Strategy and Action Plan, 2007).

The wetlands of Turkiye are important as natural ecosystem remnants providing food, water, grazing for livestock and offering wildlife habitat, biodiversity and tourist destinations, as well as functioning as important nutrient cycling capacity for maintaining water quality. These areas are under long term threats of global warming, pollution, agricultural activities and urbanization.

2.4 Wetland Ecosystem Benefits: The Functions and Values of Wetlands

Wetlands have several benefits. Many of them are directly related to quality and quantity of vegetation (Gross et al., 1989). These benefits are typically grouped into two main categories: wetland functions and wetland values (URL-3) (Table 2.3). The removal or damage of wetland system because of urbanization, agricultural activities or other factors causes the environmental problems such as water quality distortion.

Table 2.3: Wetland functions and values (URL-3).

Wetland Functions	Description
Biodiversity	Numerous species of birds and mammals rely on wetlands for food, water, and shelter, especially while migrating and breeding.
Water Treatment	They help improve water quality, including that of drinking water, by intercepting surface runoff and removing or retaining inorganic nutrients, processing organic wastes, and reducing suspended sediments before they reach open water.
Flood Protection	Wetlands store and slowly release surface water, rain, snowmelt, groundwater and flood waters. Trees and other wetland vegetation also impede the movement of flood waters and distribute them more slowly over floodplains.
Shoreline Erosion	Wetlands protect shorelines and stream banks against erosion. Wetland plants hold the soil in place with their roots, absorb the energy of waves, and break up the flow of stream or river currents.
Carbon Store	Wetlands store carbon within their live and preserved (peat) plant biomass instead of releasing it to the atmosphere as carbon dioxide, a greenhouse gas affecting global climates.
Wetland Values	Description
Recreation	Wetlands provide areas for sports hiking, bird watching.
Economical Education	Fishing and rice Faouna-Flora

2.5 Major Threats to Wetlands

Most important threat is transformation into land for non-wetland uses with driving forces such as population and economic growth. Examples of such activities include drainage to obtain land for agricultural uses, like farming and ranching, and the

transformation of wetlands into aqua cultural sites, such as rice paddies. Another problem is over-exploitation of ground water aquifers, which supports wetlands. This is a threat not only to that individual wetland, but also to others at a considerable distance from it. Discharge of industrial and/or domestic wastes, either into the water sources feeding the wetland or into the wetland itself, leads to its pollution and thus to the destruction of the ecosystem and the various habitats within it. Another source of pollution is the use/over-use of pesticides, herbicides and fertilizers in the agricultural fields around the wetland. These pollutants saturate the soil and drain into the ground water, thus contaminating its water sources. Burning and cutting reeds before, and/or during, the breeding season of bird species leads to the destruction of the food chain and a reduction in the number and variety of birds established in the ecosystem. Over-fishing is an additional cause of destruction to the ecological balance of wetlands.

The results of these threats are commonplace. They include loss of habitat for a wide range of organisms. Organic matter builds up at an accelerated rate, and reduces water quality. The combination of algae, bacteria and other microorganisms, forming the major component of the food chain, is altered to include more pollution-tolerant species, and the detrimental effects of nutrient enrichment are transmitted over wide ranges of areas. These are, in brief, the dramatic results of progressive human activities, the location of which may be quite distant from the area affected.

2.6 Wetland Loss and Degradation

The loss and degradation of wetlands in many countries all over the world is continuing at an alarming rate. Wetland loss is the loss of wetland area, due to the conversion of wetland to non-wetland habitats, because of human activity such as urbanization and agriculture; wetland degradation is the impairment of wetland functions as a result of human activity. The loss and degradation of wetlands reduces their ability to provide goods and services to humankind and to support biodiversity, and are therefore associated with economic costs.

Area of over 1,3 million ha (totally 57%) of Turkish wetlands have been disappeared as a consequence of wetland loss. The loss and degradation of Turkey's wetlands emerged from various causes such as agricultural activities, growth in industrial and residential areas, road constructions, malaria eradication, flood prevention etc.

However, because of the loss or degradation of wetlands across Turkey, wetland dependent flora and fauna species are at high risk. Nevertheless, these human interferences have caused crucial environmental degradations.

In Turkey, the total area of wetlands drained by 1986, starting in the 1950's, exceeded 190,000 ha, as a result of drainage activities related to malaria control and increased need for farmland. Decreases, in both the bird populations and the number and variety of species of nesting birds, have been observed in Anatolia. Lakes also have problems such as irrigation, drainage, pollution, over-fishing, hunting pressure, housing etc. The wetlands of the developing world are rapidly being lost for to intensified agriculture, urban development, industrial growth, and pollution.

The most common wetland type in the Mediterranean is probably the "lost wetland". In France wetlands are shrinking at a rate of 10,000 ha per year. In Roman times, 10% of Italy (3 million ha) was wetlands; by 1972 this had diminished to only 190,000 ha. In one region of Spain, 60% of the wetlands has been lost, three-quarters of this loss taking place in the last 25 years. 80% of Portuguese salt marshes were threatened with reclamation. The Bulgarian Ministry of the Environment has reported that many coastal lakes and marsh-lands have been drained or modified since 1944. Similarly, the Yugoslav Commission for the Environment has reported that the majority of larger wetland complexes have been drained and put under cultivation or into pasture since 1945. In Greece a 60% loss of wetlands, mainly lakes and marshland, has taken place as a result of land drainage for agriculture. In Egypt, it is reported that there has been a sustained contraction of wetland areas because of continuous land reclamation. Lake Burullus, for instance, now a Ramsar site, was reduced from 58,800 ha to 46,100 ha between 1913 and 1974.

3. REMOTE SENSING OF WETLANDS

3.1 Introduction

To conserve and manage wetland resources, it is important to inventory and monitor wetlands and their adjacent uplands (Özeşmi and Bauer, 2002). Given the significant extent of wetland degradation and loss in Turkey, these sensitive regions need to identify and map. Wetland maps are an extremely useful source of information on the status of existing wetlands for management and protection activities such as . land use planning, environmental impact assessment, and habitat analysis.

Digital remote sensing has been used with some success to monitor wetlands and provide input to better manage the Earth (Skidmore et al, 1997). Satellite remote sensing has several advantages and powerful tool for monitoring and mapping wetland resources, especially for over large geographic areas due to its ability to acquire timely digital data on a repetitive basis (Rundquist et al, 2001). Remote sensing also offers several advantages over traditional field methods of collecting wetland information including synoptic coverage, cost effectiveness, and short analyzing time (Butera, 1983; Rundquist et al, 2001). As a result, remotely sensed data has become an attractive and popular tool for wetland researches. Improved spectral resolution of multispectral data provide increased spectral information allowing better differentiation of land cover, and improved spatial resolution increases the likelihood that “pure” pixels are collected for specific land cover types. Remote sensing techniques, together with ground truth, are widely used to collect information on the qualitative and quantitative status of biodiversity of natural resources (Chopra et al, 2001). Remote sensing specifications for mapping wetland vegetation vary greatly, depending on desired map accuracy and spatial patterns in the vegetation community.

This chapter summarizes the literature on remote sensing of wetlands, includes what kind of data and which classification method were more successful for wetlands monitoring, management, mapping.

3.2 Remote Sensing Research in Wetland Ecosystems

There are different types of wetlands and these wetlands have studied by using different remotely sensed data. Multispectral images that are Landsat MSS, Landsat TM, SPOT, IRS-1B, LISS-II, IKONOS, and QUICKBIRD are the major satellite systems that have used to study wetlands; radar systems, including JERS-1, ERS-1 and RADARSAT, space and airborne-based hyperspectral images CASI, HyMap, AVIRIS, Hyperion and other systems are NOAA AVHRR, SPOT VEGETATION.

Remote sensing of wetlands by satellites dates back Landsat-1, launched 1972. Work and Gilmer, 1976 used Landsat-1 MSS imagery to invent lake and pond. Butera, 1983 compared medium resolution MSS with high resolution airborne MSS to predict area of *Phragmites Communis*. Landsat-1 MSS appeared to overpredict the total area. With the high resolution, it was able to distinguish vegetation species in a mixed wetland environment. Jensen et al. (1986) used Landsat MSS imagery to develop a regional map of wetlands. The U.S. Fish and Wildlife Service used Landsat imagery for National Wetland Inventory in 1979, but the service concluded that the Landsat MSS could not provide the needed classification detail and accuracy requirements, and mid- and high-altitude color infrared aerial photography adopted in wetland studies. This technique used to identify and map vegetative communities and wetland boundary (Gammon and Carter, 1979). The Thematic Mapper (TM) multispectral instrument, first launched on Landsat-5 in 1984, brings increased spatial resolution (30 m) and increased spectral resolution (6 bands) to bear on the problem of wetland remote sensing. TM performances for discriminating wetlands from uplands, producing coastal wetlands habitat maps, delineating forested wetlands and discriminating wetlands communities within wetlands were tested by using different classification methods (supervised, unsupervised and hybrid) (Jensen et al, 1986; Johnston and Barston 1993; Berberoglu et al, 2000; Berberoglu et al, 2004; Baker et al, 2006).

Other popular satellite used for wetland remote sensing is the French System Pour l'Observation de la Terre or SPOT satellite (20 m resolution MS and 10 m PAN and 2.5 m PANSAHRP). SPOT imagery and Indian Remote Sensing (IRS-1) platform (36.5 m resolution) used to map wetlands and to determine the seasonal changes of wetland vegetation changes (Hardisky et al, 1986; Jensen et al, 1993; Jensen et al, 1995; Houhoulis et al, 2000).

Wetlands are complex and small environments. Satellite images with medium spatial resolution not enough to map and delineate wetlands (Nagendra, 2001). To solve this mix pixel problem, high resolution satellite images with better spatial resolution such as IKONOS, Quickbird and SPOT 5 data used for wetland evaluation studies (Dechka et al, 2002; Mumby and Edwards, 2002).

A synthetic aperture-radar (SAR) sensor, such as onboard the Canadian RADARSAT satellite, is sensitive to the dielectric constant and the geometric properties of the target. Since an empirical relationship exists between the dielectric constant of a natural object and its water content (Herkelrath et al, 1991), SAR images are useful for detecting the presence of water (Kasischke and Bourgeau-Chavez, 1997). Radar pulses can penetrate vegetation to a degree dependent on canopy density. RADARSAT imagery has been shown to be useful for flood delineation in open areas and in deciduous vegetation during leaf-off conditions (Crevier et al, 1996; Kushwaha et al, 2000). Floodwater boundaries, vegetation communities at the land–water fringe, and upland versus wetland vegetation should be discriminated more efficiently by using combined optical and radar data (Augusteijn and Warrender, 1998; Toyra et al, 2001).

A relatively new form of remote sensing provides another means to acquire information on three-dimensional habitat heterogeneity. Light detection and ranging (Lidar) is based on the use of laser light emitted from a source and reflected back to a sensor as it intercepts objects in its path (Dubayah et al, 2000). As the reflected light is detected at the sensor, it is digitized, creating a record of returns that are a function of the distance between the sensor and the intercepted object. This entire stream of reflected laser returns is referred to as a waveform. Topography of subcanopy, canopy height, basal area, stem diameter, canopy height profiles, canopy cover and biomass have all been successfully derived from large-footprint lidar waveform data in a variety of forest types (Drake et al, 2002). Digital Elevation Model (DEM) of the study area produced to examine relationship of vegetation and topography in flooded area (Toyra et al, 2002). Combination of the optical data with Lidar data offers the potential to map and monitor plant communities based on their spectral and structural characteristics.

Hyperspectral remote sensing data with the advantage of many narrow spectral bands used for wetland vegetation discrimination and wetland mapping (Bakker and

Schmidth, 2002; Schmidth and Skidmore, 2003 and Ramsey III et al, 2005). The wealth of spectral information provided by hyperspectral sensors allows for the species-level detection necessary to map vegetation species (Underwood et al, 2003). High spectral resolution data provide an increased ability to differentiate land cover types. Airborne and spaceborne based hyperspectral data such as HyMap, Hyperion, Aviris used for different wetland vegetation studies with vegetation index and field collected spectra data especially for invasive alien species analysis and vegetation species discrimination (Schmidt and Skidmore, 2003; Goodenough, 2003; Galvao et al, 2005; Galvao, et al, 2009; Guerschman et al, 2009).

Work on wetland mapping and monitoring involving extensive areas at low detail levels has been undertaken using NOAA imagery (Klemas et al, 1993). Very little work has presently taken place on semi-arid wetland applications for the coarse resolution VEGETATION sensor system that formed part of the SPOT 4 payload in April 1998 (URL-4). Work has been more focused on such topics as land cover changes and boreal forest resource assessments. Generally it may be considered that low resolution sensors such as NOAA-AVHRR or SPOT 4 (VEGETATION) are inadequate to map or monitor detailed ecological change in wetlands, however the extent of their potential usefulness in wetland semi-arid environments has rarely been previously documented (Ringrose et al, 2003).

3.3 Conventional Approaches to Wetland Ecosystems

Classification and change detection monitoring of wetland is difficult task because wetland types and spatial distribution can change dramatically from season to season, especially when nonpersistent species are present. Change information of wetland is essential and necessary to the management of wetland and relative decision-making of protection. As a prelude to their conservation, it is necessary to map wetland, determine whether or not they have changed over specified time periods and quantify these changes (Jensen et al, 1993; Munyati, 2000).

This task often may require temporal and synoptic data collection and analysis. Change detection studies have taken advantage of the repeat coverage and archival data available with satellite remote sensing. Aerial photograph interpretation has traditionally been used to monitor and determine changes in wetlands (Ramsey and Laine, 1997).

The variety of image data sources and classification techniques presently used has led to the development of numerous change detection techniques (Coppin et al, 2004).

- Post-classification comparison has been applied to wetland studies to determine the total area of wetland change and to identify specific locations of such changes (Ramsey and Laine, 1997; Munyati, 2000).
- Simple differencing of spectral bands that includes image subtraction and threshold is a common technique for quantifying spectral change. This method may provide spurious results due to influence of data noise, inconsistencies between individual sensors, and limitations of detecting change with a single spectral band (Coppin et al, 2004).
- Simple differencing of vegetation indices (e.g., Normalized Difference Vegetation Index (NDVI)) is less susceptible to noise interference (Hayes and Sader 2001). Index differencing is more spectrally dynamic than simple differencing, although these techniques are also heavily dependent on the radiometric resolution of only two spectral bands (Johnson and Kasischke 1998, Dymond and Johnson 2002).
- Orthogonal spectral data transformations compress spectral data into linear combinations of spectral components that can accurately detect diverse ecosystems (Collins and Woodcock 1994, Oetter et al. 2001, Dymond and Johnson 2002, Parmenter et al. 2003). Principle components analysis (PCA) Lillesand and Keifer, (1979); and Tasseled Cap (TC) Collins and Woodcock (1994); Parmenter et al. (2003) are two commonly applied orthogonal data transformations. TC transformations have effectively isolated wet sites on a landscape Dymond et al. (2002) and improved distinctions between moist and senescent vegetation (Crist et al. 1986).
- Spectral libraries in conjunction with hyperspectral and multispectral data have used and evaluated to determine spatial and temporal changes in wetlands areas to monitor and control of the loss of wetlands (Schmidt, 2003).

Wetland classification is difficult because of spectral mixing with other land cover classes and among different types of wetlands (Ozesmi and Bauer, 2002). Detailed wetland maps can be updated using satellite imagery.

Improved vegetation maps have been produced using traditional supervised and unsupervised classifiers on high spatial resolution multispectral and hyperspectral data (e.g., Belluco et al, 2006; Pengra et al, 2007). Previous work on the classification of marsh vegetation using multi-temporal image data (Belluco et al, 2006) and LiDAR data (Rosso et al., 2006) relies on judicious identification of endmembers, often derived from extensive field measurements. A layered, hybrid or rule-based approach may give better results than more traditional methods.

3.4 Field Spectroscopy

Spectroscopy can provide information about a substance by relating the interaction of electromagnetic radiation as a function of wavelength to its chemical composition and physical properties (Kokaly and Clark, 1999). All vegetation contains the same basic constituents: chlorophyll and other light-absorbing pigments, water, proteins, starches, waxes, and structural biochemical molecules such as lignin and cellulose (Elvidge, 1990). All of these components contribute to the reflectance spectra of vegetation. Figure 3.1 shows laboratory reflectance spectra of vegetation foliage in the fresh and dry state (adapted from Beerli et al, (2007)).

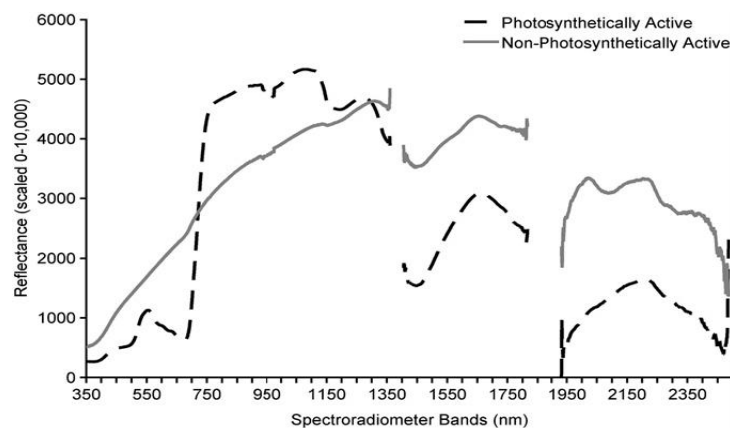


Figure 3.1 : Spectral signatures for photosynthetically and non- photosynthetically active vegetation recorded using a handheld spectroradiometer adapted from Beerli et al, (2007) .

The wavelength regions in which the basic plant components have strong absorption features are indicated on this plot. Because of pigment absorptions, the visible region of green plants shows a maximum reflectance at approximately 0.55 μm and lower reflectance in the blue (0.45 μm) and red (0.68 μm). Beyond visible wavelengths (longer than 0.70 μm), the spectra of fresh plants show a strong rise in reflectance.

The region of high plant reflectance at the short-wavelength end of the near-infrared (0.75–1.30 μm) is called the near-infrared plateau (NIR-plateau). The high reflectance results from an increased amount of light scattering at cell-wall interfaces because of a change in the index of refraction, the absence of pigment absorptions, and the weakening of overtone absorption of water in leaves at those wavelengths. Two absorption features centered near 0.98 and 1.20 μm are evident on the NIR-plateau. At 1.40 μm , a strong water-absorption feature reduces the reflectance. For fresh leaves, another, even stronger, water absorption is present at 1.90 μm . In dried vegetation, the water absorptions no longer conceal the absorption features at 1.73 μm , 2.10 μm , and 2.30 μm that are caused by organic bonds in plant biochemicals. Proteins, lignin, and cellulose all contribute to these features. The waveband region and importance for the vegetation quality and quantity analysis is given in Table 3.1

Table 3.1 : Wavelengths of importance for vegetation studies and their role.

WaveBand μm	Region	Importance
0.470	Blue	Sensitive to carotenoid content (Blackburn, 1999)
0.495- 0.499	Blue	Sensitive to ageing and browning conditions (Thenkanbail et al.,1999,2000)
0.555	Green	Maximum reflectance peak in the visible region, sensitive to chlorophyll content (Blackburn, 1999; Thenkanbail et al., 2002)
0.611	Red	Sensitive to biomass and LAI (Thenkanbail et al., 2004b)
0.635	Red	Sensitive to chlorophyll b (Blackburn, 1999)
0.670	Red	Maximum absorption region for chlorophyll a (Gitelson and Merzlyak, 1997)
0.680	Red	Sensitive to chlorophyll a (Blackburn, 1999)
0.692	Red	Sensitive to growth conditions, biomass and LAI (Thenkabail et al., 2004b)
0.722	Red Edge	Sensitive to vegetation stress and structure, but resilient to soil background and atmospheric noise/radiation contribution (Dawson and Curran, 1998)

Table 3.1 (contd.) : Wavelengths of importance for vegetation studies and their role.

0.783	NIR	Sensitive to chlorophyll content (Curran et al., 1991)
0.845	NIR	Sensitive to chlorophyll content (Schepers et al., 1996)
0.895	NIR	Reflectance peak for most vegetation species, sensitive to biomass, chlorophyll and protein content (Thenkabail et al., 2002)
0.943	NIR	Absorption area due to vegetation water content (Thenkabail et al., 2004b)
0.970- 0.980	NIR	Sensitive to vegetation water content (Thenkabail et al., 2002; Penuelas et al., 1993)
1.054	NIR	Sensitive to vegetation water content (Thenkabail et al., 2004b)
1.094	NIR	Sensitive to biomass and LAI (Thenkabail et al., 2004b)
1.104	NIR	Sensitive to biomass and LAI (Thenkabail et al., 2004b)
1.145	NIR	Sensitive to biomass and water content (Thenkabail et al., 2004b)
1.215	NIR	Sensitive to vegetation water content (Thenkabail et al., 2004b)
1.285	NIR	Sensitive to biomass and LAI (Thenkabail et al., 2004b)
1.467	MIR	Sensitive to starch, lignin, cellulose and water content (Thenkabail et al., 2004b)
1.518	MIR	More sensitive to changes in water content than NIR wavebands (Jensen, 2000)
1.659	MIR	Sensitive to biomass, starch, lignin and assists the discrimination of leaf types (Gausman, 1973)
2.022	MIR	Sensitive to water content (Thenkabail et al., 2004b)
2.052	MIR	Sensitive to water content and protein (Kumar et al., 2001)
2.050- 2.140	MIR	Lignin absorption area (Kumar et al., 2001)
2.264	MIR	Sensitive to water content changes (Jensen., 2000)
2.315	MIR	Sensitive to water content, lignin, starch and stress (Thenkabail et al, 2004b)

Several studies demonstrate significant spectral differences between marsh plant species in both field reflectance data (Hardisky et al, 1986; Zhang, 1999; Schmidt & Skidmore, 2003; Gao & Zhang, 2006) and hyperspectral (Gross & Klemas, 1986) reflectance data at various times during the growing season.

4. REMOTE SENSING, FIELD SPECTROSCOPY AND GEOSTATISTICS

4.1 Image Processing

The image processing techniques conducted in this research to obtain past and present accurate land cover map of the study area were explained in the following sections. Using the produced land cover maps, land cover changes in the area were determined and detailed, and accurate wetland vegetation map was produced. The relationships between field collected data and remotely sensed data were investigated. The potential of integrated field collected reflectance data and hyperspectral remote sensing data was analysed based on different classification methods.

4.1.1 Radiometric and Atmospheric Correction

The electromagnetic radiation signals travelling through the atmosphere are altered because of the process of absorption and scattering caused by gases, and aerosols within atmosphere. These atmospheric processes have a dual effect on remotely sensed data. The radiation reaching the top of the atmosphere (TOA) from the Sun (extraterrestrial irradiance), is altered as it travels through the atmosphere to the surface of the Earth; and the radiation reflected or emitted from the surface of the Earth is not equal to the radiation measured by sensors in orbit around Earth. As a result, remotely sensed data are not solely dependent on the spectral properties of targets on the surface of the Earth, but also on the content of the atmosphere. Changes in scene illumination, atmospheric conditions, viewing geometry and instrument response cause radiometric distortions over satellite image. Therefore, satellite sensor images are radiometrically and atmospherically corrected to eliminate system errors and to minimize contamination effects of atmospheric particles through absorption and scattering of the radiation from the earth surface (Teilet, 1986; Song et al, 2001; Liang, 2004).

The atmospheric contribution to the measured radiation can be very important and can cause considerable errors if TOA values are used to take quantitative measurements of surface parameters; moreover, it will never be constant since the atmospheric content is temporally and spatially variable; therefore, TOA data collected over different locations or time are not directly comparable. Atmospheric correction is a very important processing step of quantitative remote sensing because most of the inversion algorithms such as canopy models, are based on surface reflectance that are retrieved from atmospheric correction (Liang, 2004). Atmospheric contamination is a major source of error in several vegetation monitoring applications Liang (2001) hence, it is common practice to remove it in cases when quantitative measurements are needed, or data collected over different dates and/or areas need to be used together.

The objective of radiometric correction is to recover the “true” radiance and/or reflectance of the target of interest (Lathrop, 1988).

Units of electromagnetic radiation namely irradiance, radiance and reflectance should be considered since they will be used in radiometric and atmospheric correction procedure.

- *Irradiance* - radiant flux incident on a receiving surface from all directions, per unit surface area, $W m^{-2}$
- *Radiance* - radiant flux emitted or scattered by a unit area of surface as measured through a solid angle, $W m^{-2} sr^{-1}$
- *Reflectance* - fraction of the incident flux that is reflected by a medium

Conversion from Digital Number (DN) to radiance (analog signal) was conducted by using calibration parameters such as gain and offset. These are available in published sources and image header files.

The following equation is used for the calculation of radiance values from DN values:

$$L=DN/A_k \tag{4.1}$$

- $L (W m^{-2} sr^{-1} \mu m^{-1})$ = top of atmosphere (TOA) upwelling radiance
- $A_k (W^{-1} m^2 sr \mu m)$ = calibration factor for spectral band k
- DN = Digital numbers

given by SPOT-Image (Doxaran, et al, 2002).

L was converted to TOA reflectance, R^* (unitless) using the following equation (4.2) (Vermote et al, 1997)

$$\rho_{\lambda} = \frac{\pi * L_{\lambda} * d^2}{ESUN_{\lambda} * \cos(Z)} \quad (4.2)$$

Where

- Z = Solar zenith angle in degrees
- $ESUN_{\lambda}$ ($W\ m^{-2}\ \mu m$) = Mean solar Exoatmospheric irradiances
- ρ_{λ} = Unitless planetary reflectance
- d = Earth Sun distance
- L_{λ} = Spectral radiance at the sensor apertures

The Earth-Sun distance has been calculated from the given formula 4.3:

$$d = 1 - 0.01674 * \cos(0.9856 * (Jday - 4)) \quad (4.3)$$

- Jday = Julian day for day of satellite pass

Offset and bias parameters for SPOT sensors depicted in Table 4.1.

Table 4.1: Offset and bias parameters for SPOT sensors.

	Band	XS1	XS2	XS3	XS4
	Parameters				
Sensor	A_i = Offset				
	B_i = Bias				
SPOT 4	A_i	1.50348	1.91117	1.31882	9.28470
	B_i	0	0	0	0
SPOT2	A_i	1.13449	1.19372	1.27471	
	B_i	0	0	0	
SPOT5	A_i	1.301197	1.586822	1.307911	3.7207
	B_i	0	0	0	0
SPOT1	A_i	0.86920	0.83512	1.00380	
	B_i	0	0	0	
SPOT4	A_i	2.02977	1.82072	0.90380	8.15451
	B_i	0	0	0	0
SPOT5 PAN	A_i	1.937671			
	B_i	0			

Solar spectral irradiances for SPOT images are given in the following Table 4.2.

Table 4.2: Solar spectral irradiances for SPOT images.

	SPOT 1	SPOT 2	SPOT 3	SPOT 4	SPOT 4	SPOT 5
Spectral Band	HRV1	HRV1	HRV1	HRV1R1	HRVR2	HRG1
P/M	1.680	1.705	1.668	1.568	1.586	1.762
XS1	1.855	1.865	1.854	1.843	1.851	1.858
XS2	1.615	1.620	1.580	1.568	1.586	1.573
XS3	1.090	1.085	1.065	1.052	1.054	1.043
SWIR				0.233	0.240	0.236

Hyperion image DN values were converted radiance value by using the equation 4.4 and 4.5.

$$L_{VNIR} = DN/400 \quad (4.4)$$

$$L_{SWIR} = DN/800 \quad (4.5)$$

L = Spectral radiance at the sensor apertures

DN = Digital Number

Atmospheric correction procedures are designed to minimize scattering and absorption effects due to the atmosphere. Scattering causes and increase in brightness and shorter wavelengths (visible region) are strongly influenced by scattering due to Rayleigh, Mie and nonselective scattering. On the other hand, absorption decreases brightness and longer wavelengths (infrared region) are strongly influenced by water vapor absorption (Lathrop, 1988).

Atmospheric correction consists of two major steps: atmospheric parameter estimation and surface reflectance retrieval. There are two types of atmospheric correction techniques namely relative and absolute atmospheric correction. Different models have been developed to minimize the noise introduced by atmospheric processes on the signal received by the satellite, ranging from simple methods based on information contained in the image.

Some of the developed simple methods can be listed as Dark Object Subtraction (DOS)-based methods Chavez, (1996) and empirical line model Karpouzli and Malthus (2003). Complex radiative transfer models such as a simplified method for the atmospheric correction (SMAC) Rahman and Dedieu, (1994), 6S Vermote et al, (1997), MODerate spectral resolution atmospheric TRANSmittance (MODTRAN) Berk et al, (1999), that simulate the atmosphere/light interactions between the sun surface and surface-sensor. In this study, FLAASH atmospheric correction method

was used for atmospheric correction of Hyperion data (ENVI, 2009). FLAASH works based on MODTRAN.

4.1.1.1 Dark Object Subtraction (DOS)/Haze Removal

A “dark object subtraction” method was used to correct for atmospheric scattering in the path. Dark object subtraction is an image-based approach that assumes dark objects exist within an image and these objects should have values very close to zero (such as water bodies), and that radiance values greater than zero over these areas can be attributed to atmospheric scattering and thereby subtracted from all pixel values in an image (Moran et al, 1992; Gilabert et al, 1994). In fact, very few targets on the Earth’s surface are absolute black, so an assumed one-percent minimum reflectance better than zero percent (Chavez, 1996). The pixel values are selected for each individual band with the histogram method and subtracted from all pixel values for the corresponding band across an image (Liang 2001, 2004) to remove haze from the image. To employ this method, brightness values were examined in an area of shadow or for a very dark object (such as a large clear lake) and the minimum value was determined. The minimum DN value was selected as the darkest DN with at least a thousand pixels for the entire image (Song et al, 2001). The correction is applied by subtracting the minimum observed value, determined for each specific band, from all pixel values in each respective band.

Since scattering is wavelength dependent the minimum values will vary from band to band, therefore each band must be evaluated independently.

4.1.1.2 Scene-to-scene normalization/ Invariant Object Method / Pseudo Invariant Feature (PIF)

Assuming that there are some pixels in a scene whose reflectance are quite stable through time. A linear relationship based on the reflectance of these “invariant objects” can be used to normalize imagery acquired at different times. This method is example to relative atmospheric corrections. If there are simultaneous ground reflectance measurements available or some assumptions about surfaces can be made, it can be an absolute correction procedure such as empirical line correction in Figure 4.1 (Liang 2001, 2004).

N “invariant” pixels can be identified from all M imagery occurred at different times. If we can select a clear image, J, as the reference, all other images can be normalized to image J using a linear regression based on these N pixels (Liang 2001, 2004).

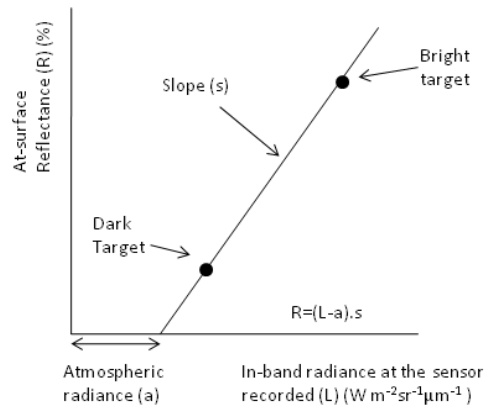


Figure 4.1 : Scene-to-scene normalization

Equation 4.6 was used to calculate the linear relationship between reflectance and radiance values of the images.

$$L_{jk} = a_{ik} + b_{ik} \cdot L_{ik} \quad (4.6)$$

Where

- L_{jk} = Reflectance of reference imagery J
- L_{ik} = Radiance of any other images
- k = Band
- a and b = Two coefficients are used for normalizing all other pixels of band k for each image i

Ideally, we need to identify “invariant” pixels with variable brightness from dark to bright in each band.

4.1.1.3 FLAASH

FLAASH is a MODTRAN4-based atmospheric correction software package developed by the Air Force Phillips Laboratory, Hanscom AFB and Spectral Sciences, Inc (SSI) (Adler- Golden et al., 1999). It provides accurate, physics-based derivation of apparent surface reflectance through derivation of atmospheric properties such as surface albedo, surface altitude, water vapor column, aerosol and cloud optical depths, surface and atmospheric temperatures from data.

FLAASH offers the additional option of correcting for light scattered from adjacent pixels. Spatially averaged reflectance is used to account for the “adjacency effect”

radiance contributions that, because of atmospheric scattering, originate from parts of the surface not in the direct line of sight of the sensor (Adler- Golden et al, 1999). Schematic process flow for FLAASH showing basic steps involved in radiance to reflectance conversion is given in Figure 4.2, adopted from Griffin and Hsiao-hua, (2003). FLAASH provides additional flexibility when compared to the other two atmospheric correction programs in that it allows custom radiative transfer calculations for a wider range of conditions including off-nadir viewing and all MODTRAN standard aerosol models.

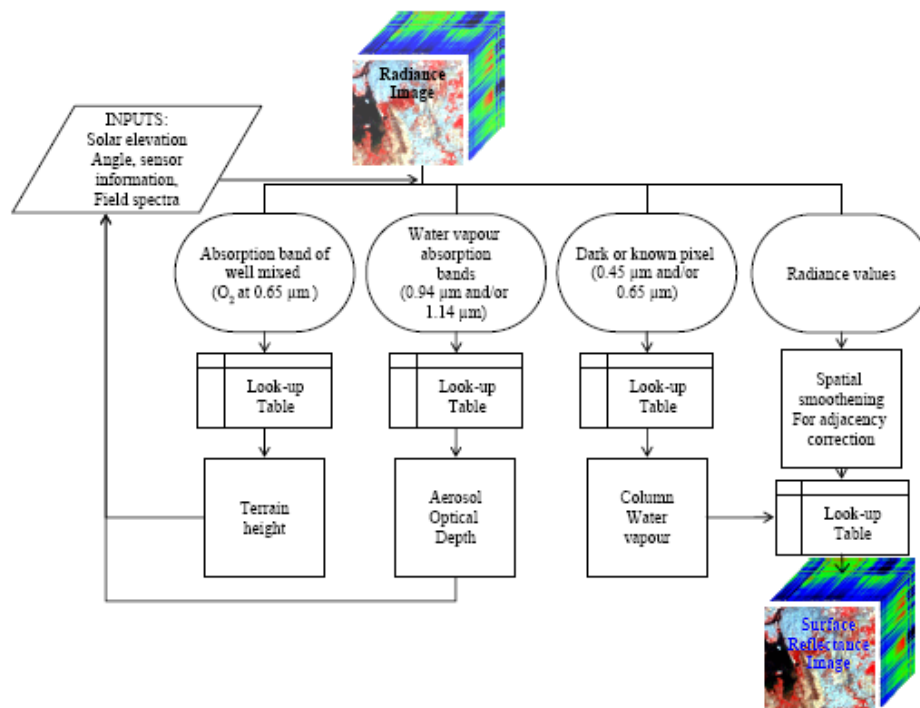


Figure 4.2 : Basic processing flow used in FLAASH (Griffin and Hsiao-hua, 2003).

4.1.2 Geometric Correction

There are both systematic and non-systematic geometric errors in remotely sensed imagery. The rotation of the earth during the image acquisition, the curvature of the earth, variations of the platform altitude, attitude and velocity, the finite scan rate of some sensors, the wide IFOV of some sensors and panoramic effects related to the imaging geometry are potential reasons of these geometric errors. The detailed information about the effects is given by (Richards and Jia, 2006).

Systematic distortions can be corrected by using mathematical formulas during preprocessing and non systematic errors can be only corrected statistically by using the Ground Control Points (GCPs). The most widely used geometric correction

process involves selecting and identifying GCPs on a satellite image with their corresponding geographic coordinate system to derive the geometric relation between the two by determining a mathematical transformation for the correction of image geometry. Empirical geometric correction models are based on the positional relationship between points on a satellite image and points on a reference system such as geometrically corrected satellite image, topographic maps, GPS coordinates (Turker and Gacemer, 2004) (Figure 4.3). This positional relationship can be used to correct image geometry without knowledge of the source and type of the distortion. These models include conventional polynomials, affine and the rational function model (RFM) (Jensen, 1996). Geometric registration error between two images is expressed in terms of an acceptable total Root Mean Square Error (RMSE), which represents a measure of deviation of corrected GCP coordinate values from the original reference GCPs used to develop the correction model. Robust and unbiased estimates of RMSE should be calculated using independent GCPs not used in model formation (Kardoulas et al., 1996).

Several authors recommend a maximum tolerable RMSE value of < 0.5 pixels (Jensen, 1996), but others have identified acceptable RMSE values ranging from 0.2 pixels to, 0.1 pixels, depending on the type of change being investigated (Townshend et al., 1992).

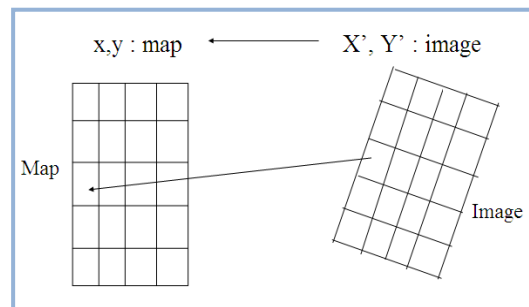


Figure 4.3 : Transforming coordinates from one system (map) to another one (image)

In this research, 1st order transformation (also referred to as an affine transformation) was used to geometrically correct the images. The affine transformation can be expressed by the following equation 4.7 and 4.8.

$$X_i' = a_0 + a_1x_i + a_2y_i \quad (4.7)$$

$$Y_i' = b_0 + b_1x_i + b_2y_i \quad (4.8)$$

In these equations X_i' , Y_i' and x_i , y_i refer the coordinates of point i in the original image and reference coordinate system, respectively. a_0 and b_0 are the translations and a_1 and b_1 , a_2 and b_2 are both the rotation and scaling of x and y directions, respectively.

The selection of GCPs is very important for geometric correction. If the GCPs can be selected correctly, the derived geometric relation between the images and the geographic coordinate system will be of high quality. Different images will then be projected onto the same geographic coordinate system and thematic analysis of multi-temporal data series such that spatial and temporal changes in surface properties can be detected and analyzed (Song et al., 2001). Accurate per-pixel registration of multi-temporal remote sensing data is essential for change detection since the potential exists for registration errors to be interpreted as land-cover and land-use change, leading to an overestimation of actual change (Stow, 1999).

4.1.3 Hyperion EO-1 Hyperspectral Data Pre-processing

Since Hyperion operates from a space platform with consequently modest surface signal levels and full-column atmospheric effects, its data demand careful processing to manage sensor and processing noise (Datt, et al, 2003). Hyperion L 1 radiometric data processing chain included band selection (Datt, et al, 2003), correction for bad lines (Han, et al., 2002), striping pixels (Datt, et al, 2003) and smile (Goodenough, et al, 2003), a pixel-based atmospheric correction using FLAASH and a geometric correction. A MMTG-A (Mapping Technologies group) extensions that embedded in ENVI software (Cudachy et al., 2001) was used for pre-processing of Hyperion EO-1 data. A brief explanation of these is provided as follow.

4.1.3.1 Band Selection

There are 242 unique spectral channels collected by Hyperion resulting in a complete spectrum covering the 357-2576 nm region. The level 1 radiometric product has a total of 242 bands but only 198 bands are calibrated (band 8 to 57 for VNIR and 77 to 224 in SWIR region) (Pearlman, at al, 2003; Datt et al., 2003) because of an overlap between VNIR and SWIR focal planes are only 196 unique channels (Table 4.3). The bands that are not calibrated are set to zero.

Table 4.3: Hyperion EO-1 bands.

	Hyperion bands (from-to)	Average wavelength interval (nm)	Calibration type	Spectrum region	Reason
1	B1-B8	355.59-426.82	Non		Low SNR
2	B9-B57	436.99-925.41	Calibrated	VNIR	
3	B58-B77	935.58-902.36	Non	VNIR	Overlap
4	B78-B225	912.45-2405.6	Calibrated	SWIR	
5	B226-B242	2415.7-2577.08	non		Low SNR
Σ	196		SNR=Signal	Noise Ratio	

Atmospheric water vapor bands which absorb almost the entire incident and reflected solar radiation and the bands that have very severe vertical stripping are usually identified by visual inspection of the image data or atmospheric modeling were excluded from the hyperspectral data.

4.1.3.2 Bad Band Selection

Hyperion has pushbroom scanner instrument, in that a detector cell may differently respond compared to other cells in the detector. This differently behaving cell is termed as a bad pixel. In other words, this can be described as differences between the DN values of pixels along the line. To solve this problem interpolation or extrapolation methods are used.

A pixel is known as ‘bad’ if it is completely different from the entire detector array row based on mean or standard deviation calculations (Mason, 2002). After visual testing with different window sizes a standard deviation window to replace the values of bad cells with ones interpolated from, neighboring good cells was applied to data for correcting bad bands.

4.1.3.3 Bad Line Detection and Correction

A pushbroom sensor instrument also has calibration differences in the detector arrays that cause vertical stripes in the image. The first 12 bands and many SWIR bands of Hyperion are influenced by striping. The differences between gain and offset are the main reason for this vertical striping problem and to solve this full linear correction was attempted to try to adjust the difference through the entire detector cell statistics. This bad lines and stripes were balanced by Mapping Technologies group- A (MMTG-A) extensions that embedded in ENVI software (Cudachy et al., 2001).

4.1.3.4 Minimum Noise Fraction (MNF)

The Minimum Noise Fraction (MNF) transform (Green *et al*, 1988) is an algorithm consisting of two consecutive data reduction operations. The first operation is based on an estimation of noise in the data as represented by a correlation matrix. This transformation decorrelates and rescales the noise in the data, by variance. The second operation accounts for the original correlations, and creates a set of components that contain weighted information about the variance across all bands in the raw data set. The algorithm retains specific channel information because all original bands contribute to each of the components' weighting. Often, most of the surface reflectance variation in a data set can be explained in the first few components, with the rest of the components containing variance as contributed primarily by noise. Weighting values for each component can also be examined, pointing to the raw bands that are contributing most to the information contained in the dominant components. The dominant components are then used to transform the data back to its original spectral space, resulting in the same number of transformed channels as the original data provided.

4.1.4 Classification

Classification is the process of grouping pixels of images into patterns of varying gray tones or assigned colors that have similar spectral values to transfer data into information for determining earth resources. Multispectral image classification is one of the most often used methods for information extraction. There are many classification methods to produce land cover/use map or to determine change detection. Before classification, the optimum bands were selected for reliable and accurate results.

4.1.4.1 Selection of Appropriate Band Combinations

In remote sensing, usage of best band combinations of multispectral data helps to derive reliable and accurate information to many studies. In general, correlation matrix of satellite bands is used to decide selection of appropriate band combinations.

Optimum Index Factor (OIF) is an index that can be used to determine which combination of bands for an image contains the most information to produce the best

composite (Chavez et al, 1984). OIF was computed by dividing the sum of the variances of the three bands by the sum of the correlation coefficients of the three bands. The best three band combination is the one with the highest OIF because this combination has the highest variance (and do the most information) and the least correction among bands (and so the least redundancy). The OIF index applied to 2003 and 2007 dated SPOT 4 and SPOT 5 images to find out the best band combinations for the study. Equation 4.9 was used for the selection of the appropriate bands.

$$OIF = \frac{\sum_{i=1}^3 \delta_i}{\sum_{i=1}^3 \sum_{j=i+1}^3 |r_{ij}|} \quad (4.9)$$

Where

δ_i = Standart deviation of the band i

r_{ij} = Correlation between the band i and j

4.1.4.2 Spectral Separability Analysis

Signature separability is a statistical measure of distance between two signatures. Separability can be calculated for any combination of bands that is used in the classification, enabling the user to rule out bands that are not useful in the results of the classification. Many methods have been developed for separability analysis such as Euclidean distance (ED), divergence, transformed divergence (TD) and Jefferies-Matusita (JM) distance. TD method is more effective than the other methods (Jensen, 1996). In this study, transformed divergence method used based on covariance and mean values of spectral bands.

Transformed divergence (TD_{ij}) can be calculated using the following formulas 4.10 and 4.11.

$$D_{ij} = \frac{1}{2} \text{tr}\{(C_i - C_j)(C_i^{-1} - C_j^{-1})\} + \frac{1}{2} \text{tr}\{(C_i^{-1} - C_j^{-1})(\mu_i - \mu_j)(\mu_i - \mu_j)^T\} \quad (4.10)$$

$$TD_{ij} = 2000 \left\{ 1 - \exp\left(-\frac{D_{ij}}{8}\right) \right\} \quad (4.11)$$

Where

- i and j = the two signatures (classes) being compared
- C_i and C_j = covariance matrix for i and j classes
- tr = trace function

D_{ij} = divergence
 μ_i and μ_j = mean vector for i and j classes

The TD gives an exponentially decreasing weight to increasing distances between the classes (Jensen, 1996). The scale of the divergence values can range from 0 to 2,000.

4.1.4.3 Unsupervised Classification

Spectral classes, which are groups of pixels that are uniform (or near-similar) with respect to their brightness values in the different spectral channels of the data, are grouped based on the numerical information in the data. Natural groupings or structures in the data are determined using clustering algorithms (Schowengerdt, 1997).

Iterative Self- Organizing Data Analysis (ISODATA) is the most commonly used unsupervised technique and also used in this research with the other classification methods.

In the first step, pixels are grouped into the number of clusters that user defined previously. These groups are called spectral classes. Classified groups are then labeled with user expertise, if the result classes are satisfactory then result classified image is used for further analysis. If the result classes are not satisfactory then numbers of clusters or some other statistical parameters such as separation distance, covariance values are changed and classification is conducted again until satisfactory result is achieved.

4.1.4.4 Supervised Classification

In supervised classification, spectrally similar areas on an image are identified by creating 'training' sites of known targets and then extrapolating those spectral signatures to other areas of unknown targets (Schowengerdt, 1997). Training sites in the image that are homogeneous representative samples of the different surface cover types in the study area.

It relies on the a priori knowledge of the location and identity of land cover types that are in the image. These are called information classes. Familiarity with the geographical area, topographic maps and some other ancillary data are required to select appropriate training areas.

The computer is trained using the numerical information in all spectral bands for the pixels comprising training areas to recognize spectrally similar areas for each class.

As a supervised classification Maximum Likelihood (ML) classifier is selected in this study. The ML classifier assumes that the statistics for each class in each band are normally distributed and calculates the probability that a given pixel belongs to a specific class. Unless a probability threshold is selected, all pixels are classified. Each pixel is assigned to the class that has the highest probability. If the highest probability is smaller than a threshold, the pixel remains unclassified.

4.1.4.5 Hybrid Classification

Hybrid classification is the use of both supervised and unsupervised techniques to classify an image. Hybrid method combines the benefits of both techniques. Supervised and unsupervised methods, when taken singularly, have their drawbacks. There have been many hybrid classification methods (Schowengerdt, 1997). In this study a hybrid classification method for remote sensing data was used, incorporating both a unsupervised and supervised classification methods with principal component analysis, to increase the mapping accuracy compared to methods using either a supervised or unsupervised method.

4.1.4.6 Spectral Angle Mapper (SAM) classification

The Spectral Angle Mapper (SAM) is a physically based hyperspectral classification technique by determining the spectral similarity between an endmember spectrum and a pixel spectrum in an n dimensional space, by calculating the angle between the spectra. Smaller angles indicate closer matches to the reference spectrum. Pixels further away than the specified maximum angle threshold in radians are not classified (Kruse et al., 2003). Since this method uses only the direction of a vector and not its length, it is insensitive to illumination and albedo. The spectral angle can be calculated by equation (4.12)

$$\alpha = \cos^{-1} \left[\frac{\sum_{i=1}^n t_i r_i}{\sqrt{\sum_{i=1}^n t_i^2} * \sqrt{\sum_{i=1}^n r_i^2}} \right] \quad (4.12)$$

where

n = number of bands

t_i = test spectrum
 r_i = reference spectrum
 α = spectral angle

In general, pixels belonging to the same class have small spectral angle, and spectral angles of pixels of different types are large. In this study, endmember spectra of each land cover types at different bands were extracted directly from the Hyperion image and ASD field spectra measurements.

The result of SAM is an angular difference measured in radian ranging from zero to $\Pi/2$ which gives a qualitative estimate of similarity between image spectrum and ASD spectrum. Small spectral angle values correspond to high similarity between image spectra and ASD spectra. Larger angle values correspond to less similarity.

4.1.4.7 The Coordination of Information on the Environment (CORINE) Land Cover Data Set

The Coordination of Information on the Environment (CORINE) Program was established by the European Commission to create a harmonized Geographical Information System on the state of the environment in the European Community (Moos and Wyatt 1994).

The CORINE land cover nomenclature/classification was designed to include the diverse land cover of the European Union (EU) countries (URL-5). The legend of the CORINE land cover is standard for the whole of Europe, which as a result is quite extensive with 44 classes of Corine Land Cover describing land cover (and partly land use) according to anomenclature of 44 classes organized hierarchically in three levels (Table 4.4) (Willems et al, 2000; Gulinck et al, 2001; Han et al, 2004; European Environment Agency 2005; Yilmaz, 2009).

The first level (five classes) corresponds to the main categories of the land cover/land use (artificial areas, agricultural land, forests and seminatural areas, wetlands, water surfaces). The second level (15 classes) covers physical and physiognomic entities at a higher level of detail (urban zones, forests, lakes, etc); finally level 3 is composed of 44 classes (Willems et al. 2000).

Standards specified by European Union's CORINE Program were used during the classification of land uses. Within the framework of European Union's CORINE

Program, member countries take advantage of satellite images and make use of numerical land use/land cover standards to prepare maps. CORINE Program aims to compare environmental data obtained from member countries. In order to reach a standard in applications and research studies related to environment, common methodology has been applied while collecting relevant basic data on land use and land cover standards. This methodology developed by the Joint Research Center.

Table 4.4 : The CORINE land cover nomenclature.

Class 1	Class 2	Class 3
Artificial Surfaces	Urban fabric	Continuous urban fabric
		Discontinuous urban fabric
	Industrial, commercial, and transport units	Industrial or commercial units
		Road and rail networks and associated land
		Port areas
		Airports
	Mine, dump and construction sites	Mineral extraction sites
		Dump sites
	Artificial, nonagricultural vegetated areas	Construction sites
		Green urban areas
Agricultural areas	Arable land	Sport and leisure facilities
		Nonirrigated arable land
		Permanently irrigated land
	Permanent crops	Rice fields
		Vineyards
		Fruit trees and berry plantations
		Olive groves
	Pastures Heterogeneous agricultural areas	Pastures
		Annual crops associated with permanent crops
		Complex cultivation patterns
Forest and semi-natural areas	Forests	Land principally occupied by agriculture, with significant areas of natural vegetation
		Agro-forestry areas
		Broad-leaved forest
		Coniferous forests
		Mixed forests

Table 4.4 (contd.): The CORINE land cover nomenclature.

	Scrub and/or herbaceous vegetation associations	Natural grasslands Sclerophyllous vegetation Transitional woodland-scrub
	Open spaces with little or no vegetation	Sclerophyllous vegetation Transitional woodland-scrub Transitional woodland-scrub Burnt Areas Glaciers and perpetual snow
Wetlands	Inland wetlands	Inland marshes Peat bogs
	Maritime wetlands	Salt marshes Salines Intertidal flats
Water Bodies	Inland Waters	Water courses Water bodies
	Maritime waters	Coastal lagoons Estuaries Sea and ocean

4.1.4.8 Accuracy Assessment

Classification accuracy has been a focus of attention for a considerable period of time and is a topic that has developed considerably in recent years (Congalton 1991, Congalton and Green 1999, Foody 2002). Classification accuracy is the main measure of the quality of thematic maps produced and required by users, typically to help evaluate the fitness of a map for a particular purpose (Foody, 2008). Although seemingly it is a simple concept, classification accuracy is a very difficult variable to assess and is associated with many problems (Foody 2002).

The most widely used approaches for image classification accuracy assessment are site-specific methods based on the analysis of the entries in a confusion or error matrix (Congalton and Green 1999, Foody 2002). In principal, this matrix provides a simple summary of classification accuracy and highlights the two types of thematic error that may occur, omission and commission. This not only summarizes the accuracy of the classification but also may convey useful information to enhance analyses based on the classification (e.g. Prisley and Smith 1987, Fang et al. 2006).

In this research, to assess the accuracy of classification, the confusion matrix and some common measures derived from this matrix namely, overall accuracy, user's accuracy, producer's accuracy and Kappa coefficient are used. The confusion matrix is a simple cross-tabulation of the mapped class label against that observed in the ground or reference data for a sample of cases at specified locations.

The design of confusion matrix is presented in Figure 4.4. The bold elements represent the main diagonal of the matrix that contains the cases where the class labels depicted in the image classification and ground data set agree, whereas the offdiagonal elements contain those cases where there is a disagreement in the labels (Figure 4.4). In the following figure 1,2, and 3 represent the classes of water, forest, and urban, respectively. The number of classes, q, is 3 in this example. Equations 4.13 and 4.14 used for overall accuracy assessment and Kappa statistic calculations.

		Actual Class			Σ
		1	2	3	
Predicted Class	1	n_{11}	n_{12}	n_{13}	n_{1+}
	2	n_{21}	n_{22}	n_{23}	n_{2+}
	3	n_{31}	n_{32}	n_{33}	n_{3+}
Σ	n_{+1}	n_{+2}	n_{+3}	n	

Figure 4.4 : The confusion matrix and some common measures of classification accuracy that may be derived from it (Foody, 2002).

$$\text{Percentage correct} = \frac{\sum_{k=1}^q n_{kk}}{n} * 100 \quad (4.13)$$

$$\text{User's accuracy} = \frac{n_{ii}}{n_{i+}}$$

$$\text{Producer's accuracy} = \frac{n_{ii}}{n_{+i}}$$

$$\text{Kappa Coefficient} = K = \frac{n \sum_{i=1}^q n_{kk} - \sum_{i=1}^q n_{k+} n_{k+i}}{n^2 - \sum_{i=1}^q n_{k+} n_{+k}} \dots \quad (4.14)$$

where;

- q = number of classes in error matrix
- n = total number of observations in error matrix

- n_{ii} = major diagonal element for class i
- n_{i+} = total number of observations in row for class i (right margin)
- n_{+i} = total number of observations in column for class i (bottom margin)

4.2 Land Cover Change Detection

Change detection is the process of identifying differences in the state of an object or phenomenon by observing it at different times (Singh 1989). Land cover change itself represents one of the most pervasive forms of ecosystem alteration and is linked commonly to other forms of environmental degradation including erosion, habitat and biodiversity loss, biogeochemical cycle alteration, ground water depletion, and invasive species (Lambin and Strahler 1994, Flores and Yool, 2007). Change detection of land cover and land use (LCLU) is a fundamental input for monitoring, planning, management and environmental studies, such as landscape dynamics, urbanization, natural hazards, manmade risks and environmental impacts (European Commission 1998; Serra et al, 2003; Dogru et al, 2006; Balik Sanli et al, 2007; Dogru et al, 2008). For monitoring and determining the types and extent of environmental changes of large areas, change detection techniques can be applied widely with a multitemporal satellite image acquisition as a cost effective and rapid approach (Munyati 2000; Yuanbo et al. 2004; Yuan et al. 2005; Bektas and Goksel 2005).

In a remote sensing context, the goal of change detection is to compare the differences in the spatial representation of reflectance values of two points in time, while controlling the variances caused by differences in external variables (Du et al, 2002). These variables might include atmospheric conditions, illumination and viewing angles, and soil moisture (Schowengerdt 1997). Because of this reason, remotely sensed data require rigorous preprocessing such as geometric, radiometric and atmospheric correction before they used in change detection. This ensures that reflectance changes detected derive from actual changes in the land cover conditions.

Various change detection algorithms such as image differencing, image rationing, vegetation indices, principle components analysis, or “from-to” (Singh 1989; Kwarteng and Chavez 1998; Mas 1999; Fung and Siu 2000; Masek et al. 2000; Jensen 2004; Coppin, 2004; Guild et al. 2004; Yuan et al. 2005) change vector analysis are applied to determine the change or no change maps (Chen et al, 2003).

Any change detection technique possesses its own set of advantages and disadvantages, and no single approach can be considered optimal or applicable in all cases. Among the many factors governing selection of a change detection strategy are information requirements, spectral coverage, data availability and quality, image processing resources, analyst skill and experience, phenomenological knowledge, time and cost constraints, and the importance of labeling the changes that are detected. However, change detection capabilities are intrinsically limited by the spatial resolution of the digital imagery in environmental applications. The application of multi-sensor data provides the potential to detect accurately land-cover changes through integration of different features of sensor data.

4.2.1 Principal Component Analysis Based Change Detection

Principal component analysis is a statistical technique that rotates the axes of a multidimensional image space in the direction of maximum variance. The components or axes generated by this rotation are simple linear combinations of the original image data, are orthogonal to each other and, thus, have no mathematical relation. Eigenvectors are used as multiplication coefficients or loadings in PCA for each pair of input bands or images. The linear transformation can reduce data redundancy between bands and emphasize different information in the derived components (Jackson, 1983). The main difference of this approach with similar techniques is that it not only removes the correlation (redundancy) between bands, but it effectively reduces the number of bands within an image without losing or changing overall information content. Assumes that multitemporal data are highly correlated and change information can be highlighted in the new components.

Two ways to apply PCA for change detection are: (1) put two or more dates of images into a single file, then perform PCA and analyse the minor component images for change information; and (2) perform PCA separately, then subtract the second-date PC image from the corresponding PC image of the first date.

PCA is widely used in many areas, e.g., signal processing, computer graphics, statistics, colorimetry, and neural computing. In remote sensing, it is mainly applied to the classification and interpretation of satellite images by using spectral data associated with different targets, including land-cover change (Kwarteng and Chavez, 1998), urban expansion (Li and Yeh, 1998), tropical forest conversion (Jha

and Unni, 1994), forest mortality (Collins and Woodcock, 1996) and forest defoliation (Muchoney and Haack, 1994). The method of combining PCA and classification methods has been commonly use to detect temporal changes and shown satisfying results in practice (Fung and LeDrew, 1987; Jensen, 1996; Munyati, 2004; Deng et al, 2008).

4.2.2 Change Vector Analysis

Change vector analysis (CVA) is a radiometric technique, the primary utility of which is the detection of all changes present in the input multispectral data (Malila, 1980). It is also flexible enough to be effective when using diverse types of sensor data and radiometric change approaches, and it is capable of incorporating categorical information as well.

CVA has been found to be useful under circumstances encountered in a variety of change detection applications. In particular, CVA has proven to be a valuable tool when project requirements either explicitly call for capturing and distinguishing among all changes, or when doing so is a prerequisite to further analysis of changes of interest. The potential advantages of CVA over some other methods include:

- Capability to concurrently process and analyze change in all multispectral input data layers (as opposed to selected bands);
- Avoidance of compounding of spatial-spectral errors often inherent in multi-date classifications;
- The capability to detect changes both in land cover and condition;
- Computation and separation of multidimensional change vector components, and composition of change images that retain this information and facilitate change interpretation and labeling (Johnson and Kasischke, 1998).

CVA was first used to characterize magnitude and direction variations of a vector in an n-dimensional spectral space defined by the axes of bands, transforms, or spectral features from a multi-temporal dataset (Malila 1980). The change vector is defined by the position of a given pixel in Time 1 (T1) and Time 2 (T2) whenever a change occurs in its spectral response as described in equation 4.15 (Lambin and Strahler 1994).

$$c_i = P(i, T_2) - P(i, T_1) \quad (4.15)$$

where c_i is the change vector of pixel i and p is the position of pixel i in T_2 and T_1 . This vector is distinguished by a measurable magnitude, characterizing the intensity of change, and a direction, characterizing the nature of such a change in the spectral space. Vector magnitude is measured as the Euclidean distance between T_1 and T_2 in the spectral space.

$$M(i, T_2 - T_1) = \sqrt{[P_x(i, T_2) - P_x(i, T_1)]^2 + [P_y(i, T_2) - P_y(i, T_1)]^2} \quad (4.16)$$

Where $M(i, T_2 - T_1)$ is the vector magnitude of pixel i from T_2 to T_1 and $P_x(i, T_2) - P_x(i, T_1)$ is the difference in the position of pixel i in the spectral axis x from T_2 to T_1 . Vector direction is measured either through simple logic relationships or angular units according to the vector's variations in the spectral space.

Vector directions are commonly calculated using trigonometric functions as expressed in equation 4.17 for a vector direction in a bi-dimensional spectral space.

$$D(i, T_2 - T_1) = \text{Sin}\{[P_y(i, T_2) - P_y(i, T_1)]/[P_x(i, T_2) - P_x(i, T_1)]\} \quad (4.17)$$

where $D(i, T_2 - T_1)$ is the vector direction of pixel i from T_2 to T_1 . This separation of change into two components constitutes a particular strength of this approach because it can be used when different change types vary in intensity across the landscape (Warner 2005; Flores and Yool, 2007).

Discrepancies between vector direction and magnitude measurement scales have motivated development of approaches that assess the full dimensionality of vector change. Vector direction, for example, is measured through logic relationships between input images in T_1 and T_2 (Michalek et al. 1993). This approach assigns each pixel a categorical value according to its positive or negative vector shift in time (figure 4.5(a)). Another approach by Malila (1980) measures the direction angle of vector change. This protocol groups angular measures according to sectors, assuming each sector code corresponds to a different type of change (figure 4.5(b)). In both cases, code assignation and differentiation of change occurrence is usually established using arbitrary thresholds (Flores and Yool, 2007)

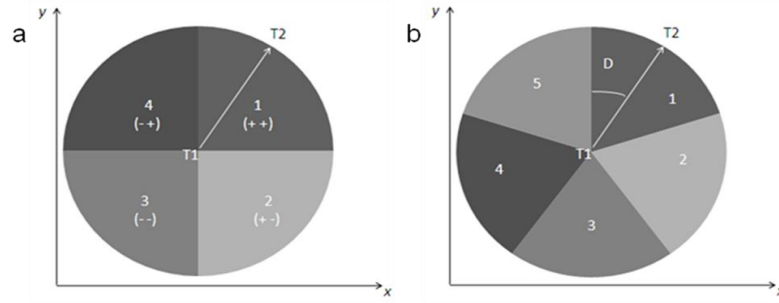


Figure 4.5 : Change vector directions represented by (a) shift sector coding and (b) angle grouping

In this study, CVA was applied to temporal SPOT data set by using Tasseled Cap Transformation (TCT) in order to determine the magnitude and direction of the changes in the Terkos Water Basin. Vector magnitude (M), the first CVA component of the model was calculated as the 3-dimensional Euclidean distance between a pixel position in the brightness (x), greenness (y) and wetness (z) axes for Time 1 (x_1, y_1, z_1) and Time 2 (x_2, y_2, z_2) according to equation (4.18)

$$M = \sqrt{(x_2 - x_1)^2 + (y_2 - y_1)^2 + (z_2 - z_1)^2} \quad (4.18)$$

Where x_1 and x_2 , y_1 and y_2 , and z_1 and z_2 correspond to brightness, greenness, and wetness from 2003 (Time 1) and 2007 (Time 2), respectively.

Vector directions were calculated in polar coordinates as longitude and colatitudes measures. The longitude angle ϕ , measured from the x axis (brightness) to the y axis (greenness) along the xy plane, was calculated using equation (4.19) (Figure 4.6).

$$\Phi = \arctan [(y_2 - y_1) / (x_2 - x_1)] \quad (4.19)$$

The colatitudes angle θ , measured from z axis (wetness) to the y axis (greenness) along the zy plane, was calculated using equation (4.20) (Figure 4.6).

$$\theta = \arctan [(z_2 - z_1) / (y_2 - y_1)] \quad (4.20)$$

Last colatitudes angle in this study is ρ , which correspond to the angle measured from the z axis (wetness) to the x axis (brightness) along the zx plane. This angle was calculated using the equation (4.21) (Figure 4.6)

$$\rho = \arctan [(z_2 - z_1) / (x_2 - x_1)] \quad (4.21)$$

The arctangent function produced results in radians; therefore, polar coordinates were transformed into degrees and then adjusted to a single hemisphere. For this adjustment, 180 were added to longitude coordinates ($\phi+180$), and each colatitudes

coordinate was subtracted from 180 ($180 - \theta$ and $180 - \rho$). The resultant vector for a given pixel changing from 2003 to 2007 is thus a vector described by magnitude and direction.

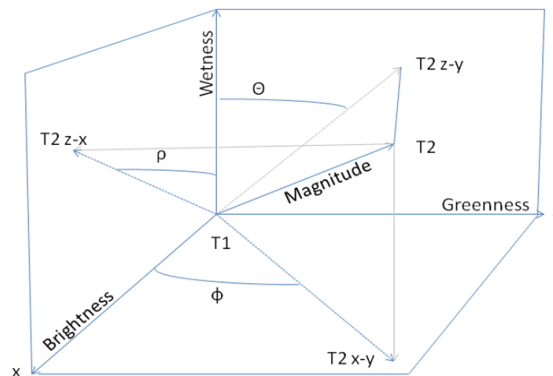


Figure 4.6 : Geometric representation of a change vector and its corresponding polar coordinates along the planes formed by the three Tasseled Cap Transforms: brightness (x), greenness (y), and wetness (z).

In Figure 4.6, vector magnitude (M) is presented by the change in position of a pixel in Time1 (T1) and Time2 (T2). Longitude Vector Direction (ϕ) is the angle between the x-axis and the projection of the vector T1-T2 in the x-y plane. Colatitude Vector Direction (θ) is the angle between the z axis and the projection of the vector T1-T2 in the z-y plane and Colatitude Vector Direction (ρ) is the angle between the z axis and the projection of the vector T1-T2 in the z-x plane.

4.2.2.1 Tasseled Cap Transformation

The Tasseled Cap Transform (TCT) is a vegetative index commonly used as an indicator of vegetation health and assessing vegetation and land cover change. The TCT presents several advantages for use in change detection and has been shown to perform well for various types of environments. It is a scene independent transformation, which means that it can be applied to any scene across dates to extract physical characteristics in a consistent and interpretable way. The three resulting features (Brightness, Greenness and Wetness) are able to relate spectral components to soil reflectance, green vegetation, and soil moisture characteristics (Crist and Kauth 1986). Brightness is defined as the weighted sum of all bands, aligned in the direction of the principal variation in soil reflectance. Greenness, orthogonal to brightness, represents the contrast between the near-infrared and visible bands, which relate strongly to the amount of green vegetation in the scene (Crist and Kauth 1986). Wetness, orthogonal to brightness and greenness, relates to

canopy and soil moisture (Lillesand and Kiefer 1987). Cohen and Fiorella (1998) demonstrated that incorporating the wetness in addition to greenness and brightness transforms, improved detection accuracy in CVA.

The Tasseled Cap transformation was therefore selected as the enhancement technique to be used for this study. The TCT requires coefficients for brightness, greenness and wetness components and these coefficients are specific to each sensor. In this study, the coefficients for components were derived by using Gram Schmidt Orthogonalization technique for SPOT data set.

4.2.2.2 Gram Schmidt Orthogonalization Technique and TCT parameters Extraction

Gram Schmidt Orthogonalization is a mathematical tool that performs a rotational transformation in n-dimensional space, resulting in a series of orthogonal axes, each of which is a linear combination of the original axes. It is a linear transform and is sometimes called Gram Schmidt Transform (GST).

The orthogonalization technique was applied to SPOT 5 data to derived TCT parameters are named Brightness, Greenness, and Wetness and detailed information given in title 4.2.2.1.

Image preprocessing steps were applied to SPOT 5 data and DN values converted to at satellite reflectance values. The image was classified in order to obtain small and homogenous clusters of pixels. Samples of bare soil, green vegetation and water objects were selected to guide the Tasseled Cap Brightness, Greenness and Wetness transformation, respectively. The samples were considered representative as being well distributed along the image. Equations from 4.22 to 4.36 used for calculations of components.

To obtain brightness, two sets of soil classes considerably differing in reflectance values were selected: bright soils (X_{bs}) and dark soils (X_{ds}). The mean of the bright and dark soil values were differenced for each of the image bands (n) to acquire the image points b_i :

$$b_i = (\overline{X_{bs}} - \overline{X_{ds}})_i \quad (4.22)$$

The Brightness coefficients (BRC_i) were calculated by dividing each of vector components (b_1, b_2, \dots, b_n) by the normalization factor B, where:

$$B = \sqrt{(\sum_{i=1}^n b_i^2)} \quad (4.23)$$

n= number of image bands, and

$$BRC_i = \frac{b_i}{B} \quad (4.24)$$

The Brightness image (BRI) was then extracted by the linear transformation of the SPOT 5 image bands with the BRC_i .

$$BRI = \sum_{i=1}^n BRC_i * X_i \quad (4.25)$$

For the Greenness component extraction, dense vegetation clusters were selected in the image and their mean values were calculated for each band. For this computed Normalized Difference Vegetation Index (NDVI) image was used as a base map to select pure vegetation samples by using equation 4.26 (Schowengerdt, 1997).

NDVI has been widely used to identify the vegetation based on spectral values. The ratio of near-infrared (NIR) and red bands is often applied to map vegetation and to verify its condition.

$$NDVI=(NIR-RED)/(NIR+RED) \quad (4.26)$$

Then, green vegetation and bright soil samples were differenced for each band of the data and Gram Schmidt Orthogonalization was applied by:

$$g_i = (\overline{X_g} - \overline{X_{bs}})_i - D_g * BRC_i \quad (4.27)$$

$$D_g = \sum_{i=1}^n (\overline{X_g} - \overline{X_{bs}})_i * BRC_i \quad (4.28)$$

In this the green vegetation vector (g_1, g_2, \dots, g_n) is orthogonal to the soil line vector (b_1, b_2, \dots, b_n). By applying normalization factor G the Greenness coefficients GRC_i were calculated for each band.

$$G = \sqrt{\sum_{i=1}^n g_i^2} \quad (4.29)$$

$$GRC_i = \frac{g_i}{G} \quad (4.30)$$

The Greenness image (GRI) was then extracted by linear transformation of the SPOT 5 image bands with the GRC_i :

$$GRI = \sum_{i=1}^n GRC_i * X_i \quad (4.31)$$

The last component Wetness image was extracted by following the same method described above, where the vector towards the wetness image point was orthogonalized to both Brightness and Greenness.

$$w_i = \overline{X_w} - \overline{X_{bs}} \quad (4.32)$$

$$B = \sqrt{(\sum_{i=1}^n b_i^2)} \quad (4.33)$$

$$g_i = (\overline{X_g} - \overline{X_{bs}})_i - D_g * BRC_i \quad (4.34)$$

$$D_g = \sum_{i=1}^n (\overline{X_g} - \overline{X_{bs}})_i * BRC_i \quad (4.35)$$

The extracted Brightness, Greenness and Wetness coefficients were tested against orthogonality by calculating the dot products of the coefficients.

For instance, for the Brightness and the Greenness coefficients for the equation (4.36) needed to be fulfilled.

$$\sum_{i=1}^n BRC_i * GRC_i = 0 \quad (4.36)$$

4.2.3 Semivariogram and spatial profile analysis

Semivariograms and spatial profile analysis tool can be use to investigate land cover and land use change. Quantity and direction of the spatial variations are related with the semivariogram parameters. These parameters such as the shape, range, nugget, and sill of the semivariograms were interpreted to determine the location of abrupt change areas (Woodcock et al, 1988; Curran, 1988; Atkinson and Lewis; 2000).

As a geostatistical tool, semivariogram measures the spatial variation in spatial data sets. It is a measure of the dissimilarity between observations separated by a distance h or lag. In Geostatistics, the digital number (DN) of a satellite image is considered to be a regionalized variable, characterized by both random and spatial correlation aspects. This variable is interpreted as a function $DN(x)$ that provides DN of a pixel x located by its geographic coordinates or by its row and column in the image. Both aspects can be jointly studied through the variogram function, which characterizes the spatial variability of the DN of a satellite image. The relation between any pair of pixels, h intervals apart (the lag distance), can be given by the average squared difference between all such pairs. As the per-pixel variance is half this value, the

semivariance (h) for pixels at distance h apart is defined as (Curran and Atkinson, 1998; Woodcock et al, 1988). Calculation of semivariance is given in equation 4.37.

$$\gamma(h) = \frac{1}{2} E[Z(x) - Z(x+h)]^2 \quad (4.37)$$

$Z(x)$ and $Z(x+h)$ are the random functions describing the property of interest Z at places separated h and E is the mathematical expectation operator.

The experimental semivariogram, obtained from real data, can be estimated along the transect where $P(h)$ pairs of observations separated by the same lag h . Their average semivariance at lag h is given by

$$\gamma_s(h) = \frac{1}{2P(h)} \sum_{i=1}^{P(h)} [Z(x) - Z(x+h)]^2 \quad (4.38)$$

The quantity $\gamma_s(h)$ is an estimate of the semivariance $\gamma(h)$ and is a useful measure of dissimilarity between spatially separate pixels and spatial patterns can be described using experimental semivariograms as the larger the semivariance, the less similar are the pixels.

After obtaining experimental semivariograms, it is necessary to fit a continuous and authorized mathematical model such as the linear, spherical, exponential or Gaussian. Lag, sill, range and nugget are terms used to describe these fitted models (Figure 4.7)

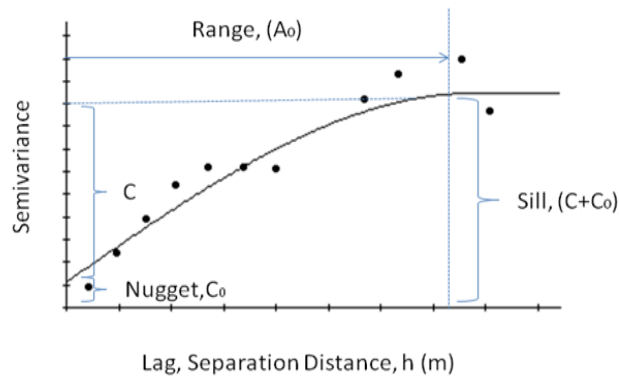


Figure 4.7 : A semivariogram

where,

Lag, h Separation distance between sampling pairs

Sill, $(C+C_0)$ The value where the semivariogram flattens off, maximum level of (h)

Range, A_0 Point on the h axis where the semivariogram reaches the sill

Nugget, C_0 Point where (h) intercepts the ordinate

The X-axis of a semivariogram shows the scale of variation; the Y-axis of a semivariogram shows the amount of variation and the shape of a semivariogram shows both. Nugget is an estimate of variance at distance (lag=0), therefore can be interpreted as a measure of variability inside the pixel cell, and is also a measure of systematic noise (Curran and Dungan, 1989). The sill indicates the amount of variability with distance, the range can be used as a measure of spatial dependency, and it is an estimate of the distance at which maximum variability (sill) is reached.

4.3 Field Spectroscopy

Field spectrometry, which was first developed by mineralogists, is a sensitive analysis tool with a great potential for use in vegetation research (Schmidt and Skidmore, 2003; Skidmore et al., 2010). Developments in the field of hyperspectral remote sensing and imaging spectrometry have opened new ways for monitoring vegetation quality and quantity.

A great deal of relevant information on vegetation properties can be extracted from passive reflectance spectra in the visible and near-infrared wavelengths by using ASD field spectroradiometer (ASD, 2007). This study describes how spectroscopy at ground-level can be used as a survey technique. Moreover, the method is also valuable in the construction of hyperspectral libraries of various vegetation types for use in different classification methods of satellite-derived imagery. Two test sites were selected and depicted in Figure 4.8.



Figure 4.8 : Selected test sites for field study.

5. STUDY AREA, DATA and CASE STUDY

5.1 Study Area

The population of Turkey was 13 648 270 in 1927 and it has increased approximately five fold in seventy three years, and reached to 67 803 927 in 2000 (Table 5.1). According to the U.S Census Bureau, the population of Turkey will reach to 82 205 000 by 2025. Istanbul is one of the most important cities in the world due to its historical, cultural, industrial and natural characteristics. Istanbul has been affected by huge immigration waves; the city population was 3 million in 1970s, it became 7.4 million in 1990s and current population is around 12 million (SIS, 2007).

Table 5.1: Population growth of Turkey and İstanbul (SIS, 2007).

Year	Population of Turkey	Population of İstanbul	Istanbul/Turkey Rate (%)	Growth Rate of Population in Turkey (%)	Growth Rate of Population in İstanbul (%)
1927	13.648.270	806.863	5.91		
1935	16.158.017	883.599	5.47	18	10
1940	17.820.950	991.237	5.56	10	12
1945	18.790.174	1.078.399	5.74	5	9
1950	20.947.188	1.166.477	5.57	11	8
1955	24.064.763	1.533.822	6.37	15	31
1960	27.754.820	1.882.092	6.78	15	23
1965	31.391.421	2.293.823	7.31	13	22
1970	35.605.176	3.019.032	8.48	13	32
1975	40.347.719	3.904.588	9.68	13	29
1980	44.736.957	4.741.890	10.6	11	21
1985	50.664.458	5.842.985	11.53	13	23
1990	56.473.035	7.309.190	12.94	11	25
2000	67.803.927	10.018.735	14.78	20	37

It has an annual incoming migration flow of about 400.000. Rapid industrialization and population increase have caused changes in landscape characteristics of İstanbul.

This urban growth causes severe problems in the use of natural resources such as fresh water supplies (Goksel et al., 2001). In the provincial boundary of İstanbul,

there are 12 water basins; however, only 11 of them provide water to the City of Istanbul. Due to intense urban developments surrounding the lake, Küçükçekmece basin no longer provides water to the City of Istanbul and has been removed from the list of drinking water resource basins. Instead, its sub-portion, named Sazlıdere Basin, is preserved for the same purpose. From west to east, water basins are on the European side Terkos, (5), Büyükçekmece (6), Sazlıdere (7), Alibeyköy (8), and Küçükçekmece (9), and on the Asian side, Elmalı (10), Ömerli (11), and Darlık (12) water basins in Figure 5.1.

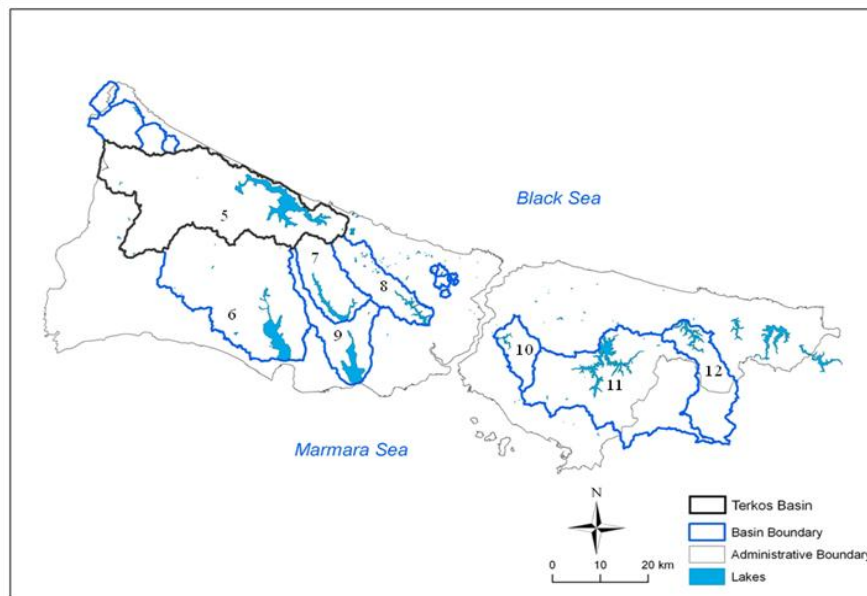


Figure 5.1 : Surface water resources basins in the province of Istanbul.

A significant portion of Ömerli and Darlık water basins lay out of the provincial boundary of Istanbul.

According to the research carried out by the Istanbul Water Board Authority, the annual water source capacity of the city is 1034 million cubic meters per year. It is projected that the estimated water requirement of the city will rise up to 4 461 000 m³ day⁻¹ in 2010 (Maktav et al, 2002).

Terkos Water Basin is one of the most important drinking water source of Istanbul was selected as study area. The natural freshwater Lake Terkos is located in the northwest Istanbul and is separated from the Black Sea with a thin land barrier, and the natural structure of the seaside coasts is sandy beach (Figure 5.2). It lies between the latitude of 40°19'N and 41°42'N, and longitude of 28°29'E and 28°32'E. The area

of the basin is 632 km² and the area of the Terkos Lake is 42 km². Lake Terkos provides 25% of the water demand of Istanbul (Coşkun et al, 2006).

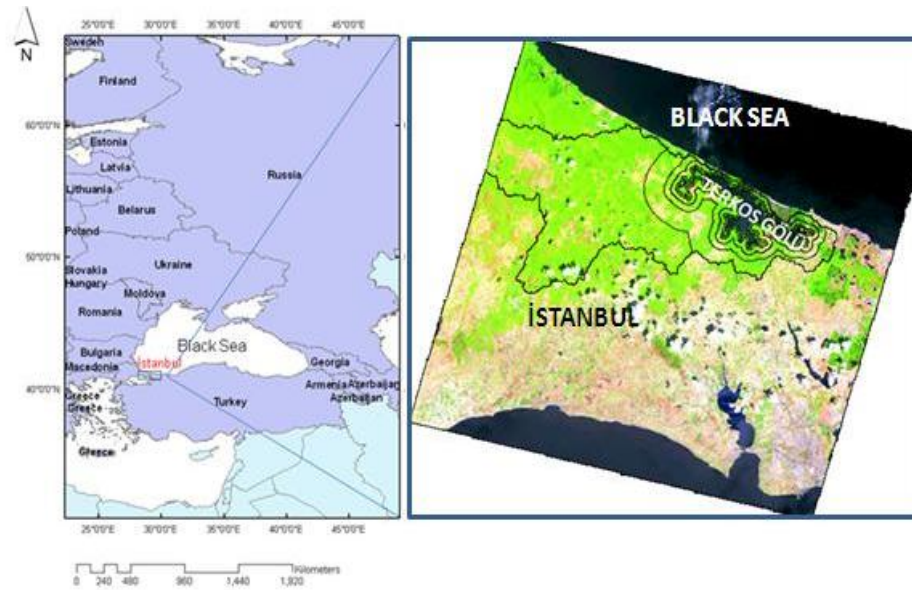


Figure 5.2 : Location of Istanbul and Terkos Water Basin.

The water quality of Lake Terkos is still acceptable as a water supply reservoir because it has relatively low population and limited industrial activities (Baykal et al, 2000). Protection and management of the drinking water reservoirs are important and inevitable especially for the global warming scenarios. The Istanbul Water and Sewerage Administration is responsible for maintaining the water quality of the supply from all catchment areas of Istanbul. Protection zones around drinking water resources are also subjected to the Turkish Water Pollution Control Federation (TWPCR), which restrict residential, industrial and agricultural activities in the catchment areas. Protection zones such as absolute, short, medium and long-range established in the catchment area and activities that are permissible in each of these zones evaluated by TWPCR (Coşkun et al, 2002).

3% of the Terkos water basin is under conservation and the basin is known as important vegetation, fish and bird area with its sand dunes, aquatic vegetations, marshes and wetlands (Özhatay et al, 2003). The basin has 13 of 73 endemic species of Turkey. There are three different vegetation types in the basin. First one is sand dune vegetation species between the Black Sea coast and lake boundary. Second one is very rich wetland vegetation species in the lake, very close to lake boundary and to the mouth of the rivers. The last one is mixed forest and scrub (Byfield, 2009).

Lake Terkos is an important wetland as well as being a drinking water reservoir of Istanbul. The medium protection zone of Terkos Basin was selected as the study area. The geographic location of the basin is one of the most important reasons to select Terkos as study area among the other important vegetation areas in Istanbul. Terkos basin is a very important vegetation area because the region includes very rich Euro-Siberian and Mediterranean vegetation species, especially wetland vegetation species. More than 50 wetland vegetation species can be seen in different parts of the Terkos Lake (Özhatay et al, 2003). Some wetland vegetation (i.e. *Ceratophyllum demersum*, *Myriophyllum spicatum*, *M.verticillatum*, *Najas marina*, *N.minor*, *Potamogeton crispus*, *P.lucens*, *P.perfoliatus* (can be seen only in this region), *Utricularia australis* ve *Vallisneria spiralis* (can be seen less than five different region in Turkey), *Hydrocharis morsus-ranae*, *Lemna* spp., *Nuphar lutea*, *Polygonum amphibium*, *Salvinia natans*, *Trapa natans* and *Nymphaea* sp., *Phragmites australis*, *Typha angustifolia*, *T.latifolia*, *T.laxmannii* ve *Schoenoplectus lacustris* ssp. (can be seen, especially where the streams flow into the lake) can be seen in Lake Terkos (Özhatay et al, 2003). Different types of aquatic vegetation can be seen in Lake Terkos in different seasons. Figure 5.3 shows some of the vegetation types in Lake Terkos.



Figure 5.3 : Wetland vegetation types in Lake Terkos.

Wetland vegetation types depicted in Figure 5.3 include a) *Epipactis palustris* b) *Leucojum aestivum* c) *Íris pseudocorus* d) *Butemus umbellatus* e) *Typha latifolia* f) *Ranunculus aquatilis* g) *Natans* h) *Nymphaea alba* i) *Vallisneria spiralis* j) *Trapa natans* k) *Polygonum amphibium*, l) *Nuphar lutea* m) *Lemna spp* n) *Hydrocharis orsusranae* o) *Utricularia australis* p) *Stratiotes aloides* r) *Potamogeton perfoliatus* r) *Potamogeton crispus* s) *Najas minors* t) *Myriophyllum spicatum* u) *Ceratophyllum* (Ozhatay et al., 2003). Five of the twenty vegetation species (e, h, i, j and m) were selected for further analysis based on their spatial distribution in the test sites and field reflectance spectra were collected during summer season.

The natural resources of the basin has been under human threats such as construction of houses and their increasing quantity of waste water, filling wetlands for new agricultural areas and cutting sedges and over fishing and bird hunting.

5.2 Remote Sensing Data

In practice, the criteria selecting suitable remotely sensed data set depending on the objectives and requirements of a project must take into account spatial resolution, spectral resolution, temporal resolution, data availability, data quality, acquisition cost, and even processing time. It is indispensable and even necessary for some special applications to work with multitemporal data from different sensors.

For the change detection, it is important to use the same sensor, same radiometric and spatial resolution data with anniversary or very close to anniversary data to eliminate the effects of external sources, such as sun angle, seasonal, and phonological differences. However, acquiring the same sensor data in anniversary multitemporal format is sometimes difficult especially if you are looking for change detection for a long term.

SPOT scenes from different dates 1991 and 2003 were available for the study covering an area of at least 60 km x 60 km, each with the 20 m spatial resolution. In order to test the ability of high resolution satellite data in the wetland vegetation study 2007 dated SPOT 5 multispectral and panchromatic data with the spatial resolution 10 m and 2.5m were used. As a hyperspectral test example 2007 dated Hyperion EO-1 hyperspectral data with the resolution 30 m and 242 bands were used in the study. Detailed satellite data descriptions are given in Table 5.2.

Table 5.2: The characteristics of the satellite data used.

Sensors	Satellites	Acquisition date	Spatial Resolution	Band Range (μm)
Hyperspectral	Hyperion EO-1	08-07-2007	30 m	0.45-1.35
				1.40-2.48
High Spatial	SPOT 5 PAN	14-08-2007	2.5 m	0.48 – 0.71
			or 5 m	
Multispectral	SPOT 5 MS	14-08-2007	10 m	0.50 – 0.59
			10 m	0.61 - 0.68
			10 m	0.78 – 0.89
			10 m	1.58 – 1.75
	SPOT 2 MS	10-08-1991	20 m	0.50 – 0.59
			20 m	0.61 - 0.68
			20 m	0.78 – 0.89
	SPOT 4 MS	24-07-2003	20 m	0.50 – 0.59
			20 m	0.61 - 0.68
			20 m	0.78 – 0.89
				1.58 – 1.75
Sensors	Satellites	Acquisition date	Spatial Resolution	Radiometric Resolution
Hyperspectral	Hyperion EO-1	08-07-2007	30 m	16 bit
High Spatial	SPOT 5 PAN	14-08-2007	2.5 m	8 bit
			or 5 m	
Multispectral	SPOT 5 MS	14-08-2007	10 m	8 bit
	SPOT 2 MS	10-08-1991	20 m	8 bit
	SPOT 4 MS	24-07-2003	20 m	8 bit

The SPOT sensor acquires information using a linear array of detectors. This approach is superior since there are no moving parts (i.e. a rotating mirror that scans back and forth across the orbit path). This design provides for a longer ‘dwell-time’ or radiance integration period over a target (Schowengerdt, 1997) and thereby provides increased sensitivity to radiometric contrasts between surfaces. The SPOT system’s overall capability was enhanced significantly in 1998 with the addition of a mid-infrared channel on the SPOT-4 sensor, providing greater utility for land-cover and land-use monitoring (Stroppiana et al., 2002). The SPOT-5 sensor (launched in 2002) collects panchromatic, visible and near-infrared, and mid-infrared data at 5, 10 and 20 m spatial resolution, respectively (URL-4). Further, following the availability of these data, many projects began to employ image fusion techniques, using panchromatic and multispectral information for improved land-cover and land-use monitoring.

The Hyperion sensor is an experimental space-born hyperspectral instrument on the Earth Observing (EO-1) satellite, which was launched by NASA in 2000 (Pearlman et al., 2003). Hyperion level 1 product is available in only HDF with the band stored in BIL format. The standard new USGS FORMAT 42 km long acquisitions comprising of 242 bands with an image size of 256 samples and 3129 lines for Hyperion (URL-6) (Table 5.3). The instrument is a pushbroom scanner, measuring an entire row of the image and the two detector arrays simultaneously measure the complete wavelength range. The spectral resolution, however, is far superior to multispectral satellite imagery, with 10 nm spectral bandwidth and 242 wavebands over 400 to 2500 nm range. The wavelength range is consistent with ASD field spectrometers.

Table 5.3: Hyperion EO-1 detailed sensor characteristics.

Sensor altitude	705 km	Number of rows	256
Spatial resolution	30 m	Number of columns	3129
Radiometric resolution	16 Bit	VNIR range (µm)	0.45-1.35
Swath	7.2 km	SWIR range (µm)	1.40-2.48
IFOV(mrad)	0.043		

5.3 Field Spectroscopy Data

Hyperspectral data were obtained from the 1-nm-wide narrowband FieldSpec Pro FR spectroradiometer manufactured by Analytical Spectral Devices (ASD) measuring spectra over a spectral range of 0.4–2.5 μm (ASD, 2007). Gathering spectra at any given location involved optimizing the integration time (typically set at 17 ms), providing foreoptic information, recording dark current, collecting white reference reflectance, and then obtaining target reflectance. A 18° field of view (FOV) was used. At each sampling location, target reflectance was measured from wetland vegetatin species. Using handheld GPS, 30 field plots (30 by 30 m) were located within the south- east section of the Terkos Lake. There was difficulties to sample the plots randomly because of the water depth problem some areas was not reachable by boot for representing a range of wetland vegetation characteristics. Plots constrained to be easily reachable and distributed according to region properties by existing high resolution satellite images. Field sampling took place in the middle of the day (i.e. 2 hours before and after true midday) during the summer season (i.e. from June to July 2006 and 2007), while plants were still fresh; there was no evidence of wilting or senescence.

At each site, 20 reflectance measurements consistently taken for at least three vegetation samples. Mean and standard deviations were calculated for each sampling plot to have homogeneity. Field collected reflectance data were analyzed using ASD pre-processing programs for integration with Hyperion Data. Mean and the spectral variability of the canopy reflectance spectra of sample plots ($n = 35$) in Terkos Water Basin, Istanbul is given in Figure 5.4.

Hyperspectral image spectra as well as field spectra are generally more noisy as compared to the controlled laboratory situation, due to the Sun's variable illumination, and the greatly reduced incoming signal. Detectors of spectrometers are built to work in a specific spectral range, in other words the signal to noise ratio decreases at the extreme of the spectrum where the focus of sensors deteriorates (Schmidt and Skidmore, 2003). Therefore, the noise in spectra crossing several detector types generally has increased noise where sensors meet. Also, where the incoming radiation becomes too weak for the sensors to detect a signal, the noise intensifies.

This usually happens where the atmosphere absorbs most of the Sun's radiation namely around 2500, 1950 and 1450 nm and wavelengths shorter than 300 nm.

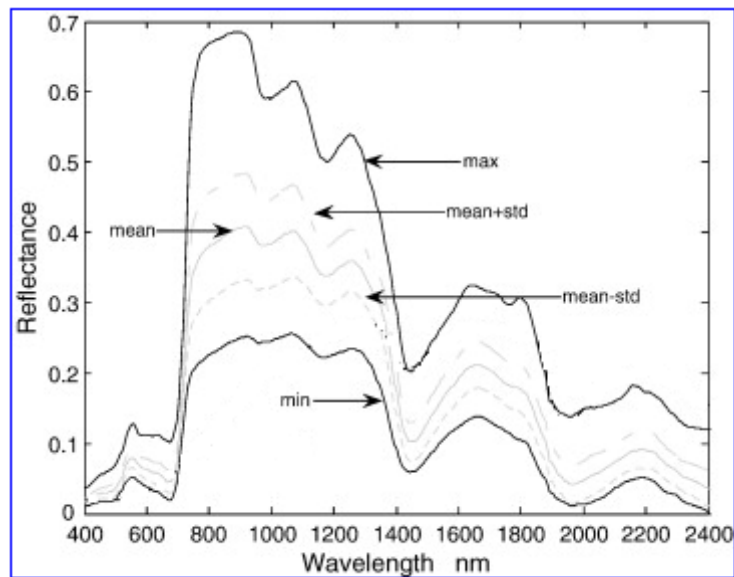


Figure 5.4 : Mean and the spectral variability of the canopy reflectance spectra of sample plots in Terkos Water Basin, Istanbul.

The location of the collected reflectance were recorded by using handheld GPS (Global Positioning System). Examples of ground photos were given in Figure 5.5. Spectroradiometer data of marshes were analyzed using ASD pre-processing programs for integration with Hyperion Data.

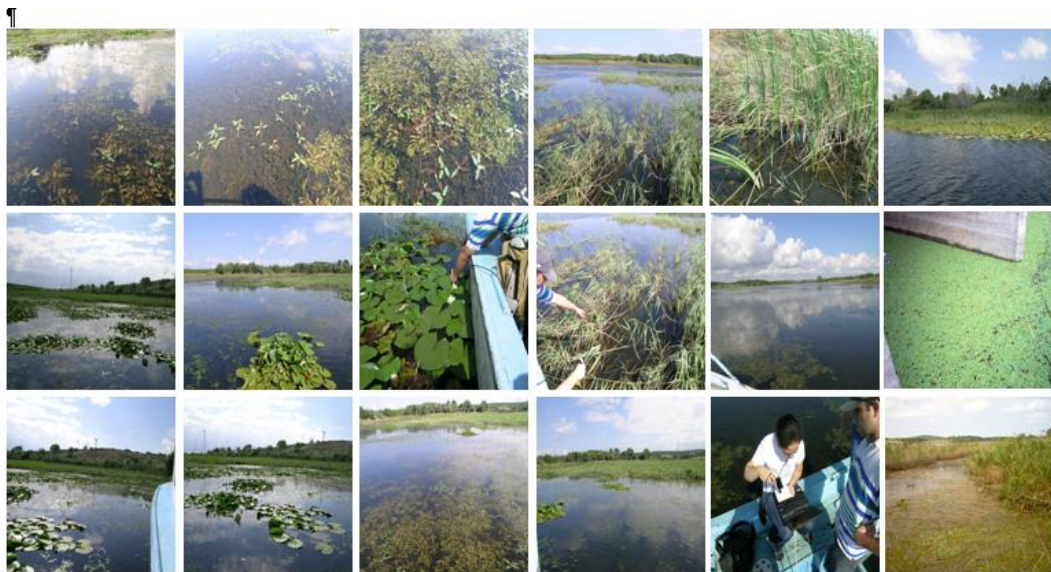


Figure 5.5 : Typical field sites showing the wetland vegetation layer with water.

5.4 Meteorological Data

Station data including daily temperature (min, max and average), daily average wind, and daily total precipitation were obtained from the State Meteorological Office of Turkey for the study area (Table 5.4). Especially, meteorological station data were obtained for the exact acquisition data of remotely sensed data from 1991 to 2007. Field studies were made under the sun without any clouds to collect ASD field reflectance.

Table 5.4: Meteorological information on image acquisition date.

Date	Temperature (°C)	Precipitation (%)
10/08/1991	28	64
24/07/2003	20	4
08/07/2007	25	52
14/08/2007	26	61

5.5 Digital Image Pre-Processing of Satellite Data Set

Several digital image processing techniques were applied to remove atmospheric, radiometric and geometric distortions available within multispectral and hyperspectral satellite images to extract meaningful and reliable information. Then, images were classified by using different transformation methods such as PCA, TCT and MNF with the help of unsupervised, supervised and SAM classification techniques. Furthermore, PCA based change detection and CVA applied to data set. CORINE legend were used in the study. All the results were compared based on accuracy assessment of classification methods. Methodology of the study is depicted in Figure A.1.

5.5.1 Radiometric and Atmospheric Correction

Digital numbers (DN) of all images converted into radiance then to at satellite reflectance values. Equations, gain and offset parameters presented in title 4.1.1 were used for the procedure. Calculation of radiance was given with following example for the value DN=100 for the first band of SPOT 5 image.

Gain: $1.301197 \text{ W}^{-1} \text{ m}^2 \text{ sr } \mu\text{m}$

$L=100/\text{Gain}$

$L=76.852314 \text{ W m}^{-2}\text{sr}^{-1}\mu\text{m}^{-1}$

Before radiance, transformation band sequential of the SPOT 5 data was checked by comparing with band histogram and they stacked in the correct order.

Atmospheric correction of the SPOT 2, SPOT 4 and SPOT 5 data were performed using dark object subtraction (DOS) method since this approach is a widely used by many scientists and it is simple as explained in title 4.1.1.

Dark objects having very small surface reflectance namely lakes, seas or other water bodies were selected for each SPOT data set by using histograms. It is assumed that these minimum reflectance values in the histograms from the entire scenes are attributed to the effect of the atmosphere. The correction is applied by subtracting the minimum observed value, determined for each specific band, from all pixel values in each respective band. After employment of DOS, haze was removed, and the surface features blocked by haze were recovered.

For Hyperion DN values were converted radiance value by using the equ.4.4 and 4.5. Radiance values were converted reflectance by using FLAASH atmospheric correction method.

5.5.2 Geometric Correction

Geometric correction applied to correct systematic and non-systematic distortions by using mathematical formulas during preprocessing by using the Ground Control Points (GCPs) (Figure 5.6). Different dated SPOT data were geometrically corrected by using affine transformation model. Different images projected onto the Universal Transverse Mercator (UTM) coordinate system. Homogeneously distributed locations that can easily and accurately identified such as highway, road intersections and bridges were selected as GCPs. Ground coordinates of these points were provided from 1:25,000 topographical map and other satellite sensor images. It is of vital importance to change detection applications that the multitemporal imagery is registered to the precision of at most ± 0.5 pixel Root Mean Square error (RMSE). An RMSE at the level of more than ± 0.5 pixel may result in the identification of

spurious areas of change among the datasets. Each geometric correction has RMSE lower than 0.5 pixel. Detailed information is given in the Table 5.5.

The registration of each image was performed using the nearest neighbour resampling algorithm. The accuracy of geometric correction was checked by using test points.

Table 5.5: Geometric correction information.

Satellite Data	Ground Control Points	RMSE	Test Points	RMSE
SPOT 1991	25	0.46	7	0.62
SPOT 2003	28	0.40	7	0.65
SPOT 2007	28	0.48	7	0.52
Hyperion 2007	15	0.47	6	0.56

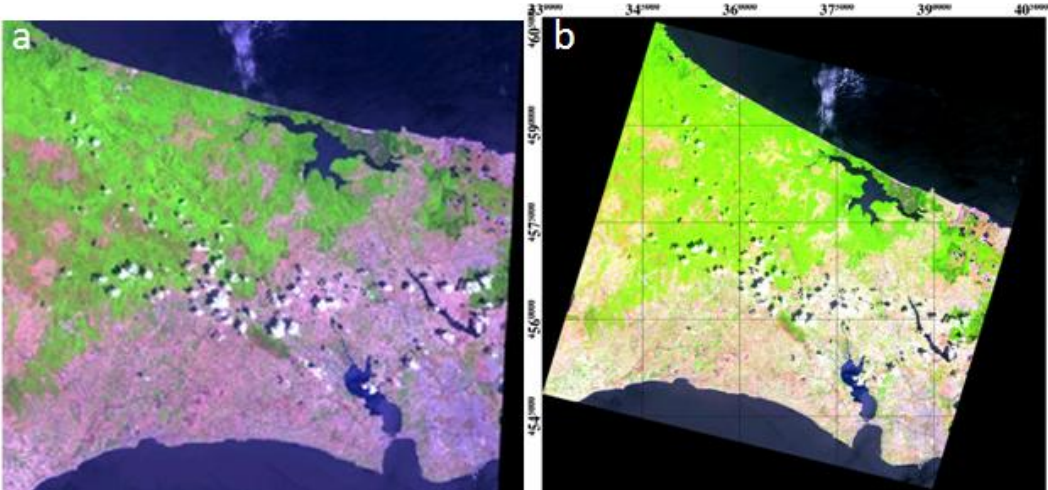


Figure 5.6 : 2003 dated SPOT data (4,3,2) a) Original data b) Geometrically corrected data.

5.5.3 Radiometric Normalization

Radiometric normalization is important to separate real changes in surface features from radiometric changes linked with the different dated images. Pseudo-invariant features (PIF) were selected and a regression model produced for the radiometric normalization. This technique was applied by selecting a reference image (2007 dated SPOT MS) and 2003 dated SPOT 4 image. In this study, the technique was applied with the assumption that there are targets with constant reflectance values over time. The PIFs were selected objectively with PCA and quality control.

Ten invariant targets including impervious areas, and bare lands were selected. Vegetation was excluded as invariant targets because they tend to show seasonal trends. The accuracy of the radiometric normalization was assessed with PCA. A mean of 3 pixels for each target was calculated for both images.

The linear correlation coefficients (R^2) of PIFs were calculated and used to convert 2003 values to 2007 equivalent values (Table 5.6).

Table 5.6: Linear regression analysis between 2003 and 2007 image by using PIF.

Spectral Bands	Linear Equations	R^2 values
Band 1	$Y=0.514x+0.047$	0.993
Band 2	$Y=0.706x+0.039$	0.978
Band 3	$Y=0.744x+0.033$	0.978
Band 4	$Y=0.773x+0.021$	0.957

5.5.4 Hyperion Pre-processing

Hyperion L 1R radiometric data processing operations included band selection (Datt, et al, 2003), correction for bad lines (Han, et al, 2004), striping pixels (Datt, et al, 2003) and smile (Goodenough, et al, 2003), a pixel-based atmospheric correction using FLAASH and a geometric correction. A brief explanation of these steps is given as follow.

5.5.4.1 Band Selection

The level 1 radiometric Hyperion EO-1 product has a total of 242 bands but only 198 bands are calibrated (band 8 to 57 for VNIR and 77 to 224 in SWIR region) (Datt et al., 2003) because of an overlap between VNIR and SWIR focal planes are only 196 unique channels. Detailed information was given in title 4.1.3.1. 196 bands of the Hyperion data checked one by one and bands without any problem used in the next process steps. Selected and unselected bands were given in the Figure 5.7.

355.50	579.45	803.30	1006.81	1013.30	1235.27	1457.23	1679.20	1901.17	2123.14	2345.11
365.76	589.62	813.48	1016.98	1023.40	1245.36	1467.33	1689.30	1911.27	2133.24	2355.21
375.04	599.80	823.65	1027.16	1033.50	1255.46	1477.43	1699.40	1921.37	2143.34	2365.21
386.11	609.97	833.83	1037.33	1043.59	1265.56	1487.53	1709.50	1931.47	2153.34	2375.30
396.20	620.15	844.00	1047.51	1053.69	1275.66	1497.63	1719.60	1941.57	2163.43	2385.40
406.47	630.32	854.18	1057.68	1063.79	1285.76	1507.73	1729.70	1951.56	2173.53	2395.50
416.64	640.50	864.00	1067.92	1073.89	1295.86	1517.83	1739.69	1961.66	2183.63	2405.60
426.82	650.67	874.18	1078.01	1083.99	1305.96	1527.92	1749.79	1971.76	2193.73	2415.70
436.99	660.85	884.35	1088.19	1094.09	1316.05	1537.92	1759.89	1981.86	2203.83	2425.80
447.17	671.02	894.53	1098.19	1104.18	1326.05	1548.02	1769.99	1991.96	2213.93	2435.90
457.34	681.20	904.70	1108.28	1114.18	1336.15	1558.12	1780.09	2002.06	2224.02	2445.99
467.52	691.37	914.88	1118.26	1124.28	1346.25	1568.22	1790.19	2012.16	2234.12	2456.09
477.69	701.55	925.05	1128.15	1134.38	1356.35	1578.32	1800.29	2022.25	2244.22	2466.09
487.87	711.72	935.23	1138.54	1144.48	1366.45	1588.42	1810.38	2032.35	2254.22	2476.19
498.04	721.90	945.41	1148.64	1154.58	1376.55	1598.51	1820.48	2042.45	2264.32	2486.29
508.22	732.07	955.58	1158.73	1164.68	1386.64	1608.61	1830.58	2052.45	2274.42	2496.39
518.39	742.25	965.76	1168.82	1174.77	1396.74	1618.71	1840.58	2062.55	2284.52	2506.49
528.57	752.43	975.93	1178.91	1184.87	1406.84	1628.81	1850.68	2072.65	2294.62	2516.58
538.74	762.60	986.11	1188.99	1194.97	1416.94	1638.81	1860.78	2082.75	2304.71	2526.68
548.92	772.78	996.28	1199.08	1205.07	1426.94	1648.91	1870.87	2092.84	2314.81	2536.78
559.09	782.95	1006.46	1209.17	1215.17	1437.04	1659.01	1880.97	2102.94	2324.91	2546.88
569.27	793.13	1016.62	1219.30	1225.17	1447.14	1669.10	1891.07	2113.04	2335.01	2556.98

Figure 5.7 : Selected and unselected 242 bands of Hyperion EO-1 data.

108 bands selected among the 242 Hyperion bands for further analysis. No image data were available for the following ranges: 355.6 to 416.61, 915.23 to 983.08, and 2445.99 to 2556.98. Good image data were available for the following ranges: 426.82 to 905.05, 993.17 to 1114.18, 1164.68 to 1336.05, 1507.73 to 1769.99 and 2032.35 to 2042.45. Relatively poor data were available in the following ranges: 1124.28 to 1154.58, 1346.25 to 1497.63, and 1780.09 to 2435.90. Atmospheric water vapor bands, which absorb almost the entire incident and reflected solar radiation and the bands that have very severe vertical stripping are usually identified by visual inspection of the image data were excluded from the hyperspectral data. After visual inspection, 108 selected bands were subset from the Hyperion image and these bands are listed in Table 5.7 based on spectral region.

Table 5.7: Selected bands from Hyperion based on spectrum region.

Spectral Region	Wavelengths (nm)	Number of Bands
VIS	427-660	24
NIR	671-905	24
SWIR-1	993-1336	31
SWIR-2	1507-2042	29
		$\Sigma = 108$

5.5.4.2 Bad Detection Element

Bad pixel problem in Hyperion was solved by using interpolation and extrapolation method. Most of the noisy cells were detected in column 1 and 126 of the detector array. Visual inspections showed that some of the good cells were identified as noisy cells. These cells were deselected from the detector array.

After visual correction and testing different window sizes a standard deviation window is used to replace the values of bad cells with ones interpolated from neighboring good cells. Figure 5.8 depicts the differences between the neighbor columns and the vertical stripe problem because of this difference. Therefore, corrected image is given in the Figure 5.8 b.

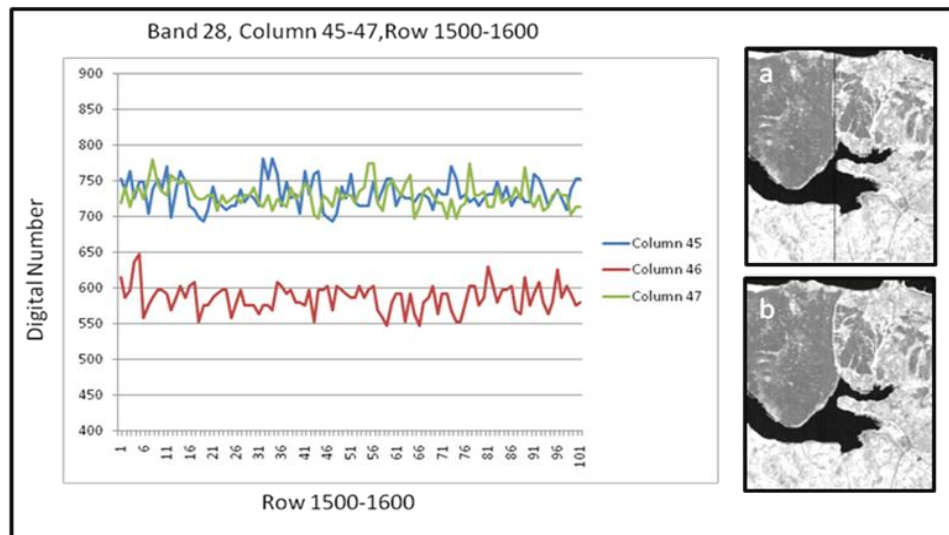


Figure 5.8 : Differences between columns a) Bad column in Hyperion EO-1 image b) Corrected bad column in image.

5.5.4.3 Bad Line Detection and Correction

A pushbroom sensor instrument also has calibration differences in the detector arrays that cause vertical stripes in the image. The first 12 bands and many SWIR bands of Hyperion are influenced by striping (Figure 5.9). The differences between gain and offset are the main reason for this vertical striping problem and to solve this full linear correction was attempted to try to adjust the difference through the entire detector cell statistics. This bad lines and stripes were balanced by Mapping Technologies group- A (MMTG-A) extensions that embedded in ENVI software.

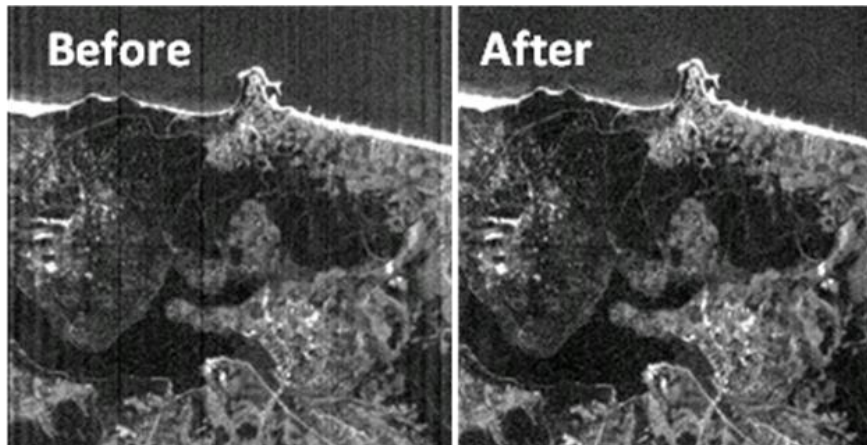


Figure 5.9 : Striping problem and after correction applied by MMTG-A.

5.5.4.4 FLAASH Atmospheric Correction

FLAASH atmospheric correction method applied to Hyperion data to minimize the scattering and absorption effects due to the atmosphere and to retrieve the reflectance value from the data. The Hyperion radiance values from the 108 bands were converted into surface reflectance images using the Fast Line-of-Sight Atmospheric Analysis of Spectral Hypercubes (FLAASH) algorithm. A correction for adjacency effects applied using this algorithm. Model parameters included a mid-latitude summer atmosphere and a rural aerosol model. Therefore, sensor type, flight date, sensor altitude (km), ground elevation (km), pixel size (m) and flight time were used for retrieving reflectance values. Hyperion bands covering the 1135-nm water vapor band were used to estimate precipitable water vapor on a per-pixel basis.

The comparison between ASD resampled spectra and Hyperion spectra after FLAASH demonstrated that the atmospheric correction using FLAASH is very effective and these two spectra are consistent with each other and the correlation coefficient reached 0.827.

5.5.4.5 Minimum Noise Fraction Transformation

Spectral data reduction was performed using the Minimum Noise Fraction (MNF) transformation. MNF transformation was applied to the atmospherically corrected Hyperion image to separate noise from the data by using ENVI. The process applied into two steps: Forward and inverse MNF. In the first step, a forward MNF estimates noise statistics from the Hyperion reflectance data and based on this statistics,

decorrelates and rescales the noise in the data. This results in transformed data in which the noise has unit variance and no band-to-band correlations.

Next, good bands with less or no noise were selected from the MNF bands. In the final step, the selected MNF bands were transformed back to the original spectral space. MNF transformation was performed on all 108 bands after selecting bands. The first three (1-3) and the first ten (1-10) MNF bands were used for subsequent analysis as they contained high values of SNR. Figure 5.10 depicts first three MNF components of Hyperion data.

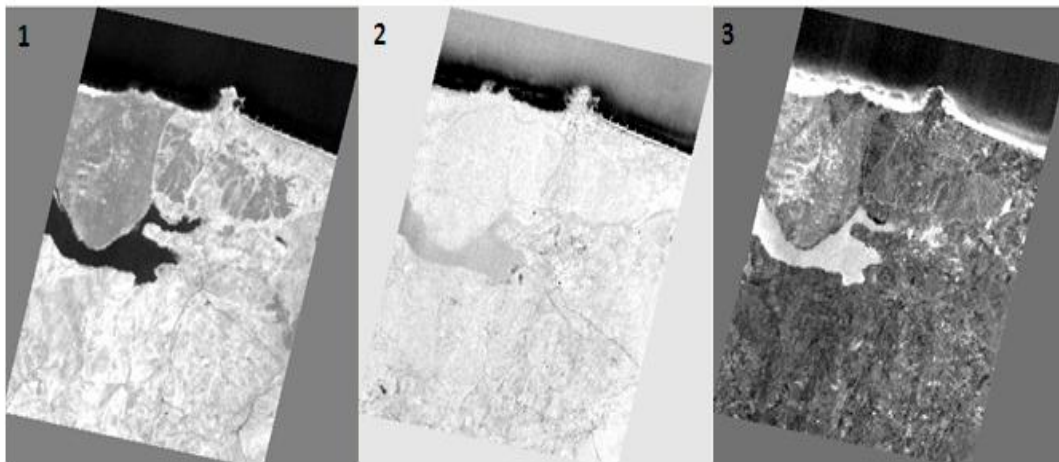


Figure 5.10 : First three components of the MNF.

5.6 Classification of Satellite Data

Hybrid classification that includes unsupervised and supervised methods was applied to determine LULC change detection based on CORINE database. Also the results from CVA analysis and classified Hyperion images were analysed by using CORINE methodology. At the first stage of this application a land use and land cover class legend was established considering both ecological and socio-cultural conditions of the region. Land cover and land use legends include three levels: five classes at the first level, seven classes at the second level and seven classes at the third level. The land use schema was determined, based on CORINE and the region's ecological and socio-cultural conditions are given in Table 5.8.

Table 5.8: The schema of the CORINE land use and land cover classes.

Level 1	Level 2	Level 3
Artificial surfaces	Urban fabric	Urban settlements (Discontinuous urban fabric)
Agricultural areas	Heterogeneous agricultural areas	Complex cultivation patterns
Forest and semi natural areas	Forests	Mixed forest
	Open space with little or/ no vegetation	Sparsely vegetated areas
	Shrub and/or herbaceous vegetation	Natural Grassland
Water bodies	Inland waters	Lake (water bodies)
Wetland	Inland wetlands	Inland marshes

5.6.1 Classification of Multispectral Satellite Data

Correlation matrix of satellite bands were used to decide selection of appropriate band combinations for more reliable and accurate classification. Table 5.9 and 5.10. depicts the correlation coefficients and standard deviations (std. dev.) of 2003 and 2007 dated SPOT 4 and SPOT 5 MS data set.

Table 5.9: Correlations and standard deviations between bands of 2003 data.

Correlation 2003	Band 1	Band 2	Band 3	Band 4	Std. Dev.
Band 1	1	0.984	0.735	0.868	18.012
Band 2		1	0.719	0.873	31.002
Band 3			1	0.944	59.403
Band 4				1	61.096

Table 5.10: Correlations and standard deviations between bands of 2007 data.

Correlation 2007	Band 1	Band 2	Band 3	Band 4	Std. Dev
Band 1	1	0.988	0.804	0.897	21.253
Band 2		1	0.746	0.860	36.580
Band 3			1	0.961	63.931
Band 4				1	66.970

In the visible region, B1 and B2 has the highest correlation approximately, 98 % for 2003 dated SPOT 4. It can be seen clearly from Table 5.9 the other coefficients are smaller than the B1 and B2 correlation. For 2007 dated SPOT data the highest correlation coefficient is between B1 and B2.

In order to assess which band combinations contained the most information and might be most useful, an OIF calculation was performed on the images. Based on the correlations of bands and standard deviation (Table 5.9), OIF was calculated with the equation 4.8 (Table 5.11). The best three band combination is the B2 B3 B4 with the highest OIF. The greatest variation was observed in by combination of bands B2 B3 B4. Greatest autocorrelation was observed in band combination B1 B2 B4 for both images.

Table 5.11: OIF values of band combinations.

Band Combination (2003)	OIF (2003)	Band Combination (2007)	OIF (2007)
B2 B3 B4	59.74	B2 B3 B4	65.24
B1 B3 B4	54.38	B1 B3 B4	57.15
B1 B2 B3	44.46	B1 B2 B3	47.97
B1 B2 B4	40.40	B1 B2 B4	45.46

Training areas for each LCLU categories based on CORINE legend were selected for classification purposes. Spectral separability of classification training areas was evaluated by using Transformed Divergence method to examine the spectral properties of individual training sample class and its separability over others (Table

5.11 and Table 5.12). These statistics can aid in determining whether the classes are “good” in terms of their separability in the multi-dimensional attribute space.

In Table 5.12 and 5.13 the number shows the LULC categories: 1) Urban Settlements 2) Complex Cultivation Patterns 3) Mixed Forest 4) Sparsely Vegetated Areas 5) Lake (Water courses) 6) Inland Marshes 7) Mining 8) Road

Table 5.12: Transformed divergence matrix (2003 SPOT 4).

TD	1	2	3	4	5	6	7	8
1	0							
2	1987	0						
3	2000	2000	0					
4	2000	2000	2000	0				
5	2000	2000	2000	2000	0			
6	1999	2000	1979	1985	1987	0		
7	1980	973	2000	2000	2000	2000	0	
8	1980	1977	2000	2000	2000	2000	1980	0

Table 5.13: Transformed divergence matrix (2007 SPOT 5).

TD	1	2	3	4	5	6	7	8
1	0							
2	1985	0						
3	2000	2000	0					
4	2000	2000	2000	0				
5	2000	2000	2000	2000	0			
6	1999	2000	1999	2000	2000	0		
7	1987	923	2000	2000	2000	2000	0	
8	1980	1975	2000	2000	2000	2000	1990	0

Separability values are between 0 and 2000. Very poor separability (0 to 1000) indicates that the two signatures are statistically very close to each other. Poor separability (1000 to 1900) indicates that the two signatures are separable to some extent. However, it is desirable to improve separability if possible.

Low signature separability is usually caused by improper combinations of image bands and/or training sites which have large internal variability within each class. Range between 1900 and 2000 indicates the good separability. Low signature separability was occurred between mining and complex cultivation patterns. Separability between these classes was improved by selecting new training areas.

5.6.2 Unsupervised Classification

In order to determine the changes in lake occurred between 1991 and 2007, Iterative Self Organizing Data Analysis (ISODATA), unsupervised classification was applied with 20 clusters, 10 iterations and a 0.95 convergence threshold (Figure 5.11). Results show that water and wetland area was 3186.10 ha in the year of 1991, and the area was 3021.92 ha in 2007. There is a decrease in the water surface area. On the other hand, the other category that includes green area and built up area around the lake is increased from 1091.66 ha to 1255.84 ha.

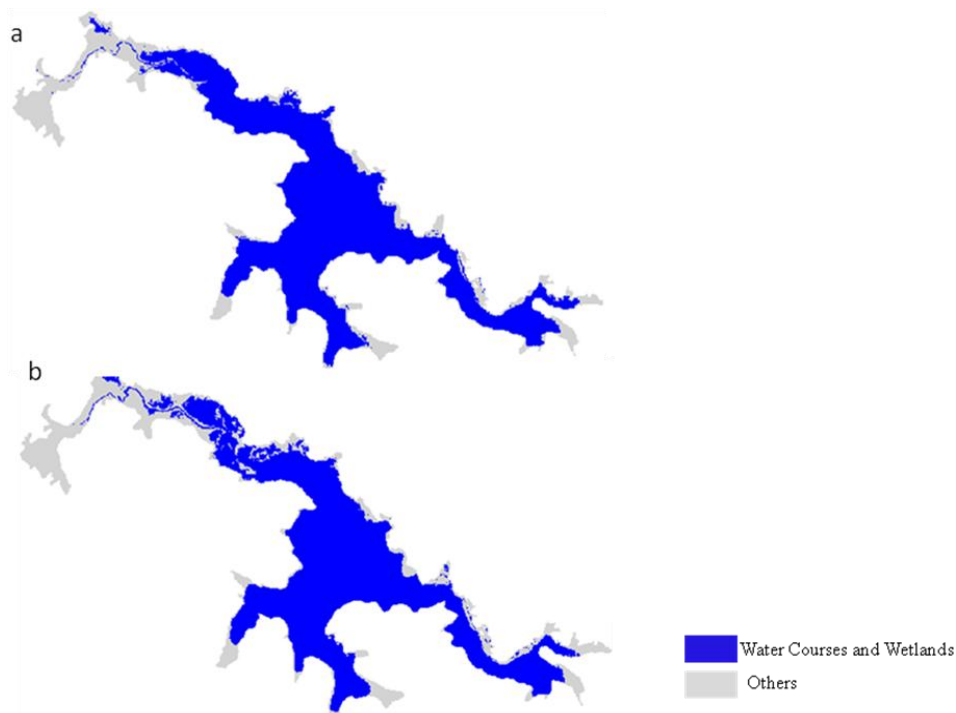


Figure 5.11 : Unsupervised classification of absolute protected area a) 1991 dated SPOT 2 and b) 2007 dated SPOT 5.

Furthermore, ISODATA, unsupervised classification method, was performed on temporal SPOT images to provide a basic set of classes for further supervised classification between the years of 2003 and 2007. 1991 dated image could not be used for this process because of the missing part of the image.

ISODATA was applied with 75 clusters, 20 iterations and a 0.95 convergence threshold to capture the most of the LULC variability from the image.

Aerial photograph, field survey data and other ancillary data were also used to evaluate classification map and assign the clusters into nine main classes based on CORINE legend. ISODATA classification results were depicted in Figure 5.12.

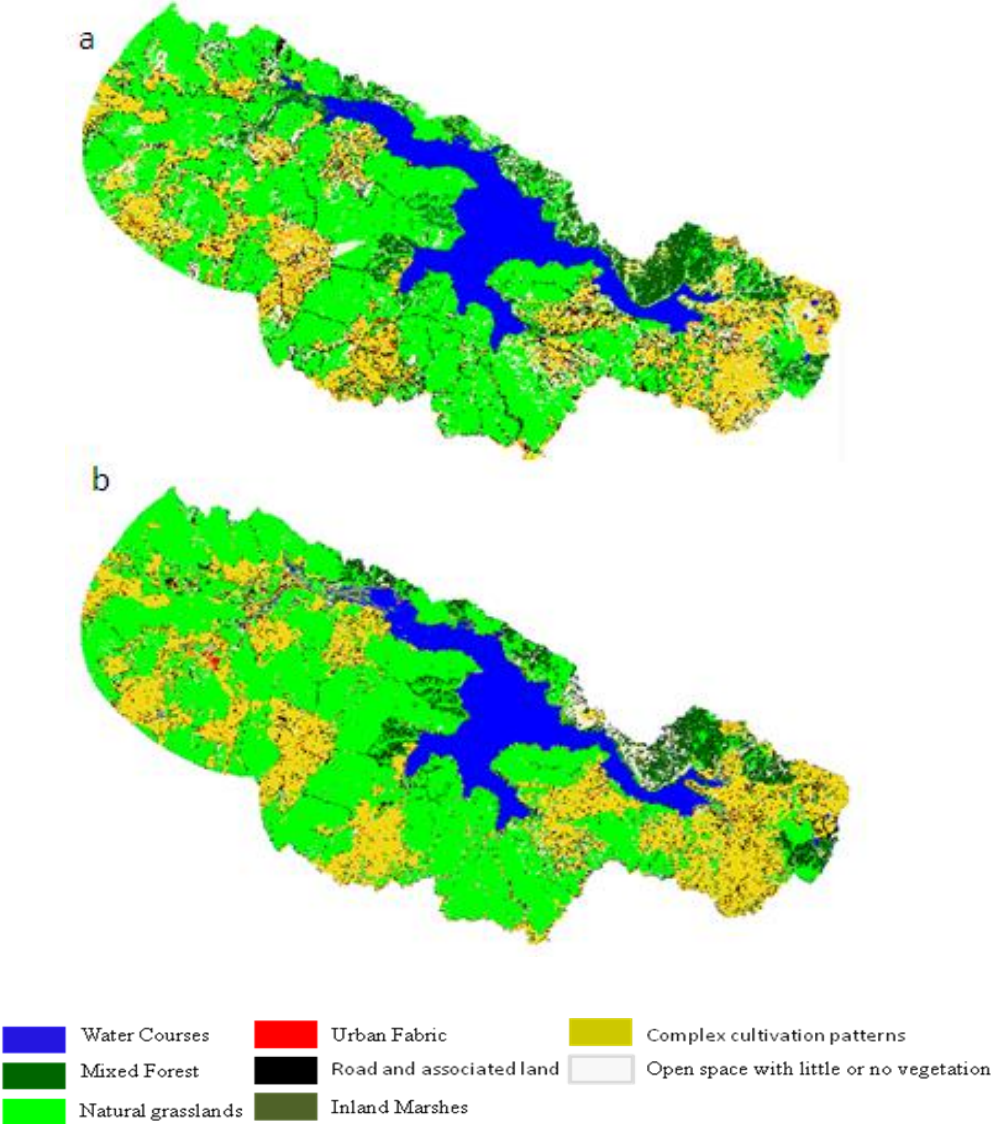


Figure 5.12 : ISODATA Unsupervised classification a) 2003 dated unsupervised image b) 2007 dated unsupervised image.

5.6.3 Supervised Classification

Maximum likelihood (ML) supervised classification algorithm was implemented on the SPOT 2003 and SPOT 2007 data. Training samples were chosen from the reference data set of unsupervised classification. As a result of classification different LULC categories for 2003-2007 were labelled as depicted in Figure 5.13 and statistical results were given in Table 5.14.

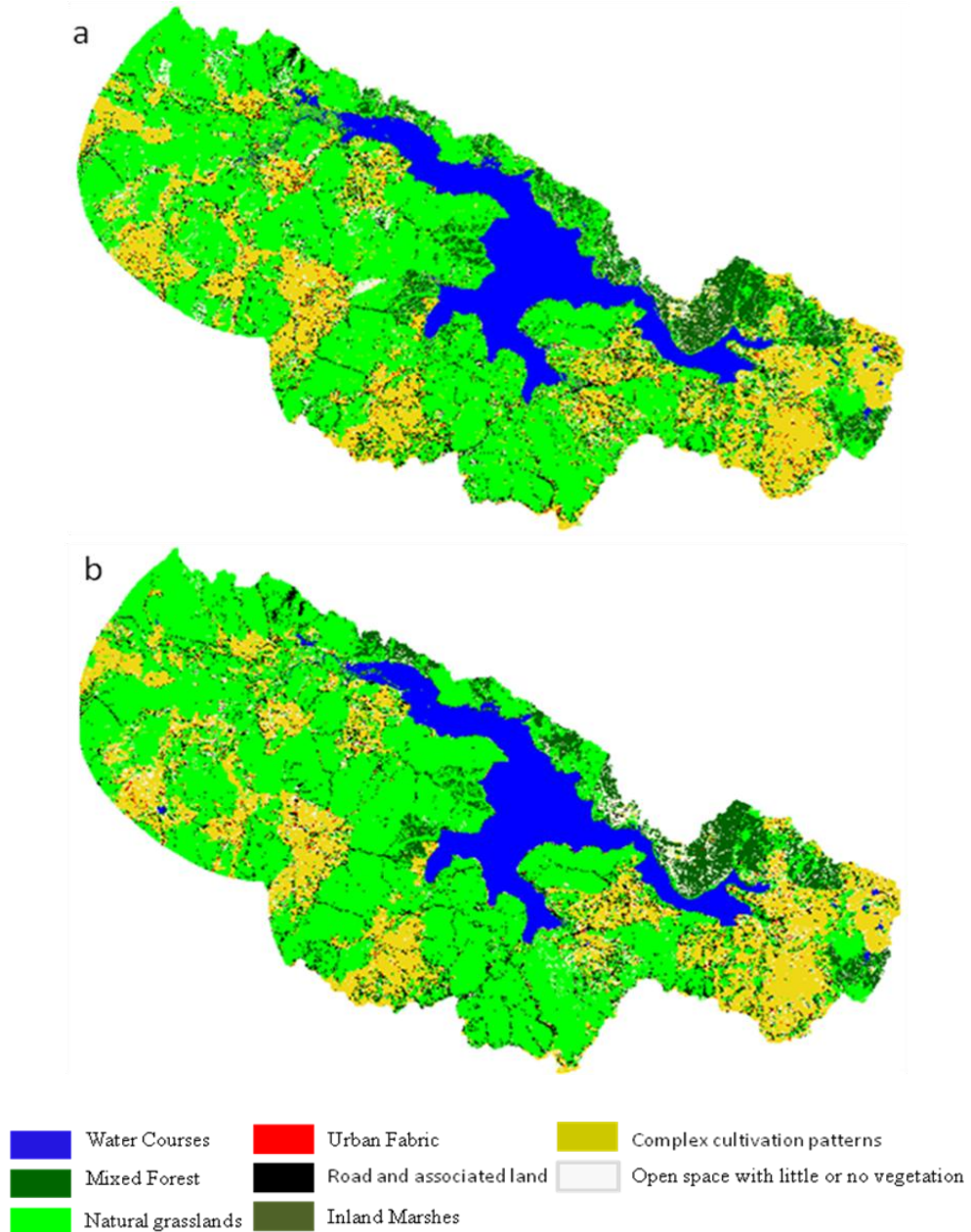


Figure 5.13 : Maximum likelihood supervised classification a) 2003 dated b) 2007 dated.

Table 5.14: Statistical results of supervised classification.

Area (ha)	Water Courses	Inland Marsh	Open Space	Natural Grasslands	Mixed Forest	Urban	Agriculture	Road
2003 Supervised	3214.5	407.72	1745.80	15056.6	1705.52	291.84	4886.4	1260.24
2007 Supervised	2926.78	249.32	1596.84	13553.4	1637.84	345.32	6936.52	1322.6
Difference (2003-2007)	287.48	158.40	148.96	1503.20	67.68	53,48	2050.12	62.36

The statistical results shows that between the years of 2003 and 2007 the LCLU changes occurred in the study area. Especially, the wetland areas decreased during this period and agricultural and open spaces were increased. The decrease in the forest area can be seen clearly from the Table 5.14. Road and urban areas were increased in the study area.

5.7 Change Detection

5.7.1 Principal Component Analysis Based Change Detection

Different dated images were stacked to store multitemporal data in one image and the principal component analysis (PCA) was used to enhance the change information from stacked multitemporal data. Figure 5.14 shows the methodology of the PCA based change detection.

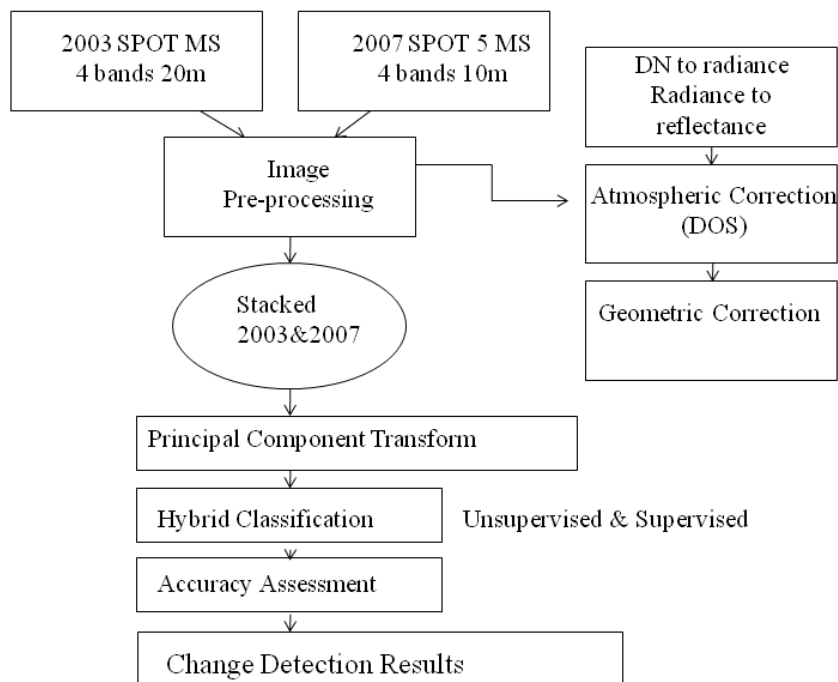


Figure 5.14 : Methodology of the PCA based change detection.

PCA is used to reduce the dimensionality of a dataset consisting of a large number of interrelated variables, while still retaining the maximum information of the variation present in the dataset (Li and Yeh, 1998; Deng et al. 2008). Principal components of stacked bands were given in Figure 5.15 for all stacked bands.

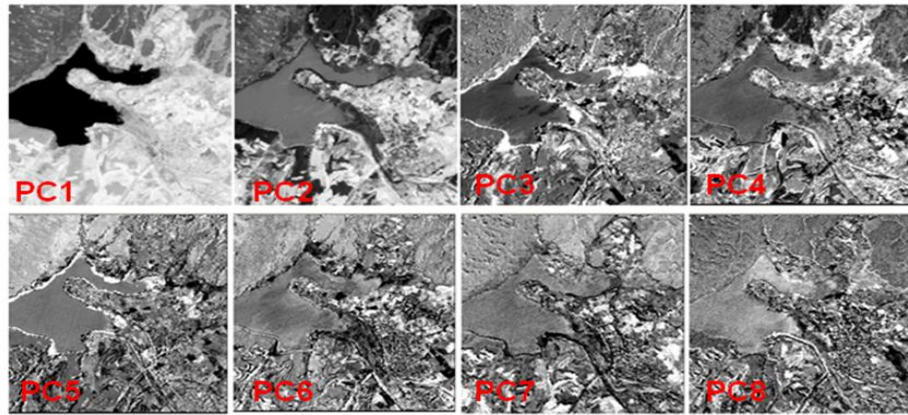


Figure 5.15 : Principal components of stacked eight SPOT bands.

Spatial and temporal changes in land use and cover were detected and quantified by using hybrid classifier combining unsupervised and supervised methods based on PCA. In this study, the images with n/m bands taken at two different times are combined into one image with (n+m) bands, and then the combined bands are transformed into (n+m) PCs.

There will be a high correlation between two images for the unchanged areas, and a relatively low correlation between the significantly changed areas. Standardized PCA was applied to the stacked multitemporal images. Most change information demonstrated in the first four components is depicted in Figure 5.15.

5.7.1.1 Change-information extraction and labelling using Hybrid classification

Pre-classification spectral change-detection methods, such as PCA, actually enhance the change information from original images, they have difficulty in labelling and obtaining 'from-to' change class information. In fact, classification intrinsically impacts the whole accuracy of change detection. In this study, a hybrid classification process combining unsupervised and supervised approaches is performed on the PCA-enhanced multitemporal change image. This hybrid classifier has the potential to produce class signatures that are numerically separable in feature space and land-use classes that are meaningful to the analyst for more accurate change detection.

Unsupervised classification using the Iterative Self-Organizing Data Analysis Technique (ISODATA) algorithm is first performed on a multitemporal change image to produce an unlabelled cluster map and providing a basic set of classes for further supervised classification.

The number of classes is the most crucial clustering parameter for capturing most of the land use variability from the remotely sensed data. Typically, a large number of clusters, say 50 or more, is used to ensure adequate data representation (Schowengerdt 1997). Different numbers of classes 30, 40, 50, 60, and 80 were empirically tried to find the suitable number. Sixty was found to be the optimum class number in terms of precision and processing time of the imageries. Aerial photograph, field survey data, and other ancillary data were used to evaluate the classification map and assign the clusters into two main classes, one being obviously unchanged land uses (such as grasslands, from 2003 to 2007) and the other being clearly changed land uses (including uncertain classes).

A mask generated that represented the unchanged area, so that changed areas could be accentuated in subsequent processing. Supervised classification adopting a maximum likelihood algorithm was implemented on the masking multitemporal image, which excluded the unchanged pixels identified from unsupervised classification results.

The reference data for selecting supervised training samples on the PCA-enhanced image were the same as those for unsupervised classification. Finally, the results from hybrid classifier were decomposed and labelled into different land uses for 2003 to 2007 (Figure 5.16) and conversion matrix given in Table 5.15. In the legend of the Figure 5.16 sparsely vegetated area includes natural grassland of the region.

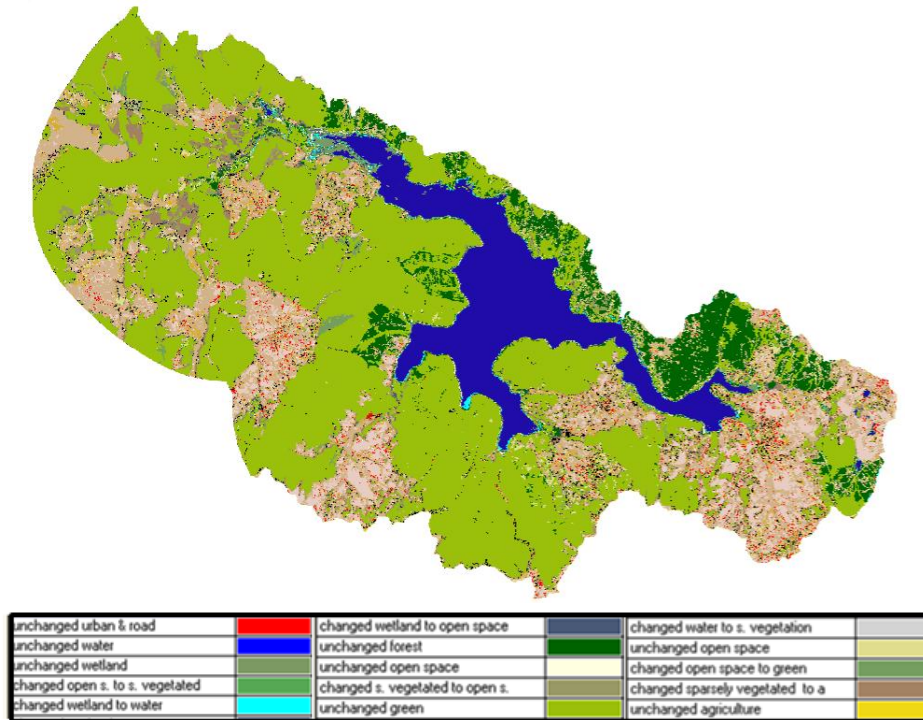


Figure 5.16 : LULC change detection by PCA and hybrid classification.

Table 5.15: LULC conversion matrix.

Area (ha)	Water	Inland Marsh	Open Space	Sparsely Vegetated	Mixed Forest	Urban & Road	Agriculture
Water	2860	40.32		31.44		69	
Inland M.	88.08	192	156.44				
Open S.			892.16	639			
Sparsely V.			562.12	13602.02			1059.88
Mixed F.					1726.64		
Urban & R.						544.76	
Agriculture							6119.96

The results depicted that major damage occurred on sparsely vegetated area of the Terkos Water Basin. 1059 ha sparsely vegetated area was converted to agricultural area and 562.12 ha of the was sparsely vegetated area changed to bare land in the study region. The above change statistics gives an explanation on the question of where LULC changes occurred between the years of 2003 and 2007. 156.44 ha area changed from wetland to open space. There is a perceivable decrease in water surface area. Total lake area decreased during three years.

5.7.1.2 Spatial Profiles and Semivariogram

In order to support the PCA based hybrid classification results a transect selected in the changed area (Figure 5.17. a). Spatial profiles and semivariogram of the transect were derived for multitemporal images to examine the spatial variation in the test region. By using classification it is possible to analyze the spectral differences in the change detection analysis. Especially for vegetation and heterogeneous areas it is difficult to delineate spectral characteristics because of very high spectral variability.

Spatial variation analysis employed as supportive method of change detection results in the study. Spatial profiles were used to visualize the spatial differences between these years (Figure 5.17.b and 5.17.c).

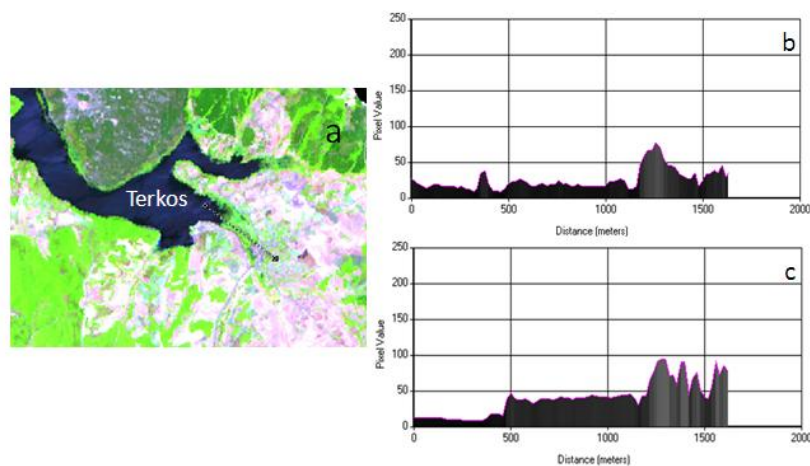


Figure 5.17 : Spatial profile analyze a) Location of the transect b) the transect view from 2003 dated SPOT 4 b) the transect view from 2007 dated SPOT 5.

Spatial profiles of changed area supported the hybrid classification results. The spatial profile was taken from the near-infrared band. On all profiles, black represents the water and wetland vegetation, whereas grey tones represent land. The differences in grey colour tones represent different land-use characteristics can be seen in Figure 5.17.

Therefore, semivariogram employed as a change detection tool in this study. Semivariogram, a graphical representation of the spatial variability in a given set of data, used to assist the change detection results based on spatial information. In order to study the spatial variability in the wetlands, the semivariance has been calculated for wetland vegetations of the test area taking the values from selected transect (Figure 5.17). For the change detection analysis different semivariograms were

compared with each other for different bands. The results obtained through semivariogram analysis are presented in Figure 5.18 and Table 5.16. The results interpreted by model type and usually by three model parameters: sill, range and nugget. It was found that the semivariogram is sensitive for the changes in the images.

Gaussian and exponential models were then fitted to experimental semi-variograms using the GS+ software. Investigation of semivariograms of the same transect for different bands (Figure 5.18 left side (2003) and right side (2007)) revealed that semivariograms of the bands representing very different results.

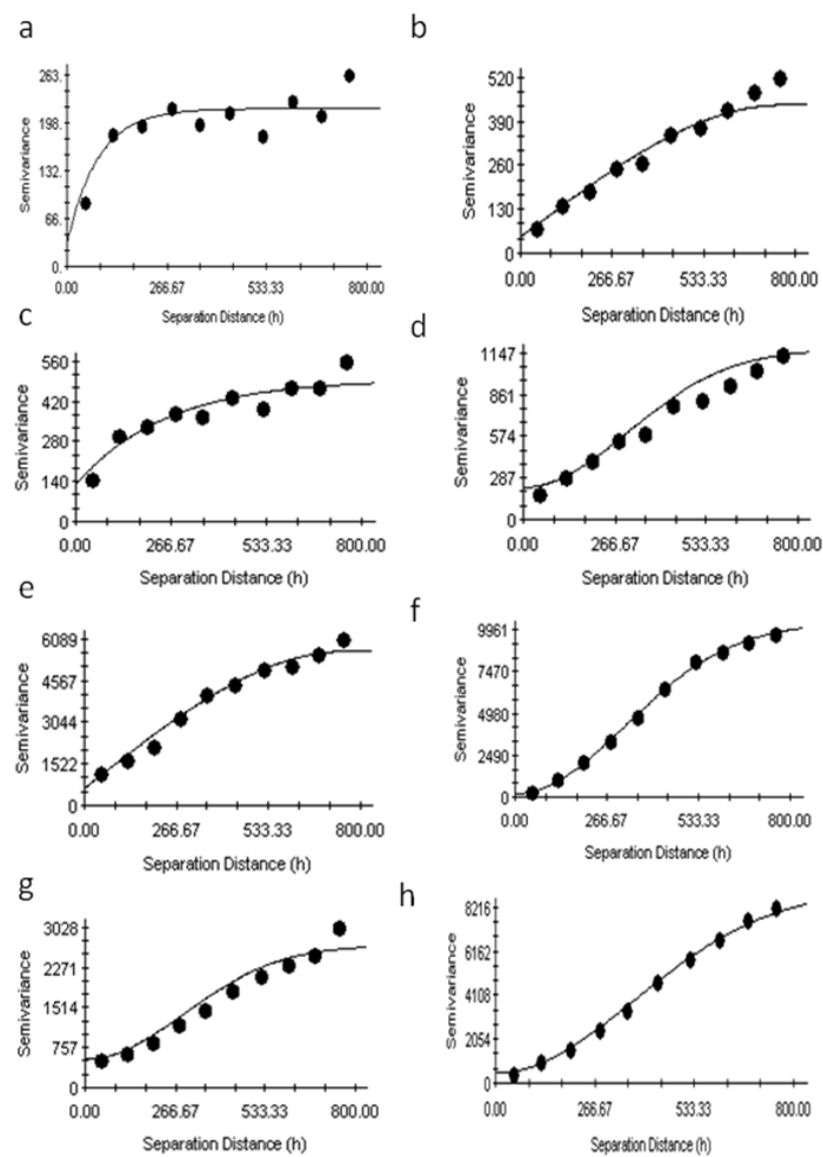


Figure 5.18 : Semivariograms of Transect, Left side: 2003 SPOT image, right side: 2007 SPOT image.

The increasing variability with the lag distance is attributed to the increasing heterogeneity in canopy structure and thus canopy diversity. The decreasing range indicates that land cover changes occurs in local scale, however increasing range shows that land cover changes occurring in large areas.

Long range indicates that DN numbers of the transect are different from each other. This means that through the transect spatial variability is increasing.

Table 5.16: Range, nugget, and sill values for selected transect.

Transect	Graph in figure	Sill	Nugget	Range (m)	R ²
2003	A	220	44	346	0,888
2007	B	435	46	622	0,976
2003	C	450	140	630	0,984
2007	D	870	190	780	0,998
2003	E	5560	507	710	0,963
2007	F	9930	10	800	0,998
2003	G	2523	504	625	0,956
2007	H	8026	680	800	0,971

5.7.2 Tasseled Cap Transformation

The Tasseled Cap Transform (TCT) is a vegetative index commonly used as an indicator of vegetation health and assessing vegetation and land cover change. Brightness, Greenness and Wetness features derived by using Gram Schmidt Orthogonalization technique given in title 4.2.2.2 based on Ivits et al., 2008. The TCT requires coefficients for brightness, greenness and wetness components and these coefficients are specific to each sensor. Therefore, these coefficients are not stable between different seasons and geographical locations. They can be used successfully for land cover discrimination if the images are transformed with parameters appropriate to the investigated season respective biogeographical zone. TCT components were produced for SPOT 5 image of the study area and derived TCT coefficients for SPOT image given in Table 5.17.

Table 5.17: Tasseled cap coefficients for SPOT 5 data at satellite reflectance.

SPOT 5	Green	Red	Near Infrared	Short Wave Infrared
Brightness	0.201	0.397	0.548	0.707
Greenness	-0.180	-0.330	0.832	-0.408
Wetness	0.388	0.573	0.013	-0.724

By using these coefficients brightness, greenness and wetness images were produced and resultant images are depicted in Figure 5.19.

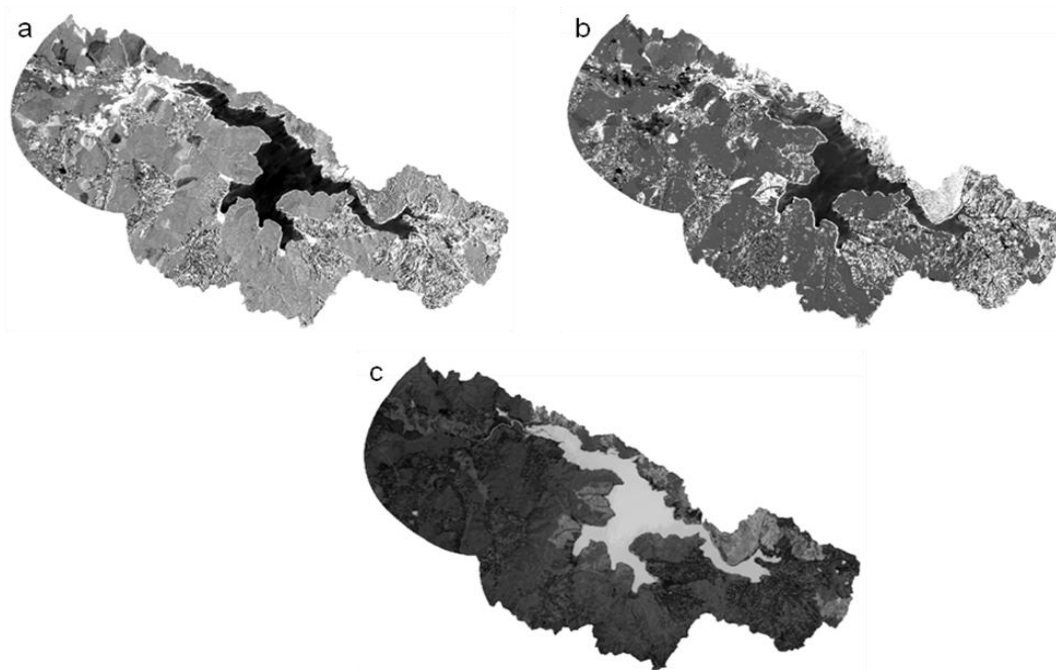


Figure 5.19 : Difference images produced by TCT a) Brightness, b) greenness and c) wetness.

The three derived axes explained greater than 99% of the variance of the test image. Given that our study area primarily consists of agricultural land, and sparsely vegetated areas. Wetland vegetation appears lighter than other green vegetation on the SPOT image in brightness and in greenness image.

5.7.2.1 Change Vector Analysis

A model in Erdas Modeler tool were produced to calculate the results of CVA. The detailed description of the model is given in Figure 5.20 and the model is produced based on Flores and Yool, 2007. This method derive the information about both the amounts and types of changes in the data. The output of the model includes the magnitude and three direction images. The magnitude image produced based on the

equation 4.14. The image obtained was used to define those areas that had significant changes between the two images. Figure 5.21 depicts the magnitude image of the study area. The direction of change was determined from the brightness, greenness and wetness direction images.

The angle of the vectors, which indicates the type of change that occurred, varies according to the number of components used (Table 5.18). In other words, each vector is a function of the combination of positive or negative changes through channels or spectral bands, which allows to distinguish 2^n types of changes. Table 5.17 shows the eight possible direction classes and their respective descriptions obtained from the three components.

Table 5.18: Change classes of raw differences in TCT components derived from the sign of the change.

Class	Brightness	Greenness	Wetness
1	+	+	+
2	+	+	-
3	+	-	+
4	+	-	-
5	-	+	+
6	-	+	-
7	-	-	+
8	-	-	-

+ indicates pixel value increase from date 2003 to 2007

- Indicates pixel value decrease from date 2003 to 2007

The change detection threshold was determined using the remote sensing analyst’s expert knowledge of the study area. Therefore, the histogram of change magnitude image is analyzed to detect change or no change threshold. Furthermore, Normalized Vegetation Index (NDVI) images of SPOT 4 and SPOT 5 were used for threshold determination. NDVI images were produced by using equation 5.1. and then depicted in Figure A.2.

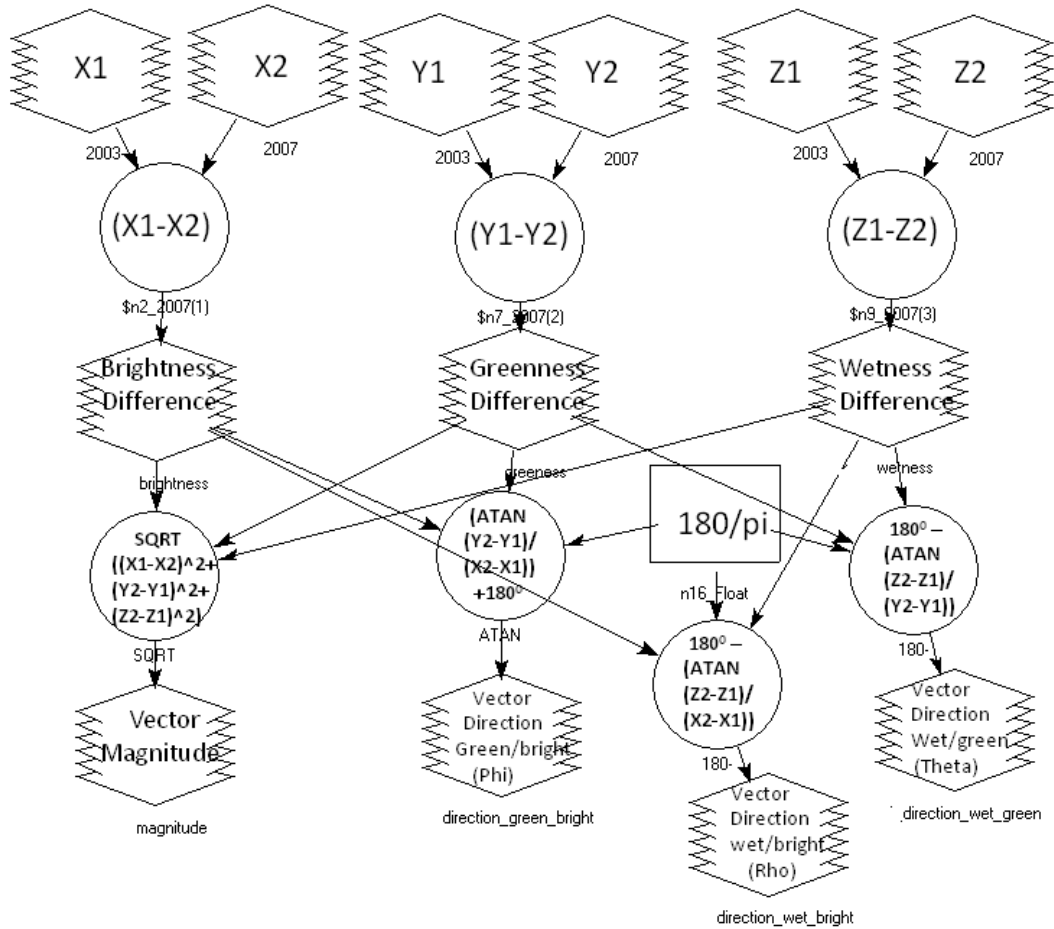


Figure 5.20 : Graphical model script of the extended change vector analysis algorithm for SPOT 4 XS 2003 and SPOT 5 XS 2007 data.

Magnitude image is shown in Figure 5.21 categorized as changed, and no changed area. White colors showed the changed area and black colors showed the non-changed areas. Gray tones can be described as minimum, lower, medium and higher changes. The classification can be grouped in three level includes Level I, Level II and Level III. The level I area is no change areas. No change is the areas, which changes spectral at very little level, so it can be ignored and consider as no change in the study period. The area in no change is water. Minimum, Lower, Medium and Higher changes can be grouped as Level II. This is spectral change areas but it does not show classes replacement.

Level II stands for the change of quality inside each class of land cover. Level III includes changed area shows the maximum spectral changes (land cover changes) in the study area.

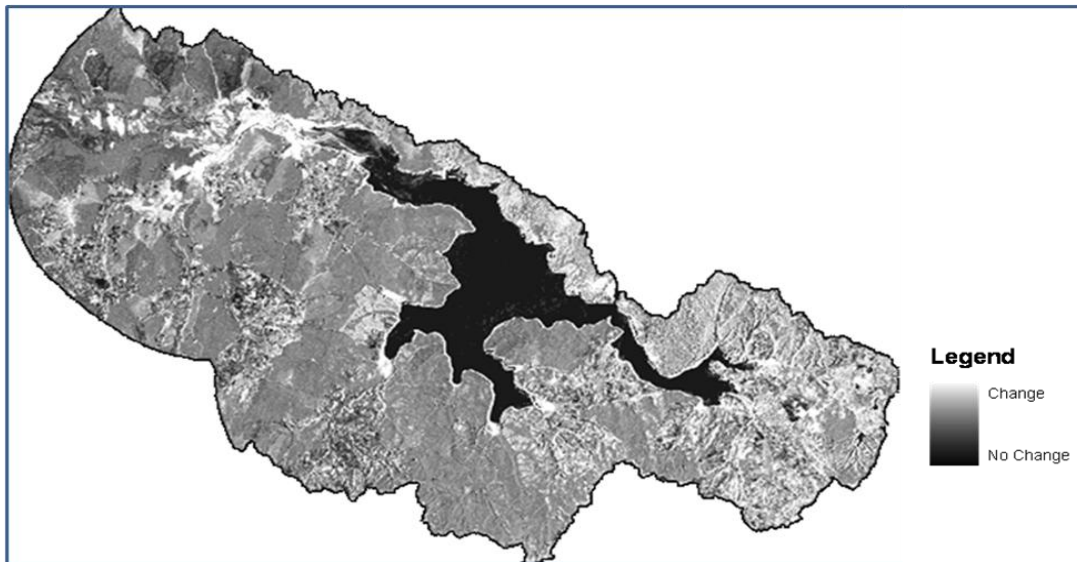


Figure 5.21 : Change vector magnitude representing the intensity of change between a pixel's brightness, greenness, and wetness in 2003 and 2007.

Magnitude image was classified as changed and non-changed area based on threshold value. This value is determined by using statistic of the magnitude image and analyst knowledge about the study region. NDVI image helped for decision of the threshold value. The resultant image depicted in Figure 5.22. As a result of this process the area of changed and unchanged was found 3853 ha and 24884.84 ha, respectively.

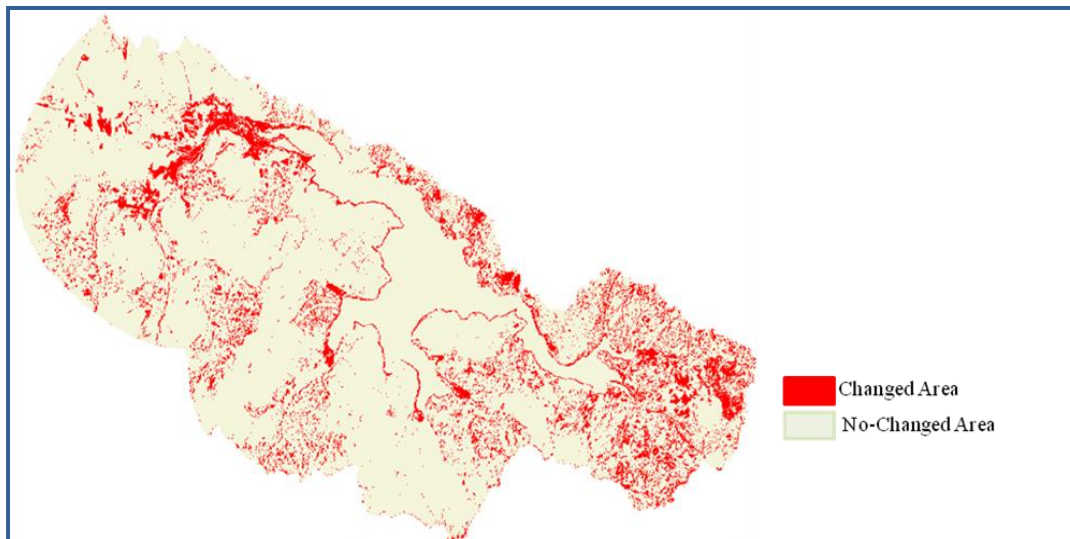


Figure 5.22 : Changed and no-changed area.

In this study, extended CVA based on the hyperspherical geometry approach implemented to measure longitude and colatitudes.

This extended approach overcomes the limitation of traditional code vector direction assignment and adds a new colatitudes measurement to increase the change extraction capabilities. Produced direction images given in Figure 5.23.

Supervised classification was applied to determine the land cover change with the help of changed and no changed area map. Three direction images stacked and unchanged areas were masked from the direction images before classification. As a result of the classification six categorized were produced only the most dynamic landscapes such as high greenness, high brightness, high wetness, medium greenness, medium brightness and medium wetness. The most dynamic landscapes were considered in this study to avoid overestimating the dynamic, from small changes occurring in the components.

Total area of change for each landscape category obtained by classifying direction and magnitude images is displayed in Figure 5.24 and the statistical results were given in Table 5.19.

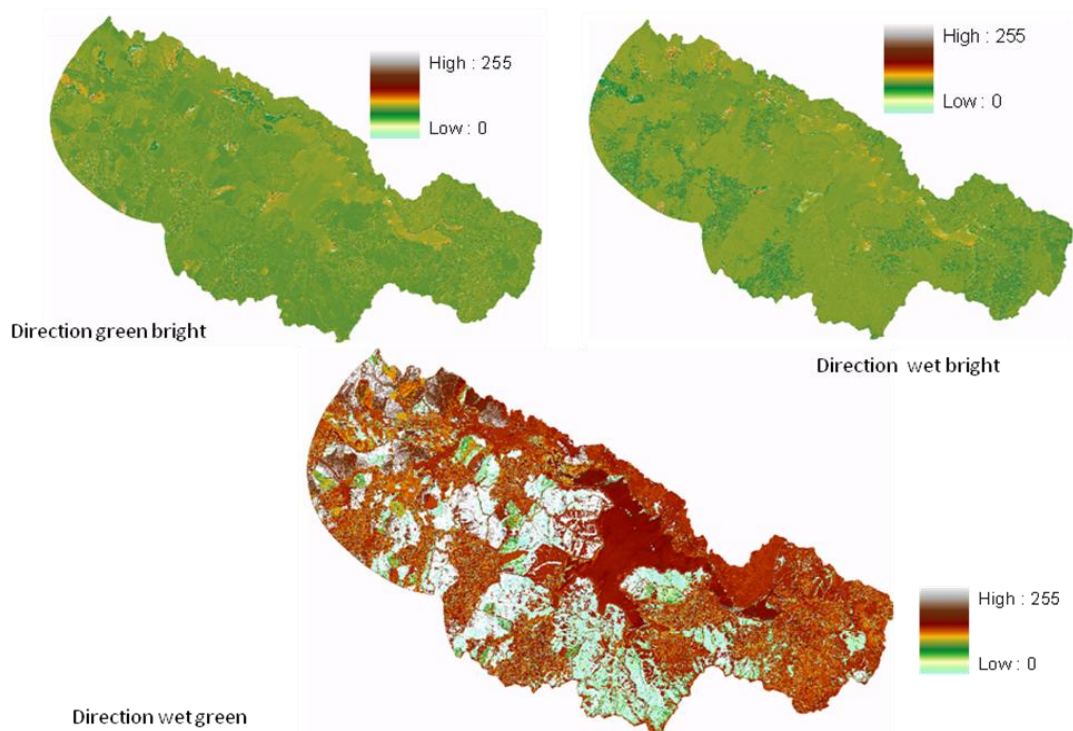


Figure 5.23 : Direction images produced by CVA.

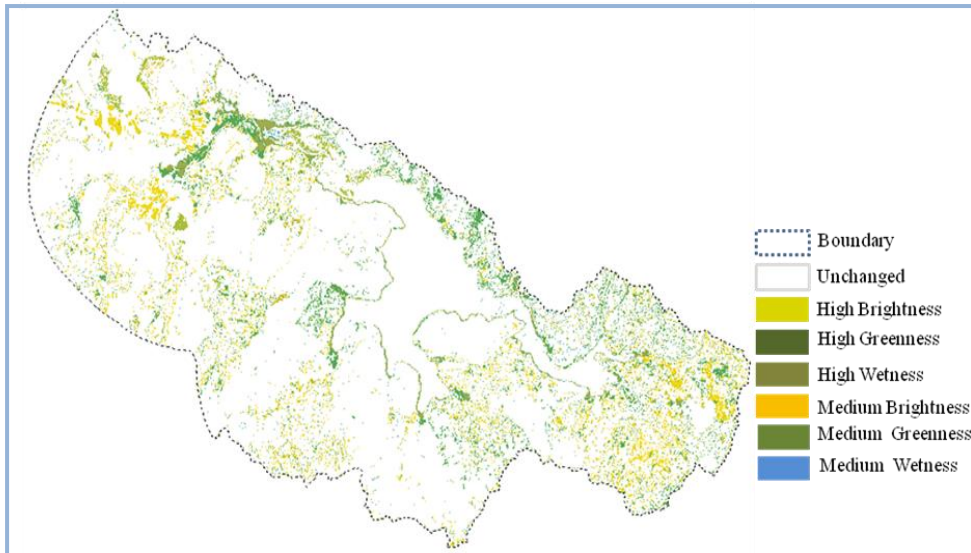


Figure 5.24 : Landscape dynamic in the Terkos derived.

Table 5.19: Landscape dynamic classes and their corresponding area in the Terkos.

Class	Value	Area (ha)	%
0	No change	24716.44	86.51
1	High wetness	350.12	1.22
2	High greenness	650.88	2.28
3	High brightness	1282.20	4.49
4	Medium wetness	131.20	0.46
5	Medium greenness	1296.60	4.54
6	Medium brightness	142.56	0.50

In Figure 5.24 each class indicates intensity of vector change in any direction within the Tasseled Cap Transformation.

5.7.2.2 Classification Accuracy Assessment

Accuracy assessment is very important for understanding the detected change results and employing these results for land management, urban land planning, and decision-making. In this study, accuracy assessment was carried out by using error matrix. The related assessment elements calculated those include overall accuracy, producer's accuracy, user's accuracy, and kappa coefficient.

Accuracy assessment of hybrid classification process was done by visual interpretation of the high resolution satellite image and field collected ground information.

Change vector analysis result was assessed by using high resolution satellite image and field collected data.

Stratified random and user-defined plots (GPS measurements) sampling methods were used for classification accuracy assessment. Congalton (1991) suggested that a good rule of thumb was to collect a minimum of 50 samples for each land-cover class in the error matrix. If the area is especially large or the classification has a large number of land-use categories, the minimum number of samples should be increased. For unsupervised and supervised classification a total of 610 reference points were selected from stratified random and user-defined plots samples to assess the classification accuracy. For the PCA based change-detection and CVA accuracy assessment at least 50 reference points were selected for the small regions. Although errors and confusion exist because of mixing problem, these two change detection methods (PCA and CVA) showed satisfying results with an overall accuracy to be 87.50% and 84.32 % and 0.85 and 0.81 for the Kappa coefficient, respectively (table 5.20). 2003 dated supervised classified image has overall accuracy of 81.41 % and Kappa value of 78 %, 2007 dated classified image has overall accuracy of 85 % and Kappa value of 83 %.

Table 5.20: Table overall accuracy and Kappa statistics result.

Accuracy Assessment	Overall Accuracy	Kappa Statistic
Unsupervised Classification 2003	76.62 %	0.74
Unsupervised Classification 2007	78.65 %	0.75
Supervised Classification 2003	81.41 %	0.78
Supervised Classification 2007	83.00 %	0.82
PCA based Change Detection	87.50 %	0.85
CVA Change Detection	84.32 %	0.81

5.8 Field Spectroscopy

The fiber optic, with the field of 8, was handheld approximately 1 m above the water surface at nadir position. The area observed by the sensor had a diameter of 18.8 cm and it was large enough to measure spectra without being influenced by the surroundings. The 20 replicate spectral measurements taken from each subplot enabled the measurement noise to be averaged out. Prior to each reflectance measurement, the radiance of a white spectralon made from a sintered poly - tetra - fluorethylene based material in other words Sintered Halon or Barium Sulfate (BaSO₄) powder and of known reflectivity was recorded for normalization of the target measurements. The field works were conducted between Jun and August in 2006 and 2007.

Spectral measurements were made on clear sunny days between 10.30 am and 2 pm in order to minimize atmospheric perturbations and BRDF effects. Terkos wetland vegetation reflectance spectra samples are depicted in Figure 5.25.

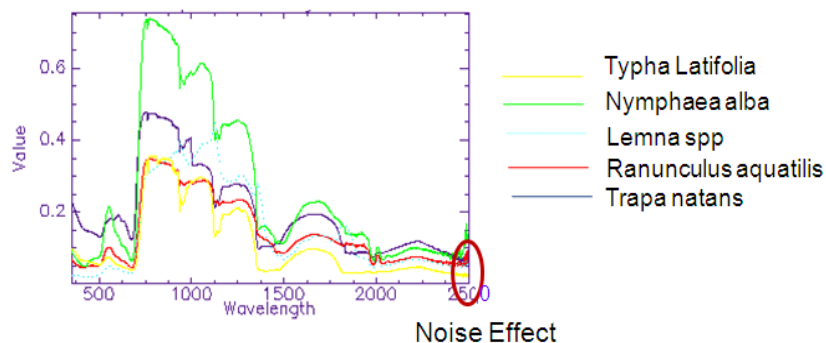


Figure 5.25 : Sample vegetation reflectance spectra from Terkos Wetlands.

The distribution of the 35 field collected reflectance data are shown in Figure 5.26.

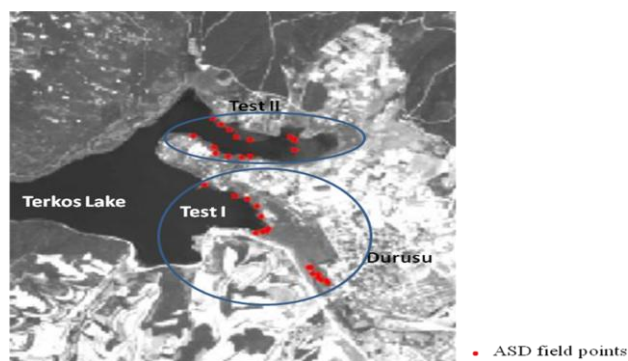


Figure 5.26 : Distribution of the field collected reflectance data.

5.8.1 Processing of field spectroscopy data

For hyperspectral remote sensing, field spectra are needed to characterize and relate the cover reflectance to image reflectance. Hyperspectral image spectra as well as field spectra are generally more noisy as compared to the controlled laboratory situation, due to the Sun's variable illumination, and the greatly reduced incoming signal. Noise is not constant over the whole spectrum; the oscillation in noise is obvious in the vegetation spectrum of Figure 5.27 a.

To minimize the noise in the measured spectral reflectance, the 20 spectra of each sample plot were averaged. Mean reflectance spectra are shown in Figure 5.25 for each sampled wetland vegetation. Bands with a wavelength less than 400 nm and more than 2400 nm displayed very high levels of noise and were excluded. The resulting wavebands were used for the analysis. A moving Savitsky-Golay filter with a frame size of 2 nd degree polynomial was applied to the averaged reflectance measurements to further smooth the spectra (Figure 5.27 b). In order to use field collected spectra with Hyperion EO-1 data, spectral resampling (downsampling) was applied to data set by using spectral response function of the image. Using spectral response function of Hyperion, that is, the wavelength center of full width at half maximum (FWHM) of each band and Gaussian filter function, ASD spectra were resampled to corresponding Hyperion bands. Resampled field spectra used in the SAM classification process to discriminate *Typha Latifolia* in the test regions.

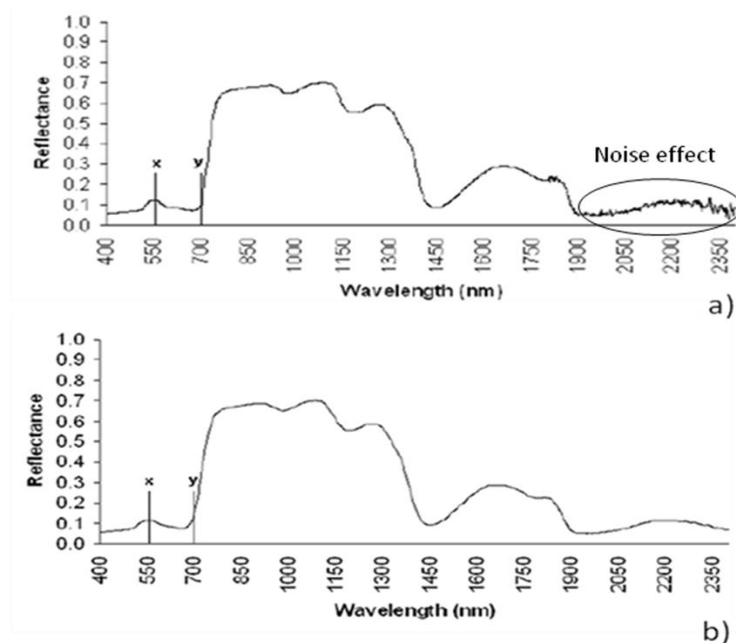


Figure 5.27 : Spectral Profile a) Mean b) Smoothed Mean.

This study aimed to investigate whether field spectrometry data could be used effectively to discriminate *Typa Latifolia* from other species occurring in the wetlands of Terkos. In other words, spectral separability analysis was used to examine whether *Typa L.* could spectrally be discriminated from the other species using field spectrometer measurements at canopy level.

One-way ANOVA (Analysis of Variance) method was used to test if the differences in the mean reflectance between *Typa L.* and the other species (*Vallisneria Spiralis*, *Lemna spp* and *Nymphaea alba*) were statistically significant. Table 5.21 shows the information about vegetation types and sample numbers. In this study, the research hypothesis that the means of the reflectance between the pairs of *Typa Latifolia* and each one of the co-existing species (VS, LS and NA) were significantly different at each measured wavelength, from 350 to 2500 nm.

The null hypothesis $H_0: \mu_1 = \mu_2, \mu_1 = \mu_3, \mu_1 = \mu_4$, versus the alternate hypothesis $H_a: \mu_1 \neq \mu_2, \mu_1 \neq \mu_3, \mu_1 \neq \mu_4$ where μ_1 , is the mean reflectance values from *Typa Latifolia* and μ_2, μ_3, μ_4 the mean reflectance values from *Vallisneria Spiralis*, *Lemna spp* and *Nymphaea alba*, respectively.

Table 5.21: *Typa Latifolia* and other wetland species in Terkos.

Species Name	Type Code	No of plots	No of measurements
<i>Typa Latifolia</i>	TL	12	60
<i>Vallisneria Spiralis</i>	VS	7	21
<i>Lemna spp</i>	LS	6	18
<i>Nymphaea alba</i>	NA	7	14

One-way ANOVA was used with a post-hoc Scheffé test at each measured wavelength for the individual class pair (TL vs. VS, TL vs.LS, and TL vs. NA). ANOVA was applied with two confidence levels: a 99% confidence level ($p < 0:01$), and a 95% confidence level ($p < 0:05$).

ANOVA results indicate that there is significant difference between the spectral reflectance and all the class pairs with a 99% confidence level ($p < 0:01$) and the 95% confidence level ($p < 0:05$). The p value was calculated 0.00 for each pairs.

5.9 Classification of Hyperion EO-1 Hyperspectral Data

Hyperion EO-1 data classified by using different methods and the results compared to determine the performance of the methods especially for the wetland vegetation and surrounded land cover mapping. After a series of preprocessing including bands removal, radiometric correction, strip removal, and geometric registration, band selection were adopted for further analysis. Hyperion EO-1 data classified based on the entire spectrum, spectrum partition analysis and spectra from MNF bands using supervised and SAM algorithm. Therefore, PCA based classification methods were applied to hyperspectral data with the help of supervised classification and SAM methods. In this stage, the following points have been addressed.

- Extracting endmember spectra for wetland vegetation.
- Exploring the uniqueness of spectral regions for the classification of wetland vegetation.
- Usability of MNF spectra coming from bands of high SNR (signal-to-noise) values for classification.
- To look at the importance of uniformity/homogeneity in vegetation cover in affective accuracy assessment.
- Usability of spectrally segmented PCA based classification for vegetation mapping.

5.9.1 Supervised and Spectral Angle Mapper (SAM) Classification

Endmember spectra of each land cover types at different bands were extracted directly from the Hyperion image and from field collected reflectance data (for wetland vegetation), and then image classified by using supervised and SAM methods. For accurate endmember collection, the center of known features (lake, grasslands, agricultural fields, etc) or known locations visited during fieldwork were selected as a sampling strategy. For the supervised *classification* field collected data used.

For the purpose of having accurate Hyperion classification a high spatial resolution multispectral base image were produced by image fusion methods. Nine different image fusion methods were applied in this study to produce a 2007 dated SPOT 5

data with four bands and 2.5 m spatial resolution. This fused data was used for ground truth data for classification process. Brovey, PCA, IHS, Multiplicative, HPF, Wavelet, LMM, LMVM and Modified IHS methods applied to SPOT 5 MS and SPOT PAN data. In order to evaluate the performance of fusion methods visual and statistical comparison methods applied. A transect is selected for statistical evaluation from the test site of the Terkos Lake (Figure 5.28). All the fusion techniques improved the resolution and the visual interpretation results. For visual comparison, a group of people interpreted the results based on spatial structure details and color distortion. Common decision was that the color conserved fusion images had the less spatial structure details. IHS, Brovey and PCA methods produced more clear spatial structures than original SPOT 5 MS data. LMM, LMVM and Modified IHS methods have the potential to keep original color. For statistical comparisons different methods were applied such as CC, RMSE, SAM, RASE and ERGAS and the results showed that LMM, LMVM and HPF have the similar spectral characteristics with the SPOT 5 MS data.



Figure 5.28 : Selected transect and test site.

Supervised and SAM classification methods were performed for the entire spectrum, VIS + NIR region (48 bands), SWIR-I region (31 bands), SWIR-II region (29 bands), bands. The results are given in Table 5.22 and Figure 5.29 for supervised classification, Figure 5.30 for SAM classification. CORINE land cover categories were followed for the classification process. Fused SPOT 5 data was used as a reference map for accuracy assessment of classification.

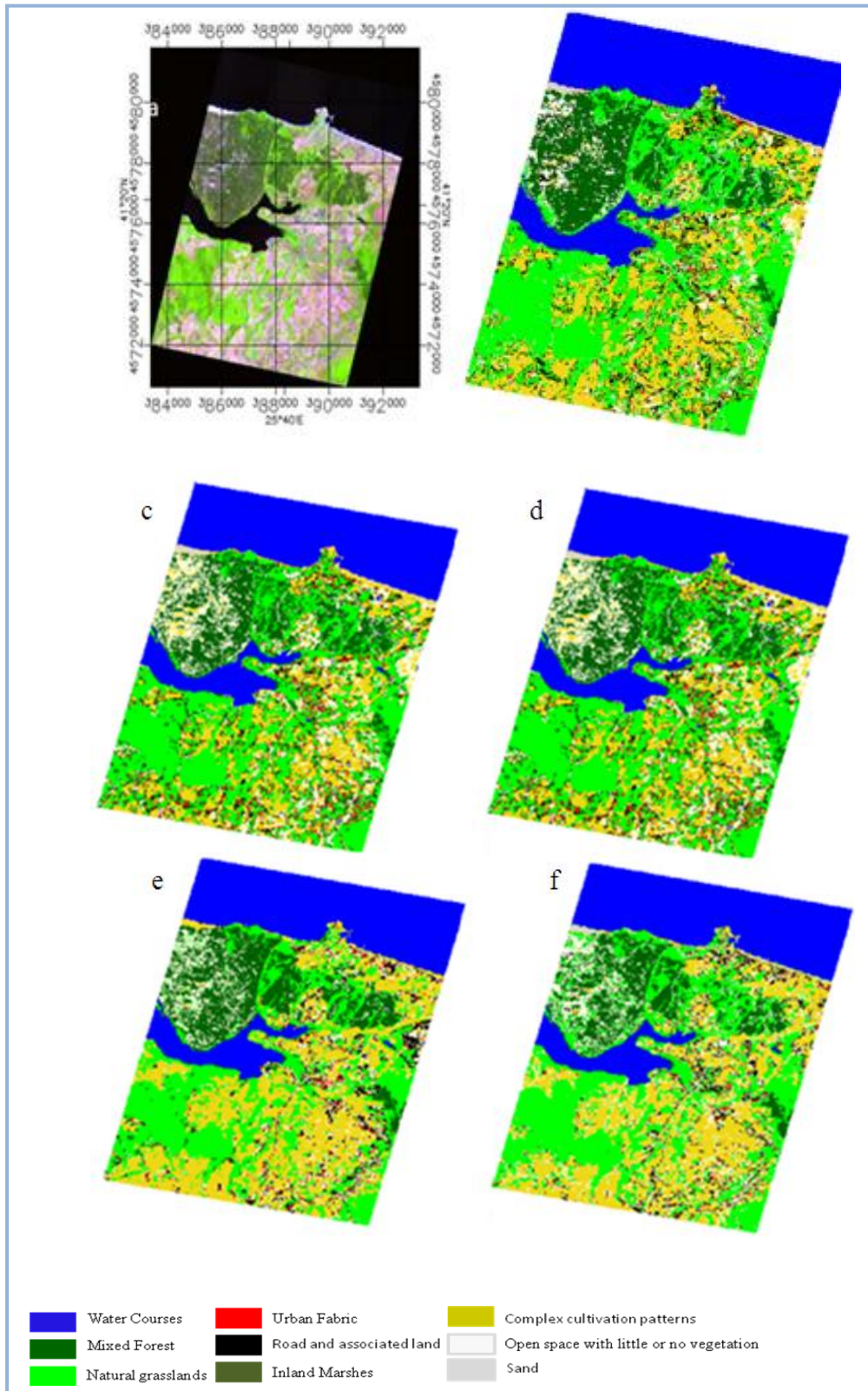


Figure 5.29 : Hyperion data classification with Maximum Likelihood.

Figure 5.29 includes a) Hyperion data (colour composite: SWIR-II – 1648 nm; NIR – 833 nm; RED – 660 nm), results of ML algorithm b) full spectrum (1–108 bands) c) VIS d)–NIR region, e) SWIR-1 region, and f) SWIR-2 region, respectively.

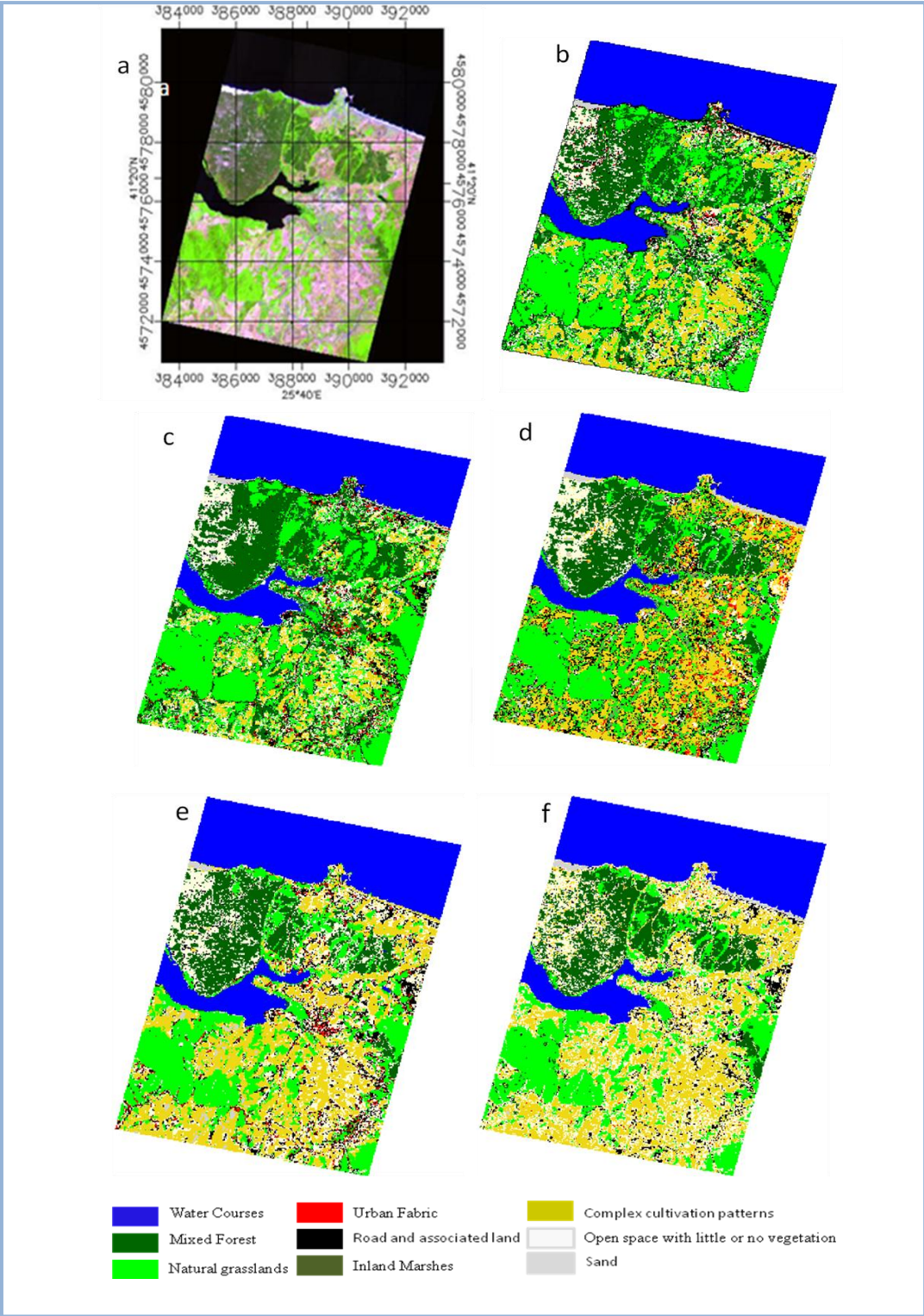


Figure 5.30 : Hyperion data classification with Spectral Angle Mapper.

Figure 5.30 includes a) Hyperion data (colour composite: SWIR-II – 1648 nm; NIR – 833 nm; RED – 660 nm), results of SAM algorithm b) full spectrum (1–108 bands) c) VIS d)–NIR region, e) SWIR-1 region, and f) SWIR-2 region, respectively.

Hyperspectral data consume large amounts of memory leading to longer processing time. Furthermore, information in the hyperspectral data is redundant to a large extent, making it difficult to extract anything useful. To overcome these difficulties, data reduction and enhancement were performed by MNF transformation using ENVI 3.6. MNF transformation was performed on all 108 bands after removing 0-value and noisy bands. The first 3 and the first 10 MNF bands were used for subsequent analysis as they contained high values of SNR. Produced MNF images were classified by using SAM algorithm to determine the performance of Hyperion EO-1 data. Results were given in Figure 5.31.

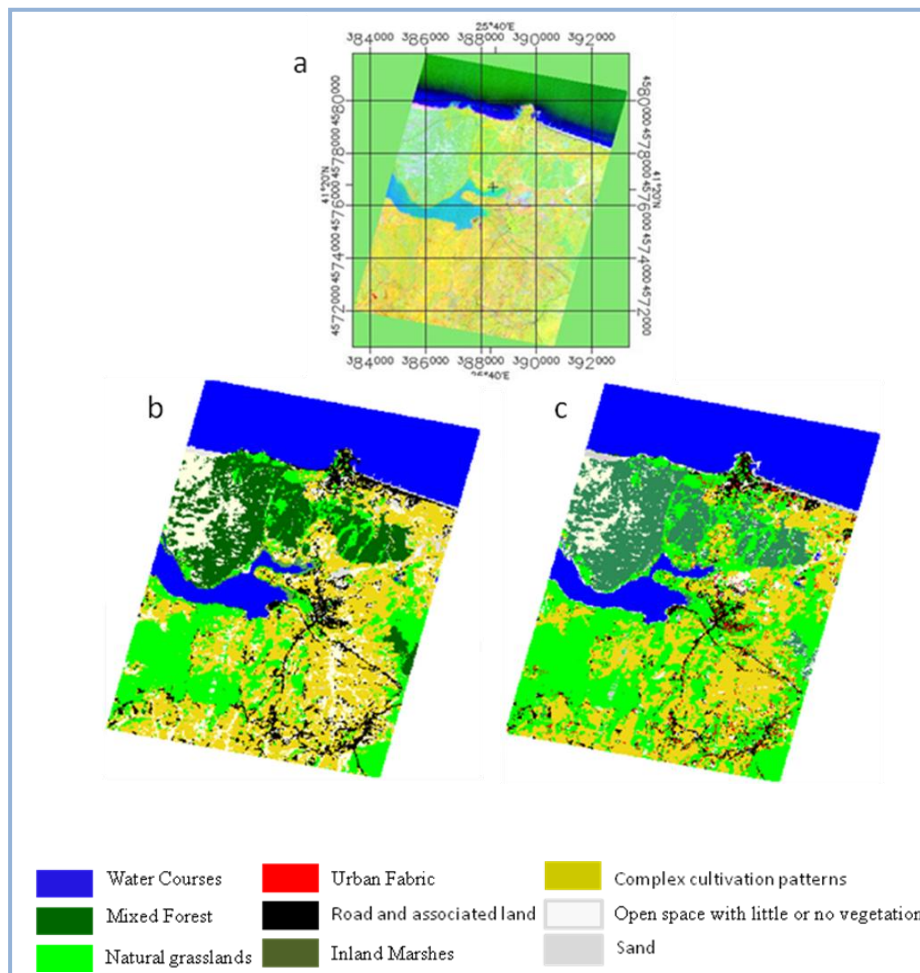


Figure 5.31 : Input data. a) MNF transformed data (colour composite of MNFbands 1–3), b) results of SAM algorithm using c) 1–10 MNF bands.

MNF used for dimensionality reduction that refers to the process by which the main components attributing to the spectral variance of the data set are identified. The aim is to reduce the information present in hyperspectral imagery so that it can be displayed in a minimized form without any alteration to the original data.

Collected GCPs and fused SPOT 5 data were used for accuracy assessment. Two measures of classification accuracy, overall accuracy and Kappa coefficient were calculated by using at least 50 training samples for some land cover types that cover small areas in the region. For the mixed forest, natural grass and agricultural categories 100 training samples were selected and used. Accuracy assessment was determined by calculating overall accuracy and Kappa statistic and the results were given in Table 5.22.

Table 5.22: Overall accuracy and Kappa statistics using different band combinations and MNF transformation.

Accuracy Assessment	Overall Accuracy		Kappa Statistic (%)	
	Supervised and SAM		Supervised and SAM	
108 bands	78.62 %	80.45%	0.76	0.78
VIS region	74.28 %	75.20	0.71	0.73
NIR region	76.65 %	78.60	0.74	0.76
SWIR I region	83.00 %	85.42 %	0.81	0.83
SWIR II region	81.65 %	82.00 %	0.79	0.80
1-3 MNF		73.38 %		0.70
1-10 MNF		70.55 %		0.68

5.9.2 Spectrally Segmented PCA Classification of Hyperion EO-1 data

One important feature of hyperspectral data is its large data volume, data redundancy and band correlation. Spectrally segmented PCA based on different spectral characteristics of vegetation over different wavelength regions were developed in this stage of the study. The method can not only reduce the large data volume but also extract helpful and reliable information to differentiate land cover categories especially wetland vegetation in the Lake Terkos Basin.

According to Bell and Baranoski (2004), the number of principal components varies from one species to another and from one region to another. They showed that conventional PCA worked effectively in visible to near-infrared regions to

reconstruct of reflectance and transmittance of different vegetation species from field collected spectra data. In this study, spectral segmentation was applied to Hyperion data based on the spectral characteristics of vegetation over different regions of wavelength.

The general procedure of spectrally segmented PCA for plant mapping was separated into several phase as illustrated in Figure 5.32 based on Tsai, et al, 2007. Supervised and SAM classification methods were applied to spectrally segmented data set. The results compared with the traditional PCA based classification result to determine the performance for the heterogeneous region.

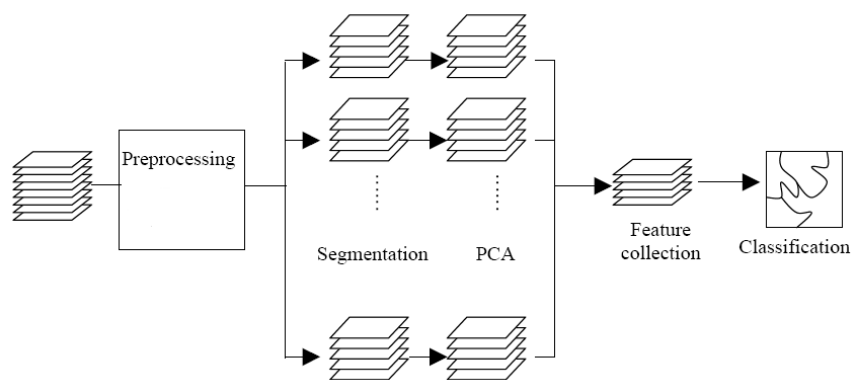


Figure 5.32 : General procedure of spectrally segmented PCA.

Preprocessed Hyperion data with selected 108 bands was cropped out as the base image for classification. After preprocessing, a vegetation index was calculated from selected suitable bands of the image. The index was used to filter out non-vegetation covered areas in the region.

In this study, band-30 (650 nm) and band-50 (854 nm) were selected to compute NDVI (Normalized Difference Vegetation Index) and a threshold was set to determine non-vegetation pixels of the image. To determine the best threshold, masking results of different NDVI thresholds were compared with fused SPOT 5 data of the study area and 0.25 was found to be the most suitable cut off for separating vegetated and non-vegetated areas in the Hyperion EO-1 data (Figure A.3).

Total 108 Hyperion bands were divided into four groups based on spectral characteristics of the vegetation over different wavelength sections. The four groups listed in Table 5.23 with wavelength and number of the bands.

Table 5.23: Four –group segmentation for spectrally segmented PCA.

Group	Wavelength (nm)	Number of bands	Description
VIS	427-660	24	Reflectance and transmittance are both relatively low because of high absorption in pigments of leaf tissues (chlorophyll).
NIR	671-905	24	Vegetation reflectance is strong because of multiple internal reflections in foliage structures.
SWIR-1	993-1336	31	Absorption is predominated by the water content.
SWIR-2	1507-2042	29	Absorption is predominated by the water content.

After the spectral segmentation, PCA applied to each spectral group independently for feature extraction. Based on Eigen analysis, the first few PCA components were collected from each segmented group for a Maximum Likelihood supervised classification and SAM. For the process three PCs in VIS, two PCs in NIR, two PCs in SWIR-1 and one PC in SWIR-2 were collected. Eight PCs from different spectral group were stacked and a new image produced. For comparison, classified image using first three PCs generated from conventional PCA.

Vegetation categories in the test site were sparsely vegetated area, natural grassland, mixed forest and inland marshes vegetation species.

ASD field spectroradiometer data were used for marshes vegetation species as ground truth data and the other reference data were extracted from fused SPOT 5 MS image. The results of all experiments are depicted in Figure 5.38. Evaluations of produced images were given in Table 5.24 with overall accuracy and Kappa values.

PCA was performed to the Hyperion image with 108 band, the first three PCs of Hyperion accounted for 99.3% of total information, which were selected to apply supervised classification and SAM, the classification result was shown in Figure 5.33 and evaluation were given in Table 5.24.

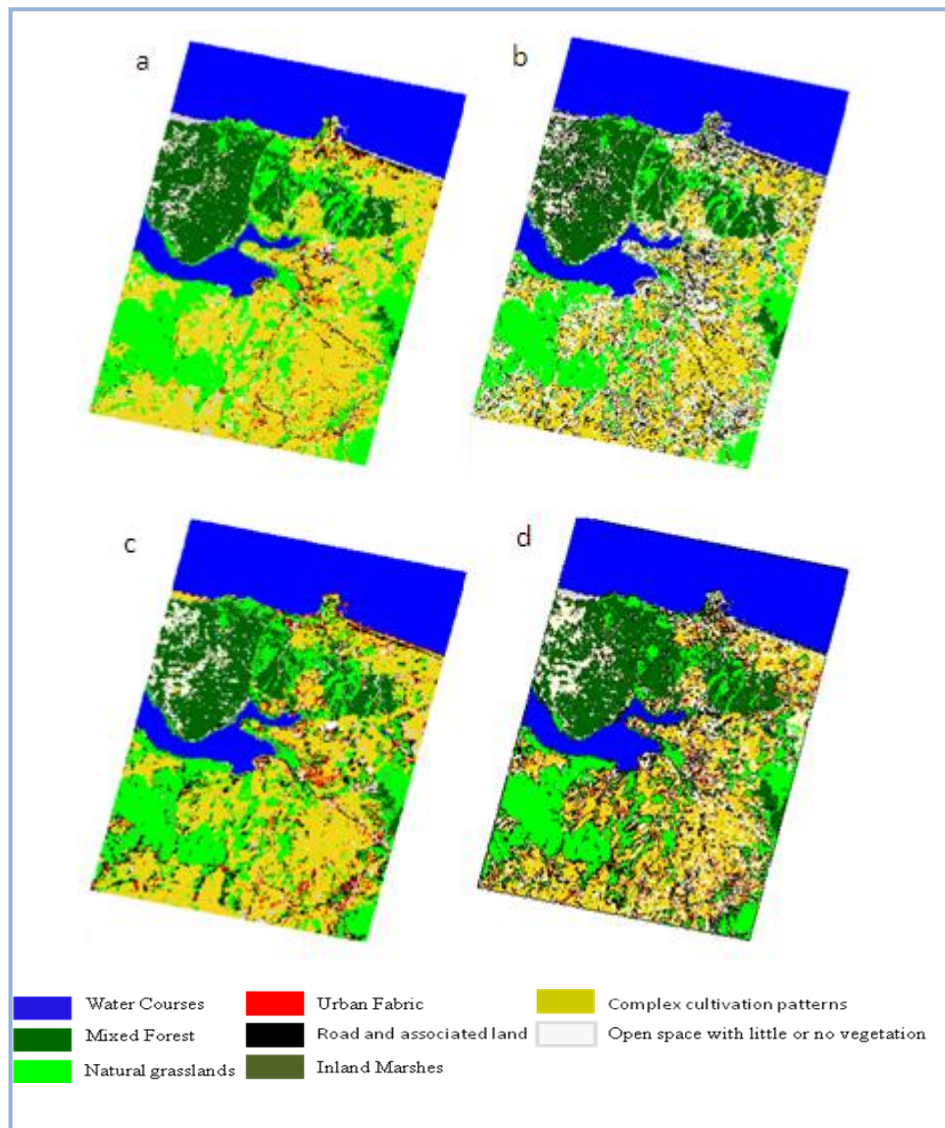


Figure 5.33 : PCA segmented and PCA all Hyperion Classification a) ML and b) SAM c) ML d) SAM.

In this study we tested the applicability of Hyperion for mapping monodominant stands of *Typha Latifolia* in the wetlands of the Terkos Lake. With PCA segmented process and SAM classification, it is possible to separate *Typha Latifolia* than other vegetation areas. It can be seen clearly from the Table 5.24 the highest overall accuracy value belongs to PCA segmented Hyperion SAM image. The lowest value belongs to PCA Hyperion ML image. The highest Kappa statistics value belongs to PCA segmented Hyperion SAM image and the lowest Kappa statistics value belongs to PCA Hyperion ML image.

Table 5.24: Overall accuracy and Kappa statistics.

Accuracy Assessment	Overall Accuracy	Kappa Statistics
PCA Segmented Hyperion ML	78.62 %	0.76
PCA Segmented Hyperion SAM	81.00%	0.79
PCA Hyperion ML	72.42 %	0.69
PCA Hyperion SAM	76.00 %	0.73

6. RESULTS AND CONCLUSIONS

Owing to the biological diversity, natural functions and financial values they have, wetlands are the most important ecosystem of the earth. Cutting reed beds, drainage for agricultural activities, and usage for drinking water supply and unplanned urbanization are the main reasons for wetlands loss and degradation. Accurate and reliable data and data processing methods are needed to preserve, manage and develop wetlands. The technology that enables production of multi-purpose maps via data support and continuous monitoring of these lands is required. Remote sensing technology is defined as a powerful and useful tool that enables providing accurate and temporal data of wetlands.

In this study, different remote sensing methods were applied to a variety of satellite data set to determine the performance of the remote sensing technology for heterogeneous natural area mapping and monitoring. Results were given in the following sections.

6.1 Preprocessing Results

First step of any image processing procedure is to apply atmospheric, radiometric and geometric corrections of satellite images to eliminate atmospheric distortions, sensor problems and geometric distortions. In this study, radiometric correction was applied by using PIF method. Atmospheric correction was applied to multispectral data by using DOS (Dark Object Subtraction) method and FLAASH was used for the atmospheric correction of hyperspectral data. For the hyperspectral Hyperion data with spectral 242 bands, band selection procedure was applied because of its noisy and overlapped bands problem. As a result, 108 bands were used for the further analysis with Hyperion. Geometric correction was applied to all data set by using ground control points. Classification was the last step to create land cover data and determine land cover changes by using multitemporal remotely sensed data.

Another important issue is to select appropriate band combinations for the study. Incorrect usage of different band combinations or panchromatic band directly affects

the results derived from satellite image data. Best band combination selection employed by using correlation matrix and Optimum Index Factor for multispectral SPOT data set. The results of this study illustrated that appropriate band selection could improve the accuracy of classification.

6.2 Change Detection Results

Land cover change detection is a very important step for natural area conservation and management. Different methods were applied in this study and their results showed that land cover changes occurred between the year of 2003 and 2007 in the basin. Three different change detection methods were applied to SPOT 4 MS and SPOT 5 MS data, such as unsupervised and supervised classification, PCA based land cover change detection and Modified Change Vector Analysis.

Unsupervised and supervised classifications were conducted for determining land cover change detection in the basin. The results showed that there is a decrease in the mixed forest, wetland and natural grassland areas in the region. Area of the wetlands decreased from 407.72 ha to 249.32 ha, and agricultural areas increased 2050.12 ha. In the region water area decreased by 287.48 ha and natural grassland decreased by 1503.20 ha. Accurate and reliable information is needed about the changes for sustainable management of the region. Because of the difficulty in labelling and obtaining 'from-to' change class information, PCA was employed to enhance the change information from original images. In fact, classification intrinsically affects the whole accuracy of change detection. A hybrid classification process combining unsupervised and supervised approaches is performed on the PCA-enhanced multitemporal change image. This hybrid classifier has the potential to produce class signatures that are numerically separable in feature space and land-use classes which are meaningful to the analyst for more accurate change detection. The results depicted that major damage occurred on natural grassland of the Terkos Water Basin. 1059 ha of natural grassland was changed to agricultural area and 562.12 ha of the natural grassland was converted into open space in the study region. An area of 156.44 ha changed from wetland to open space. There is a perceivable decrease in water surface area. Total lake area decreased during these years. This method needs field data or combining with visual interpretation of multi-date image for accurate examination of the resultant image for change detection. Therefore, mCVA method

applied to SPOT data set to determine the land cover changes by using TCT components brightness, greenness and wetness. The classification accuracy comparison between unsupervised and supervised classification, PCA based classification and mCVA analysis showed that which method can be used more effectively for complex natural area studies. For the change vector analysis, three TCT difference images, one change vector magnitude image, three vector direction images, and one final landscape dynamic image depicting the most changed landscapes were derived. For the change detection, threshold value was determined by using statistical calculations and analyst expert. Also this value checked by using Jenk's method. The advantage of the method is that it has the ability to process any number of spectral bands but it is difficult to decide changed classes and threshold value. According to the results, an increase in the agricultural and minig areas occurred. The greenness and wetness difference images show more concordant patterns. In the greenness image, especially the new forest area in the nort part of the lake has increased values together with some of the agricultural lands in the basin. In the wetness image, especially rice fields and open areas with little vegetation had high values. The largest increase in greenness was recorded in semi natural areas in the basin. Similarly, these areas showed the largest decrease in brightness. The change vector magnitude image summarizes the total change length per pixel represented as the Euclidean distance between the location of a pixel in TCT feature space in 2003 and 2007. This image represent the intensity of the change, which increases in the sand, agriculture, open spaces with little/or no vegetation and a part of vegetated areas. The largest increase in change vector magnitude is registered in agricultural fields because of the shape differences and heterogenous product type in the area. The presence of growing crops and growing young trees at the time of SPOT 5 image acquisitions resulted in extreme land cover changes in the area. The area that shows little change is urban areas and some of the agricultural fields. This area, which is under conservation by the low and urbanization is forbidden in the conservation zones. Because of this reason, urbanization is very limited in the area.

Longitude vector direction image shows a large brightness increase in the vegetated areas. Barren lands, according to classification results also show increase in brightness. Conversely, most of the semi natural and mixed forest communities register a vector direction change towards the greenness axis. The collatitude vector

direction image shows very small vector changes in the greenness-wetness plane. We can see very small changes in the open spaces with little or no vegetation. Also, it is possible to see some changes in the sand part of the study area. The colatitude vector direction is the vector direction component that shows larger variation of vector displacements. The results were quite similar from the longitude and colatitude vector direction image. Accounting for vector changes in the wetness-brightness plane, colatitude was able to enhance more bright features in the vegetated and agricultural lands. The most important disagreement of colatitude with the other two vector direction components is at the areas occupied with young generation trees in the north site of the lake (sandy area).

The accuracy assessment of classification was calculated by using error matrix for three different methods and the results were compared with each other. Based on the overall accuracy and Kappa statistics, the accuracy slightly improved from 76.62 % to 81.41 % for 2003 dated unsupervised classification and supervised classification methods with Kappa statistic increased from 0.74 to 0.78, respectively. Therefore, there was slight increase for 2007 dated unsupervised and supervised classification methods from 78.65 % to 83.00 %, with Kappa statistic increased from 0.75 to 0.82, respectively. For the PCA based change detection method the overall accuracy was 87.50 % and the Kappa value was 0.85. The overall accuracy was 84.32 % and Kappa value was 0.81 for mCVA method. PCA based change detection method had the higher overall accuracy and Kappa value than the other two methods. Comparison of accuracy assessments between three change detection methods showed that better change detection results can be obtained by using PCA based change detection method.

In this study, spatial variation analysis was employed as supportive method of change detection results. Spatial profiles were used to visualize the spatial differences between these years. A transect was selected from the test area I that includes water, wetland, urban and agricultural lands and spatial profiles were produced for the years of 2003 and 2007. Based on the gray value differences between the years spatial profiles of changed area supported the change detection results. Semivariogram, a graphical representation of the spatial variability in a given set of data used to assist the change detection results based on spatial information. With the help of the spatial information, it is possible to evaluate canopy structure

and species diversity. For the change detection analysis, different semivariograms were produced for the years of 2003 and 2007 with the help of the selected transect and the results were compared with each other for different bands. Semivariogram parameters were used to identify abrupt land cover changes within the selected region. The results showed that the semivariogram is a sensitive and effective tool to derive change detection information from satellite images. Using semivariograms and spatial profiles, regions faced with significant land cover changes were determined easily and accurately.

6.3 Field Spectroscopy Results

ASD collected field reflectance data was used as training data for wetland vegetation in the classification process of Hyperion. Field reflectance data were gathered from five different wetland vegetation species in the two test regions. Totally 35 plots were used in the study and 20 reflectance measurements consistently taken for at least three vegetation samples at each side. Mean and standard deviations were calculated for each sampling plot to have homogeneity. Collected field reflectance data were analyzed using ASD pre-processing programs for integration with Hyperion Data. A moving Savitsky Golay filter with a frame size of 2-nd degree polynomial was applied to the averaged reflectance measurements to smooth the spectra. In order to use collected spectra with Hyperion EO-1 data, spectral resampling was applied to data set by using spectral response function of the image. Resampled spectra were integrated with SAM classification process as reference data set.

In order to examine the wetland vegetation species discrimination ANOVA method was applied to ASD field spec collected reflectance values. For the study, reflectance values gathered from five different wetland vegetation species at the canopy level. To minimize the noise in the measured spectral reflectance, the 20 spectra of each sample plot were averaged. Four of the species (*Typha L.* and the other species (*Vallisneria Spiralis*, *Lemna spp* and *Nymphaea alba*) were selected for the statistical analysis. One-way ANOVA method used with a post-hoc Scheffé test at each measured wavelength for the individual class pair (TL vs. VS, TL vs.LS, and TL vs. NA). ANOVA was applied with two confidence levels: a 99% confidence level ($p < 0:01$), and a 95% confidence level ($p < 0.05$). ANOVA results indicate that there is a

significant difference in the spectral reflectance between all the class pairs with a 99% confidence level ($p < 0.01$) and the 95% confidence level ($p < 0.05$). The p value was calculated 0.00 for each pairs. The results showed that the discrimination between species is possible by using field collected spectra.

6.4 Hyperspectral Classification Results

The capability of Hyperion spaceborne hyperspectral data was analysed for discriminating land cover in a complex natural ecosystem according to the CORINE classification system . For this purpose, 2007 dated Hyperion imagery was acquired over Terkos Lake (Istanbul). Therefore, in this study applicability of Hyperion was tested for mapping monodominant stands of *Typha Latifolia* in the wetlands of the Terkos Lake. Different spectral ranges of the selected 108 bands of Hyperion were used for classification purposes with the help of different transformation methods such as MNF and PCA. Supervised and SAM classification methods applied original Hyperion with 108 bands, and Hyperion with four different spectral range (VIS, NIR, SWIR I and SWIR II). Comparisons of accuracy assessments between four spectral regions showed that better classification results can be obtained by using SWIR I region.

Furthermore, MNF was applied as a transformation method and the results of first three MNF components, and the first ten MNF components were employed for SAM classification. The overall accuracy was 73.38 % and Kappa statistic was 0.70 for first three MNF components. Based on the overall accuracy and Kappa statistics, for the first fifteen MNF components a slight decrease from 73.38% to 70.55 % and 0.70 to 0.68 were observed respectively. Comparisons of accuracy assessments between two SAM results showed that better classification results can be obtained by using first three MNF components.

PCA was applied to all 108 band data and the four spectral range data to produce new data set for SAM classification. Resampled field reflectance data collected with ASD was used as training data for wetland vegetation in the classification process. At the end of this phase it is concluded that by using Hyperion, wetland vegetation cover are distinguishable from other green lands and despite having medium spatial resolution, there is not a mixture between wetland vegetation and other vegetated areas. The classification results demonstrated the capability of the Hyperion

spaceborne hyperspectral sensor in discriminating, at the pixel level, vegetation cover up to the 3 rd CORINE Land Cover level within a fragmented landscape, such as that of Terkos Water Basin. Overall accuracy was 78.62 % and Kappa statistic was 0.76 for PCA segmented ML classification. For PCA with 108 bands ML classification, the overall accuracy was 72.42 % and the Kappa value was 0.69. The results showed that spectrally segmented PCA ML classification method had better accuracy than the other method. Overall accuracy was 76.00 % and Kappa statistic was 0.73 for PCA with 108 bands SAM classification. Among classification methods spectrally segmented PCA SAM classification had the ability to discriminate Typa L. better than the other classification methods with the 81.00 % overall accuracy and 0.79 Kappa values.

6.5 Conclusion

In this study, CORINE legend was used for multispectral and hyperspectral data classification. In this context, eight different land cover types for multispectral data and nine different land categories for hyperspectral data were examined using data from 2003 and 2007. In CORINE system, the classes define the cover types in a hierarchical structure. The results have depicted that by using multispectral SPOT 4 and SPOT 5 data, it is possible to obtain categories on the third level (last level of system) of the CORINE system. The third level, according to CORINE methodology, is formed by the sub-classes of second level classes and can be used on studies evaluated at 1/25 000–1/50 000 scales. Therefore, the results show that by spaceborn hyperspectral sensor it is possible to derive classes up to the 3 rd CORINE Land Cover level.

Mixed pixels are the main problem for this study. Trying to get wetland vegetation information from multispectral and space born hyperspectral data is generally a big issue because of the coverage of the wetland vegetation in the scene and resolution of the remotely sensed data. With this study, the ability of different remote sensing data was evaluated to produce land cover and land cover change maps of the heterogeneous natural area including water bodies, wetlands, mixed forest, open space with no or little vegetation, sparsely vegetated areas, agricultural lands, roads and urban areas.

As a result of this study it is found that spatial and spectral resolution of remote sensing data is a valuable input for wetland studies. Different data set were compared and it is concluded that wetland mapping studies with fieldwork is more expensive and more affordable than acquiring remote sensing data. When each type of imagery were analyzed separately, the results showed that there is a mixed class problem between sparsely vegetated area and wetland vegetation in medium resolution multispectral data such as SPOT XS, SPOT 4 and SPOT 5 MS due to the same reflectance properties. The improvement on accuracy of the classification can be seen clearly for hyperspectral Hyperion EO-1 data. The discrimination between wetlands and sparsely vegetated area is possible by using different classification algorithms. Especially by using spectrally segmented PCA, it is possible to determine wetland species with the help of SAM. Results of classification and change detection methods have been given in Table A1.

Wetlands need to be conserved and managed by using effective and improved technologies. Especially in Turkey we do not have the opportunity to get airborne hyperspectral data that have high spatial and spectral resolution because of restriction and rules. At the same time, it is an expensive technology. In the view of these circumstances, wetland research needs to be implemented by using available data set such as medium and high spatial resolution satellite images or spaceborn hyperspectral data set. Variety of remote sensing data can be enhanced with the help of field collected reflectance data.

For detailed classification, derived vegetation species information has huge importance and this can be achieved by using field collected spectral reflectance data. Integration of hyperspectral data with reflectance data is more valuable for wetland studies especially when there is no chance to get airborne hyperspectral data.

Overall results illustrated that different kinds of images can be used to derive past and present land cover of the concerned region. Implementing different land cover change analysis methods showed that it is possible to use medium spatial resolution data for heterogeneous natural areas taking mixed pixel problem into consideration. Evaluating different classification and transformation methods individually and together gave chance to analyze the performance of these methods for complex regions. These results can be used to produce a base guideline for Turkish wetlands research and management activities in the future studies.

For the future studies, different satellite sensor images and different digital image processing techniques can be used to derive land cover datasets for complex natural areas. Medium resolution SPOT data are alternative source of creating land cover data for finer scales and small regions but mixed class problem needs to be considered. In this context, new generation high resolution satellite images can be used. Sub-pixel mapping technology can be improved the classification results especially for vegetation species discrimination. New vegetation indices can be derived using satellite images and remote sensing techniques and these products can be integrated with satellite images to improve the accuracy of classification.

REFERENCES

- Adler Golden, S., Matthew, M. W., Bernstein, L. S., Levine, R. Y., Berk, A., Richtsmeier, S. C., Acharya, P. K., Anderson, G. P., Felde, G., Gardner, J., Hoke, M., Jeong, L. S., Pukall, B., Mello, A., Ratkowski, A., Burke, H. H.,** 1999: Atmospheric correction for shortwave spectral imagery based on MODTRAN4. *Imaging Spectrometry, SPIE*
- ASD.,** 2007: FieldSpecH 3 User Manual (Boulder, CO: Analytical Spectral Devices Inc.).
- Atlas Dergisi,** 2006: Türkiye Sulak Alanlar Haritası
- Atkinson, P.M., P, Lewis.,** 2000: Geostatistical classification for remote sensing: an introduction. *Computers & Geosciences*. Vol. **26**, pp. 361-371.
- Augusteijn, M. F., Warrender, C. E.,** 1998: Wetland classification using optical and radar data and neural network classification. *International Journal of Remote Sensing*. Vol. **19**, no. 8, pp. 1545-1560.
- Bacour, C., Jacquemoud, S., Tourbier, Y., Dechambre, M. and Frangi, J.-P.,** 2002: Design and analysis of numerical experiments to compare four canopy reflectance models. *Remote Sensing of Environment*. Vol. **79**, pp. 72-83.
- Baker, C., R, Lawrence., C, Montagne., and Patten, D.,** 2006: Mapping wetlands and riparian areas using Landsat ETM+ imagery and decision-tree-based models. *Wetlands*. Vol. **26**, no. 2, pp. 465-474.
- Bakker, W. H., Schmidt, K.S.,** 2002: Hyperspectral Edge Filtering for Measuring Homogeneity of Surface Cover Types. *Photogrammetry Engineering & Remote Sensing*. Vol. **56**, pp. 246-256.
- Balik, Sanli, F., Bektaş Balçık, F. and Goksel, C.,** 2007: Defining temporal spatial patterns of mega city Istanbul to see the impacts of increasing population. *Environmental Monitoring and Assessment*. Vol. **146**, no. (1-3),pp. 267-275.
- Baykal, B. A., Tanik, A. and Gonenc, E.,** 2000: Water quality in drinking water reservoirs of a Megacity, Istanbul. *Environmental Management*. Vol. **26**, No. 6, pp. 607–614
- Beerli, O., Phillips, R., Hendrickson, J., Frank, A.B., Kronberg, S.,** 2007: Estimating forage quantity and quality using aerial hyperspectral imagery for northern mixed-grass prairie. *Remote Sensing of Environment*. Vol. **110**, pp. 216-225.
- Bektas Balçık, F., Göksel, C.,** 2005: Remote Sensing And GIS Integration For Land Cover Analysis, A Case Study: Bozcaada Island. *Water Science and Technology*. Vol. **51**, no. 11, pp. 239-244.

- Bektas Balçık, F., Göksel, C., Doğru, A. Ö.,** 2009: Land Cover Change Detection Based on PCA and Classification, *INTERCARTO-INTERGIS on Sustainable Development of Territories: GIS Theory and Practice*, Belgium/Ghent.
- Bell, I. E., Baranoski, G. V. G.,** 2004: Reducing the Dimensionality of Plant Spectral Databases. *IEEE Transactions on Geoscience and Remote Sensing*. Vol. **42**, no. 3, pp. 570-576.
- Belluco, E., Camuffo, M., Ferrari, S., Modenese, L., Silvestri, S., Marani, A., Marani, M.,** 2006: Mapping salt-marsh vegetation by multispectral and hyperspectral remote sensing. *Remote Sensing of Environment*. Vol. **105**, pp. 54- 67.
- Berberoglu, S., Lloyd, C. D., Atkinson, P. M., Curran, P. J.,** 2000: The integration of spectral and textural information using neural networks for land cover mapping in the Mediterranean. *Computer Geoscience*. Vol. **26**, pp. 385–396.
- Berberoglu, S., Yilmaz, K.T., Özkan, C.,** 2004: Mapping and monitoring of coastal wetlands of Çukurova Delta in the Eastern Mediterranean region. *Biodiversity and Conservation*. Vol. **13**, No. 3, pp. 615-633.
- Berk, A., Anderson, G. P., Bernstein, L. S., Acharya, P. K., Dothe, H., Matthew, M.W., Adler-Golden, S. M., Chetwynd, J. H., Richtsmeier, S. C., Pukall, B., Allred, C. L., Jeong, L. S., Hoke, M.L.,** 1999: MODTRAN4 Radiative Transfer Modeling for Atmospheric Correction. *Optical Spectroscopic Techniques and Instrumentation for Atmospheric and Space Research III*, SPIE Proceeding, Vol. **3756**, p. 348-353.
- Blackburn, G. A.,** 1999: Relationships between spectral reflectance and pigment concentrations in stacks of broadleaves. *Remote Sensing of Environment*. Vol. **70**, pp. 224–237.
- Butera M. K.,** 1983: Remote Sensing of Wetlands. *IEEE Transactions on Geoscience and Remote Sensing*. Vol. **21**, no. 3, pp. 383–392.
- Byfield, A.,** 2009: Interview
- Carpenter, W. J., Lillesand T. M., Kiefer R. W.,** 1990, The use of IntensityHueSaturationtransformations for merging SPOT Panchromatic and Multispectral image data. *Photogrammetric Engineering and Remote Sensing*. Vol. **56**, pp. 459–67.
- Chavez P.S.J., Guphill, C., and Bowel,J.A.,** 1984: Image rocessing techniques for thematic mapper data. In: *proceeding of the American Society of photogrametry Conference*. Pp. 728-752, Washington.
- Chavez, P. S. Jr.,** 1996: Image-based atmospheric corrections - revisited and revised. *Photogrammetric Engineering and Remote Sensing*. Vol. **62**, pp. 1025-1036.
- Chen, J., Gong, P., He, C., Pu, R. and Shi, P.,** 2003: Land-Use/Land-Cover Change Detection using Improved Change-Vector Analysis. *Photogrammetric Engineering and Remote Sensing*. Vol. **69**, pp. 369-379.

- Chopra, R., Verma, V. K., Sharma, P. K.,** 2001: Mapping, monitoring and conservation of Harike wetland ecosystem, Punjab, India, through remote sensing. *International Journal of Remote Sensing*. Vol. **22**, no. 1, pp. 89–98
- Cohen, W.B., Fiorella, M.,** 1998: Comparison of methods for detecting conifer forest change with Thematic Mapper imagery. In R.S. Lunetta and C.D. Elvidge (Eds). *Remote Sensing Change Detection. Environmental Monitoring Methods and Applications* (Chelsea: Ann Arbor Press), pp. 89–102.
- Collins, J. B., Woodcock, C. E.,** 1994: Change detection using the Gramm-Schmidt transformation applied to mapping forest mortality. *Remote Sensing of Environment*. Vol. **50**, pp. 267-279.
- Congalton, R. G. and Green, K.,** 1999: *Assessing the Accuracy of Remotely Sensed Data: Principles and Practices* Lewis. Boca Raton, FL
- Congalton, R. G.,** 1991: A review of assessing the accuracy of classifications of remotely sensed data.. *Remote Sensing of Environment*. Vol. **37**, pp. 35-46.
- Coppin, P., Jonckheere, I., Nackaerts, K., Muys, B., Lambin, E.,** 2004: Digital change detection methods in ecosystem monitoring; a review. *International Journal of Remote Sensing*. Vol. **25**, pp. 1565-1596.
- Coskun, H. G., Bayraktar, Ö., Onur, S. and Dabanlı, O.,** 2002: Using GIS and remote sensing techniques at water basin protected areas for land use changes and water quality monitoring, *Final Proceedings of the International ISWA World Environment Congress*, Istanbul, Turkey, Vol. **4**, pp. 2477–2485.
- Coskun, H. G., Gulergun, O., Yilmaz, L.,** 2006: Monitoring of protected bands of Terkos drinking water reservoir of metropolitan Istanbul near the Black Sea coast using satellite data. *International Journal of Applied Earth Observation and Geoinformation*. Vol. **8**, pp. 49–60.
- Cowardin, L.M., Carter, V., Golet, F.C., Laroe, E.T.,** 1979: Classification Of Wetlands And Deepwater Habitats Of The United States. *U.S. Fish And Wildlife Service*. pp. 103
- Crevier, Y., Pultz, T., Lukowski, T., and Toutin, T.,** 1996: Temporal analysis of ERS-1 SAR backscatter for hydrology applications. *Canadian Journal of Remote Sensing*. Vol. 22, pp. 65-77.
- Crist, E.P., Kauth, R. J.,** 1986: The Tasseled Cap de-mystified. *Photogrammetric Engineering and Remote Sensing*. Vol. **52**, pp. 81–86.
- Cronk, J. K., Fennessy, M. S.,** 2001: *Wetland Plants: Biology and Ecology*. Boca Raton, CRC Press/Lewis Publishers.
- Cruickshank, M. M., Tomlinson, R. W., Trew, S.,** 2000: Application of CORINE land-cover mapping to estimate carbon stored in the vegetation of Ireland. *Journal of Environmental Management*. Vol. **58**, pp. 269–287.

- Cudachy, T.J., Hewson, R.D., Huntington, J.F., Quigley, M.A., and Barry, P.S.**, 2001: The performance of the satellite-borne Hyperion Hyperspectral VNIR-SWIR imaging system for mineral mapping at Mount Fitton, South Australia. *Proceedings IEEE 2001 International Conference on Geoscience and Remote Sensing*.
- Curran, P. J.**, 1988: The semivariogram in remote sensing: an introduction. *Remote Sensing of Environment*. Vol. **24**, pp. 493-507.
- Curran, P. J.**, 1994. Attempts to drive ecosystem simulation models at local to regional scales. In G. M. Foody, & P. J. Curran (Eds.), *Environmental Remote Sensing of Regional to Global Scales*. pp. 149– 166, Chichester: Wiley.
- Curran, P. J., Dungan, J. L., Macler, B. A., Plummer, S. E.**, 1991: The effect of a red leaf pigment on the relationship between red-edge and chlorophyll concentration. *Remote Sensing of Environment*. Vol. **35**, pp. 69–75.
- Curran, P.J., Atkinson, P. M.**, 1998: Geostatistics and remote sensing. *Progress in Physical Geography*. Vol. **122**, pp. 61-78.
- Curran, P.J., Dungan, J.L.**, 1989: Estimation of signal-to-noise: A new procedure applied to AVIRIS imagery. *IEEE Transactions on Geoscience and Remote Sensing*. Vol. **27**, pp.620–628.
- Datt, B., McVicar, T. R., Van Niel, T. G., Jupp, D. L. B., Pearlman, J. S.**, 2003: Preprocessing EO-1 Hyperion hyperspectral data to support the application of agricultural indexes. *IEEE Transaction on Geoscience and Remote Sensing*. Vol. **41**, no. 6, pp. 1246–1259.
- Dawson, T. P., Curran, P. J.**, 1998: A new technique for interpolating the reflectance red edge position. *International Journal of Remote Sensing*. Vol. **19**, pp. 2133–2139.
- Dechka, J.A., Franklin, S.E., Watmough, M.D., Bennett, R. P., Instrup, D.W.**, 2002: Classification Of Wetland Habitat and Vegetation Communities Using Multi-Temporal Ikonos Imagery In Southern Sakatchewan. *Canadian Journal of Remote Sensing*. Vol. **28**, no. 5, pp. 679-685.
- Deng, J. S., Wang, K., Deng, Y. H., Qi, G. J.**, 2008: PCA-based land-use change detection and analysis using multitemporal and multisensor satellite data. *International Journal of Remote Sensing*. Vol. **29**, pp. 4823-4838.
- Dogru, A. O., Bektaş Balçık, F., Balik Sanli, F., Goksel, C., Ulugtekin, N.**, 2008: Izmir Bird Paradise Change Detection Analysis: Remote Sensing and GIS Integration. *Fresenius Environmental Bulletin*. Vol. **18**, no. 1, pp. 51-56.
- Dogru, A. O., Bektaş Balçık, F., Goksel, C., Ulugtekin, N.**, 2006: Monitoring Coastal Dunes by Using Remote Sensing and GIS Integration in North West Part of Turkey: A Case Study of Kilyos Dunes. *Fresenius Environmental Bulletin*. Vol. **15**, no. 9b, pp. 1216-1220.

- Doxaran, D., Froidefonda, J. M., Lavenderb, S., Castaing, P.,** 2002: Spectral signature of highly turbid waters Application with SPOT data to quantify suspended particulate matter concentrations. *Remote Sensing of Environment*. Vol. **81**, pp. 149– 161
- Drake, J. B., Dubayah, R.O., Clark, D., Knox, R., Blair, J. B., Hofton, M., Chazdon, R.L., Weishampel, J.F., Prince, S.,** 2002: Estimation of tropical forest structural characteristics using large-footprint LIDAR. *Remote Sensing of Environment*. 79: 305-319.
- Du, Y., Teillet, P. M., Cihlar, J.,** 2002: Radiometric normalization of multitemporal high-resolution satellite images with quality control for land cover change detection. *Remote Sensing of Environment*. Vol.**82**, pp. 123–134.
- Dubayah, R., Knox, J. C., Hofton, M., Blair, J. B., Drake, J.,** 2000: Land surface characterization using lidar remote sensing. In M. J. Hill & R. Aspinall (Eds.), *Spatial information for land use management*. pp. 25–38. Singapore: International Publishers Direct.
- Dugan, P. J.,** 1990: *Sulak Alanların Korunması Genel Konular ve Gerekli Çalışmalar Üzerine Bir İnceleme* (DHKD Tarafından Türkçeye Çevrilmiş Rapor).
- Dymond, C. C., and Johnson, E. A.,** 2002: Mapping vegetation spatial patterns from modeled water, temperature and solar radiation gradients. *Journal of Photogrammetry and Remote Sensing*, Vol. **57**, pp. 69–85.
- Elvidge, C.D.,** 1990, Visible and near-infrared reflectance characteristics of dry plant materials: *International Journal of Remote Sensing*, v. 11, p. 1775-1795.
- ENVI.,** 2009: Atmospheric Correction Guide Version 4.7.
- European Commission.,** 1998: *Remote sensing of Mediterranean desertification and environmental changes (Resmedes)*. Luxembourg: Office for Official Publications of the European Communities.
- European Environment Agency.,** 2005: http://reports.eea.europa.eu/COR0-landcover/en/land_cover.pdf. Accessed 2 June 2008.
- Fang, S., Gertner, G., Wang, G., Anderson, A.,** 2006: The impact of misclassification in land use maps in the prediction of landscape dynamics. *Landscape Ecology*. Vol. **21**, pp. 233-242.
- Finlayson, C. M., Davidson, N. C.,** 1999: Summary report. In CM Finlayson & AG Spiers (eds), *Global review of wetland resources and priorities for wetland inventory*. Supervising Scientist Report 144, Supervising Scientist Group, Environment Australia, Canberra, pp 1-13.
- Flores, S. E., Yool, S. R.,** 2007: Sensitivity of change vector analysis to land cover change in an arid ecosystem, *International Journal of Remote Sensing*. Vol. **28**, pp. 1069-1088.
- Foody, G. M.,** 2002: Status of land cover classification accuracy assessment. *Remote Sensing of Environment*. Vol. **80**, pp. 185-201.

- Foody, G. M.**, 2008: Harshness in image classification accuracy assessment. *International Journal of Remote Sensing*. Vol. **29**, no. 11, pp. 3137-3158
- Fung, T., LeDrew, E.**, 1987: Application of principal component analysis to change detection. *Photogrammetric Engineering and Remote Sensing*. Vol. **53**, pp.1649 - 1658.
- Fung, T., Siu, W.**, 2000: Environmental quality and its changes, an analysis using NDVI. *International Journal of Remote Sensing*. Vol. **21**, no. 5, pp. 1011–1024.
- Galvão, L. S., Formaggio, A. R., and Tisot, D. A.**, 2005: Discrimination of sugarcane varieties in Southeastern Brazil with EO-1 Hyperion data. *Remote Sensing of Environment*. Vol. **94**, no. 4, pp. 523-534.
- Galvão, L. S., Roberts, D. A., Formaggio, A. R., Numata, I., and Breunig, F. B.**, 2009: View angle effects on the discrimination of soybean varieties and on the relationships between vegetation indices and yield using off-nadir Hyperion data. *Remote Sensing of Environment*. Vol. **113**, no. 4, pp. 846-856.
- Gammon, P., Carter, V.**, 1979: Vegetation Mapping With Seasonal Color Infrared Photographs. *Photogrammetric Engineering and Remote Sensing*. Vol. **45**, no. 1, pp. 87-89
- Gao, Z.G., Zhang, L.Q.**, 2006: Multi-seasonal spectral characteristics analysis of coastal salt marsh vegetation in Shanghai, China. *Estuarine, Coastal and Shelf Science*. Vol. 69, no. 1/2, pp.217–224.
- Gausman H. W.**, 1973. Reflectance, transmittance, and absorptance of light by subcellular particles of spinach (*Spinacia oleracea* L.) leaves. *Agronomy Journal*, 65, pp. 551– 553.
- Gilbert, M. A., Conese, C., Maselli, F.**, 1994: An atmospheric correction method for the automatic retrieval of surface reflectance from TM images. *International Journal of Remote Sensing*. Vol. **15**, pp. 2065–2086.
- Gitelson, A. A., Merzlyak, M. N.**, 1997: Remote estimation of chlorophyll content in higher plant leaves. *International Journal of Remote Sensing*. Vol. **18**, pp. 2691–2697.
- Goodenough, G., Dyk, A., Niemann, K. O., Pearlman, J. S., Chen, H., Han, T., Murdoch, M., West, C.**, 2003: Processing Hyperion and ALI for forest classification. *IEEE Transaction on Geoscience and Remote Sensing*. Vol. **41**, no. 6, pp. 1321–1331.
- Göksel, Ç., Kaya, Ş., Musaoğlu, N.**, 2001: Satellite Data use for change information : A Case study for Terkos Water Basin, İstanbul. *21. EARSeL Symposium*, Paris, France.
- Green, A. A., Berman, M., Switzer, B., Craig, M. D.**, 1988: A transformation for ordering multispectral data in terms of image quality with implications for noise removal. *IEEE Transactions on Geoscience and Remote Sensing*. Vol. **26**, no. 1, pp. 65-74.

- Griffin, M. K., Hsiao-hua, K. B.,** 2003: Compensation of hyperspectral data for atmospheric effects. *Lincoln Laboratory Journal*. Vol. **14**, no. 1, pp. 29-54.
- Gross, M. F., Hardisky, M. A., Klemas, V.,** 1989: *Applications to coastal wetlands vegetation, Theory and Applications of Optical Remote Sensing* (G. Asar, editor), John Wiley and Sons, New York.
- Gross, M. F.; Klemas, V.,** 1986: The use of Airborne Imaging Spectrometer (AIS) data to differentiate marsh vegetation. *Remote Sensing of Environment*. Vol. **19**, pp. 97-103,
- Guerschman, J. P., Hill, M. J., Renzullo, L. J., Barrett, D. J., Marks, A. S., and Botha, E. J.,** 2009: Estimating fractional cover of photosynthetic vegetation, non-photosynthetic vegetation and bare soil in the Australian tropical savanna region upscaling the EO-1 Hyperion and MODIS sensors. *Remote Sensing of Environment*. Vol. **113**, no. 5, pp. 928-945.
- Guild, L. S., Cohen, W. B., Kauffman, J. B.,** 2004: Detection of deforestation and land conversion in Rondônia, Brazil using change detection techniques. *International Journal of Remote Sensing*. Vol. **25**, no. 4, pp. 731–750.
- Gulinck, H., Mugica, M., Lucio, J. V., Atauri, J. A.,** 2001: A framework for comparative landscape analysis and evaluation based on land cover data, with an application in the Madrid region (Spain). *Landscape and Urban Planning*. Vol. **55**, pp. 257–270.
- Han, K. S., Champeaux, J. L., & Roujean, J. L.,** 2004: A land cover classification product over France at 1 km resolution using SPOT4/VEGETATION data. *Remote Sensing of Environment*. Vol. **92**, pp. 52–66.
- Hardisky, M. A., Gross, M. F., Klemas, V.,** 1986: Remote sensing of coastal wetlands. *BioScience*. Vol. **36**, pp. 453–460.
- Hayes, D. J., and Sader, S. A.,** 2001: Comparison of change-detection techniques for monitoring tropical forest clearing and vegetation regrowth in a time series. *Photogrammetric Engineering & Remote Sensing*. Vol. **67**, no. 9, pp. 1067-1075.
- Herkelrath, W. N., Hamburg, S. P., Murphy, F.,** 1991: Automatic, real-time monitoring of soil moisture in a remote field area with time domain reflectometry. *Water Resources Research*. Vol. **27**, no. 5, pp. 857–864.
- Hoffstetter, R. H.,** 1983: Wetlands in the United States. In: *Gore, A. J. P., ed. Ecosystems of the World: Mires: Swamp, Bog, Fen, and Moor*, Vol. **4B**, pp. 201-244. Elsevier, Amsterdam, Netherlands.
- Houhoulis, P. F., Michener, W. K.,** 2000: Detecting wetland change: A rule-based approach using NWI and SPOT-XS data. *Photogrammetric Engineering & Remote Sensing*. Vol. **66**, pp. 205-211

- Ivits, E., Lamb A., Langar, F., Hemphill, S., Koch, B.,** 2008: Orthogonal transformation of segmented SPOT 5 images: Seasonal and geographical dependence of the tasseled cap parameters. *Photogrammetric Engineering & Remote Sensing*. Vol. **74**, No. 11, pp. 1351-1364
- Jackson, B.B.,** 1983: *Multivariate Data Analysis: An Introduction* Irwin, Homewood, Illinois, USA.
- Jensen, J R.,** 2000: *Remote Sensing of the Environment: An Earth Resource Perspective*, Upper Saddle River, NJ: Prentice Hall, 544 pages.
- Jensen, J. R.,** 1996: *Introductory Digital Image Processing: a Remote Sensing Perspective, Second ed*, Prentice Hall, Saddle River, NJ, 316 pp.
- Jensen, J. R.,** 2004: Digital change detection. In: *Introductory Digital Image Processing: A Remote Sensing Perspective*. New Jersey, Prentice-Hall, pp. 467- 494.
- Jensen, J. R., Rutchey, K., Koch, M. S., Narumalani, S.,** 1995: Inland Wetland Change Detection In The Everglades Water Conservation Area 2A Using A Time Series Of Normalized Remotely Sensed Data. *Photogrammetric Engineering and Remote Sensing*. Vol. **61**, no. 2, pp. 199-209
- Jensen, J., Narumalani, S., Weatherbee, O., Mackay, H. E.,** 1993: Measurement of Seasonal and Yearly Cattail and Waterlily Changes Using Multidate SPOT Panchromatic Data. *Photogrammetric engineering and Remote Sensin*. Vol. **59**, no. 4, pp. 519–525.
- Jensen, J.R., Hodgson, M.E., Christensen, E., Mackey, H. E., Tinney, L.R., and Sharitz, R.,** 1986: Remote sensing of Inland Wetlands: A Multispectral Approach. *Photogrammetric Engineering and Remote Sensing*. Vol. **52**, no. 1, pp. 87-100
- Jha, C. S., Unni, N. V. M.,** 1994: Digital change detection of forest conversion of dry tropical forest region. *International Journal of Remote Sensing*. Vol. **15**, pp. 2543–2552.
- Johnson, R. D., and Kasischke, E. S.,** 1998: Change vector analysis: a technique for the multispectral monitoring of landcover and condition. *International Journal of Remote Sensing*. Vol. **19**, pp. 411–26.
- Johnston, R. M., & Barston, M. M.,** 1993: Remote sensing of Australian wetlands: An evaluation of Landsat TM data for inventory and classification. *Australian Journal of Marine Freshwater Resources*. Vol. **44**, pp. 235–252.
- Jollineau, M. Y.,** 2003: Assessing High Resolution Remotely Sensed Data for Mapping and monitoring Wetlands in southern Ontario. *PhD Thesis*, University of Waterloo.
- Kardoulas, N.G., Bird, A.C., Lawan, A.I.,** 1996: Geometric correction of SPOT and Landsat imagery: a comparison of map- and GPS-derived control points. *Photogrammetric Engineering and Remote Sensing*. Vol. **62**, pp. 1173–1177.

- Karpouzli, E., and Malthus, T.,** 2003: The empirical line method for the atmospheric correction of IKONOS imagery. *International Journal of Remote Sensing*. Vol. **24**, pp. 1143–1150.
- Kasischke, E. S., and Bourgeau-Chavez, L. L.,** 1997: Monitoring South Florida wetlands using ERS-1 SAR imagery. *Photogrammetric Engineering and Remote Sensing*. Vol. **63**, pp. 281–291.
- Klemas, V.V., Dobson, J. E., Ferguson, R. L., and Haddad, K. D.,** 1993: A coastal landcover classification-system for the NOAA Coastwatch Change Analysis Project. *Journal of Coastal Research*. Vol. **9**, pp. 862-872.
- Kokaly R.F., Clark R.N.,** 1999: Spectroscopic determination of leaf biochemistry using band-depth analysis of absorption features and stepwise linear regression. *Remote Sensing of Environment*. Vol. **67**, pp. 267–287.
- Kruse, F. A., Boardman, J.W., Huntington, J.F.,** 2003: Comparison of airborne hyperspectral data and EO-1 Hyperion for mineral mapping, *IEEE Transactions on Geoscience and Remote Sensing*. Vol. **41**, no.6, pp. 1388–1400.
- Kumar, L., Schmidt K.S., Dury S., and Skidmore A.K.,** 2001: Review of hyperspectral remote sensing and vegetation science. In Van Der Meer, F. (editor). *Hyperspectral remote sensing* (Kluwer Academic Press: Dordrecht).
- Kushwaha, S. P. S., Dwivedi, R. S., and Rao, B. R. M.,** 2000: Evaluation of various digital image processing techniques for detection of coastal wetlands using ERS-1 SAR data. *International Journal of Remote Sensing*. Vol. **21**, pp. 565–579.
- Kwarteng, A. Y., and Chavez, P. S.,** 1998: Change detection study of Kuwait City and environments using multitemporal Landsat Thematic Mapper data. *International Journal of Remote Sensing*. Vol. **19**, pp. 1651–1662.
- Lambin, E. F., and Strahler, A. H.,** 1994: Change-vector analysis: A tool to detect and categorize land-cover change processes using high temporal-resolution satellite data. *Remote Sensing of Environment*. Vol. **48**, pp. 231 244.
- Lathrop, R. G.,** 1988: The integration of remote sensing and geographic information systems for Great Lakes water quality monitoring, *PhD Thesis*, University of Wisconsin, USA.
- Li, X., Yeh, A. G. O.,** 1998: Principal component analysis of stacked multi-temporal images for the monitoring of rapid urban expansion in the Pearl River Delta of Hong Kong, Pokfulam Road, Hong Kong. *International Journal of Remote Sensing*. Vol. **19**, no. 8, pp. 1501-1518
- Liang S.,** 2004: *Quantitative Remote Sensing of Land Surfaces*, John Wiley and Sons, New Jersey, USA.
- Liang, S.,** 2001: Atmospheric Correction of Landsat ETM+ Land Surface Imagery—Part I: Methods, *IEEE Transactions On Geoscience And Remote Sensing*, Vol. **39**, no. 11.

- Lillesand, T.M., Kiefer, R.W.,** 1987: *Remote Sensing and Image Interpretation*. New York: John Wiley & Sons.
- Maktav, D. E., Sunar, F., Kabdasli, S.,** 2002: Monitoring Coastal Erosion at the Black Sea Coasts in Turkey Using Satellite Data: A Case Study at the Lake Terkos, North-West İstanbul. *International Journal of Remote Sensing*. Vol. **23**, no. 19, pp 4115-4124.
- Malila, W. A.,** 1980: Change vector analysis: an approach to detecting forest change with Landsat. *Proceedings of the 6th International Symposium on Machine Processing of Remotely Sensed Data*. Purdue University, West LaFayette, IN, USA, pp. 326–35.
- Mas, J. F.,** 1999: Monitoring land-cover changes: A comparison of change detection techniques. *International Journal of Remote Sensing*. Vol. **20**, no. 1139–1152.
- Masek, J. G., Lindsay, F. E., Goward, S. N.,** 2000: Dynamics of urban growth in the Washington DC metropolitan area 1973–1996, from Landsat observations. *International Journal of Remote Sensing*. Vol. **21**, pp. 3473–3486.
- Mason, P.,** 2002: MMTG A-List Hyperspectral Data Processing Software, 920 C, CSIRO, *Division of Exploration and Mining*. Sydney, Australia.)
- Michalek, J. L., Wagner, T. W., Luczkovich, J. L., and Stoffle, R. W.,** 1993: Multispectral Change Vector analysis for Monitoring Coastal Marine Environments, *Photogrammetric Engineering & Remote Sensing*. Vol. **59**, pp. 381-384.
- Mitsch, W. J., and Gosselink, J. G.,** 2000a: The value of wetlands: importance of scale and landscape setting. *Ecological Economics*. Vol. **35**, pp. 25-33.
- Mitsch, W. J., and Gosselink, J. G.,** 2000b: *Wetlands, 3rd edition*. John Wiley & Sons, Inc., New York.
- Moos, D., & Wyatt, B. K.,** 1994: The CORINE biotopes project: A database for conservation of nature and wildlife in the European community. *Applied Geography*. Vol. **14**, no. 4, pp. 327– 349.
- Moran, M. S., Jackson, R. D., Slater, P. N., & Teillet, P. M.,** 1992: Evaluation of simplified procedures for retrieval of land surface reflectance factors from satellite sensor output. *Remote Sensing of Environment*. Vol. **41**, pp. 169– 184.
- Muchoney, D. M., and Haack, B. N.,** 1994: Change detection for monitoring forest defoliation. *Photogrammetric Engineering and Remote Sensing*. Vol. **60**, pp. 1243–1251.
- Mumby, P. J., Edwards, A. J.,** 2002: Mapping Marine Environments With IKONOS Imagery: Enhanced Spatial Resolution Can Deliver Greater Thematic Accuracy. *Remote sensing of Environment*. Vol. **22**, no. 12, pp. 2377-2400.

- Munyati, C.**, 2000: Wetland change detection on the Kafue Flats, Zambia, by classification of a multitemporal remote sensing image dataset. *International Journal of Remote Sensing*. Vol. **21**, no. 9, pp. 1787–1806.
- Munyati, C.**, 2004: Use of Principal Component Analysis (PCA) of Remote Sensing Images in Wetland Change Detection on the Kafue Flats, Zambia. *Geocarto International*. Vol. **19**, no. 3, pp. 11 — 22.
- Nagendra, H.**, 2001: Review Article: Using Remote Sensing To Assess Biodiversity, *International Journal of Remote Sensing*. Vol. **22**, no. 12, pp. 2377-2400
- Oetter, D. R., Krankina, O. N., Cohen, W. B., and Majersperger, T. K.**, 2001: Using landsat thematic mapper data to map land cover and biomass in a Russian forest for regional carbon storage inventory. *Global Change Open Science Conference*. Amsterdam, The Netherlands.
- Ozesmi, S. L., Bauer. M. E.**, 2002: Satellite Remote Sensing Of Wetlands *Wetlands Ecology and Management*. Vol. **10**, pp. 381-402.
- Ozhatay, N. B. A., Atay, S.** 2003: Important Plant Areas of Turkey *WWF Turkiye*, MAS Press (in Turkish).
- Parmenter, A. W., Hansen, A., Kennedy, R. E., Cohen, W., Langner, U., Lawrence, R., Maxwell, B., Gallant, A., Aspinall. R.**, 2003: Land use and land cover change in the Greater Yellowstone Ecosystem: 1975–1995. *Ecological Applications*. Vol. **13**, pp. 687–703.
- Pearlman, J. S., Barry, P. S., Segal, C. C., Shepanski, J., Beiso, D., Carman, S. L.**, 2003: Hyperion, a space-based imaging spectrometer. *IEEE Transactions on Geoscience and Remote Sensing*. Vol. **41**, no. 1160–1173.
- Pengra, B. W., Johnston, C. A., Loveland, T. R.**, 2007: Mapping an invasive plant, *Phragmites australis*, in coastal wetlands using the EO-1 Hyperion hyperspectral sensor. *Remote Sensing of Environment*, Vol. **108**, no. 1, pp. 74–81.
- Prisley, S. P. and Smith, J. L.**, 1987: Using classification error matrices to improve the accuracy of weighted land-cover models. *Photogrammetric Engineering and Remote Sensing*. Vol. **53**, pp. 1259-1263.
- Rahman, H., and Dedieu, G.**, 1994: SMAC: A simplified method for the atmospheric of satellite measurements in the solar spectrum. *International Journal of Remote Sensing*. Vol. **15**, pp.123-143.
- Ramsar Convention Bureau**, 2002: The Ramsar Convention on Wetlands Homepage. |www.ramsar.org, accessed at 01.08.2007
- Ramsey III, E., Rangoonwala, A., Nelson, G., Ehrlich, R., Martella., K.**, 2005: Generation and Validation of Characteristic Spectra From EO1 Hyperion Image Data For Detecting The Occurrence of The Invasive Species, Chinese Tallow. *International Journal of Remote Sensing*, Preview Article

- Ramsey, E.W., and Laine, S. C.**, 1997: Comparison of Landsat Thematic Mapper and high resolution photography to identify change in complex coastal wetlands. *Journal of Coastal Research*. Vol. **13**, pp. 281–292.
- Richards, J. A., Jia, X.**, 2006: *Remote Sensing Digital Image Analysis An Introduction*. 4 th Edition Springer-Verlag New York, Inc
- Ringrose, S., Vanderpost, C., Matheson, W.**, 2003: Mapping ecological conditions in the Okavango Delta Botswana using fine & coarse resolution systems including simulated SPOT VEGETATION imagery. *International Journal of Remote Sensing*. Vol. **24**, no.5, pp.1029–1053.
- Rosso, P.H., Ustin, S.L., Hastings, A.**, 2006: Use of LiDAR to study changes associated with Spartina invasion in San Francisco Bay marshes. *Remote Sensing of Environment*. Vol. **100**, pp. 295 - 306.
- Rundquist, D. C., Narumalani, S., Narayanan, R, M.**, 2001: A Review of Wetlands Remote Sensing and Defining New Considerations. *Remote Sensing Reviews*. Vol. **20**, pp. 207-226
- Schepers J. S., Blackmer, T. M., Wilhelm, W. W., Resende, M.**, 1996: Transmittance and reflectance measurements of corn leaves from plants with different nitrogen and water supply. *Journal of Plant Physiology*. Vol. **148**, pp. 523–529.
- Schmidt, K. S.**, 2003: Hyperspectral Remote Sensing of Vegetation Species Distribution in a Saltmarsh. *PhD Thesis*, International Institute for Geo-Information Science and Earth Observation and Wageningen University.
- Schmidt, K. S., Skidmore, A. K.**, 2003: Spectral discrimination of vegetation types in a coastal wetland. *Remote Sensing of Environment*. Vol. **85**, no. 1, pp. 92-108.
- Schowengerdt, R.A.**, 1997: *Remote Sensing: Models and Methods for Image Processing, Second ed*, Academic Press, San Diego, pp. 522.
- Serra, P., Pons, X., & Saurí, D.**, 2003: Post-classification change detection with data from different sensors: Some accuracy considerations. *International Journal of Remote Sensing*, Vol. **24**, no. 16, pp. 3311–3340.
- State Institute of Statistics (SIS)**, 2007:-:www.die.gov.tr , accessed at 14.07.2007
- Singh, A.**, 1989: Digital change detection techniques using remotely sensed data. *International Journal of Remote Sensing*. Vol. **10**, pp. 989–1003.
- Sipple, B.**, 2002: Wetland Functions and Values. US EPA, Office of water. |<
www.epa.gov/watertrain/wetlands/text.html>, accessed at 14.07.2006
- Skidmore, A. K., Ferwerda, J., Mutanga, O., Van Wieren, S, Prins, H. H. T, Bektas Balcik, F., Venus, V.**, 2010: Forage quality of savannas - simultaneously mapping foliar protein and polyphenols for trees and grass using hyperspectral imagery. *Remote Sensing of Environment*. Vol. **114**, no. 1, pp. 64-72.

- Skidmore, A. K., Turner, B.J., Brinkhof, W., Knowles, E.,** 1997: Performance of a neural network: mapping forests using GIS and remotely sensed data. *Photogrammetric Engineering and Remote Sensing*. Vol. **63**, pp. 501-514
- Song, C., Woodcock, C. E., Seto, K., Lenney, M. P., Macomber, S.,** 2001: Classification and change detection using Landsat TM data when and how to correct atmospheric effects. *Remote Sensing of Environment*. Vol. **75**, pp. 230–244.
- Stow, D.A.,** 1999: Reducing mis-registration effects for pixel-level analysis of land-cover change. *International Journal of Remote Sensing*. Vol. **20**, pp. 2477–2483.
- Stroppiana, D., Pinnock, S., Pereira, J. M. C., Gregoire, J. M.,** 2002: Radiometric analysis of SPOT-VEGETATION images for burned area detection in Northern Australia. *Remote Sensing of Environment*. Vol. **82**, no. 1, pp. 21–37
- Teilet, P. M.,** 1986: Image correction for radiometric effects in remote sensing, *International Journal of Remote Sensing*. Vol. **7**, no. 12, pp. 1637 – 1651.
- The National Biological Diversity Strategy and Action Plan.,** 2007: <http://www.cbd.gov.tr/documents/NBSAP-2007.pdf>
- Thenkabail P. S.,** 1999: Characterisation of the alternative to slash-and burn benchmark research area representing the Congolese rainforests of Africa using near-realtime SPOT HRV data. *International Journal of Remote Sensing*. Vol. **20**, no. 5, pp. 839– 877.
- Thenkabail P.S., Smith R.B., and De Pauw E.,** 2000: Hyperspectral Vegetation Indices and Their Relationship with Agricultural Crop Characteristics. *Remote Sensing of Environment*. Vol. **71**, pp. 158-182.
- Thenkabail P.S., Smith R.B., De Pauw, E.,** 2002: Evaluation of narrowband and broadband vegetation indices for determining optimal hyperspectral wavebands for agricultural crop characterization. *Photogrammetric Engineering and Remote Sensing*. Vol. **68**, pp. 607–621.
- Thenkabail, P. S., Enclona, E. A., Ashton, M. S., Legg, C.,and Dieu, J. D, M.,** 2004b: Hyperion, IKONOS, ALI, and ETM+ sensors in the study of African rainforests. *Remote Sensing of Environment*. Vol. **90**, no. 1, pp. 23-43.
- Townshend, J. R. G., Justice, C. O., Gurney, C., McManus, J.,** 1992: The effect of mis-registration on the detection of vegetation change. *IEEE Transactions on Geosciences and Remote Sensing*. Vol. **30**, pp. 1054–1060.
- Toyra, J., Pietroniro, A., Martz, L. W., and Prowse, T. D.,** 2002: A multisensor approach to wetland flood monitoring. *Hydrological Processes*. Vol. **16**, pp. 1569–81.
- Toyra, J., Pietroniro, A., Martz, L. W.,** 2001: Multisensor hydrologic assessment of a freshwater wetland. *Remote Sensing of Environment*, Vol. **75**, pp. 162–173.

- Tsai, F., Lin, E. K., Yoshino, K.**, 2007: Spectrally segmented principal component analysis of hyperspectral imagery for mapping invasive plant species. *International Journal of Remote Sensing*. Vol. **28**, pp. 1023-1039.
- Turker, M., and Gacemer, A. O.**, 2004: Geometric correction accuracy of IRS-1D PAN imagery using topographic map versus GPS control points. *International Journal of Remote Sensing*. Vol. **25**, no. 6, pp. 1095–1104
- Underwood, E., S. Ustin, and D. DiPietro.**, 2003: Mapping nonnative plants using hyperspectral imagery. *Remote Sensing of Environment*. Vol. **86**, no. 2, pp. 150–161.
- Url-1** <<http://www.fao.org/>>, accessed at 29.08.2006
- Url-2** <<http://soils.usda.gov/use/worldsoils/mapindex/wetlands.html>>, accessed at 29.08.2006
- Url-3** <<http://www.epa.gov/watertrain/wetlands/text.html>>, accessed at 29.08.2006
- Url-4** <<http://www.spot.com/>>, accessed at 01.05.2009
- Url-5** <<http://www.eea.europa.eu/publications/COR0-landcover>>, accessed at 01.09.2009
- Url-6**<<http://www.eo1.usgs.gov>>, accessed at 10.03.2008
- Vermote, E. F., Tanre, D., Deuze, J. L., Herman, M., Morcrette, J. J.**, 1997: Second simulation of the satellite signal in the solar spectrum: An overview. *IEEE Transactions on Geoscience and Remote Sensing*. Vol. **35**, pp. 675– 686.
- Warner, T.**, 2005: Hyperspherical direction cosine change vector analysis. *International Journal of Remote Sensing*. Vol. **26**, no. 6, pp. 1201 - 1215
- Willems, E., Vandervoort, C., Willekens, A., Buffaria, B.**, 2000: Landscape and land cover diversity index:
<http://europa.eu.int/comm/dg06/publi/landscape/ch3.htm>
- Woodcock, C. E., Strahler, A. H., and Jupp, D. L. B.**, 1988: The use of semivariograms in remote sensing I: Scene models and simulated images. *Remote Sensing of Environment*, Vol. **25**, no. 323-348.
- Work, E.A., Gilmer, D.S.**, 1976: Utilization of satellite data for inventorying prairie ponds and lakes. *Photogrammetric Engineering and Remote Sensing*. Vol. **42**, No. 5, pp.685-694.
- Yilmaz, R.**, 2009: Monitoring land use/land cover changes using CORINE land cover data: a case study of Silivri coastal zone in Metropolitan Istanbul. *Environmental Monitoring and Assessment*. Online available.
- Yuan, F., Sawaya, K. E., Loeffelholz, B. C., & Bauer, M. E.**, 2005: Land cover classification and change analysis of the twin cities (Minnesota) Metropolitan Area by multitemporal Landsat remote sensing. *Remote Sensing of Environment*. Vol. **98**, pp. 317–328.

Yuanbo, L., Nishiyama, S., & Yano, T., 2004: Analysis of four change detection algorithms in bi-temporal space with a case study. *International Journal of Remote Sensing*, Vol. **25**, no. 11, pp. 2121–2139.

APPENDICES

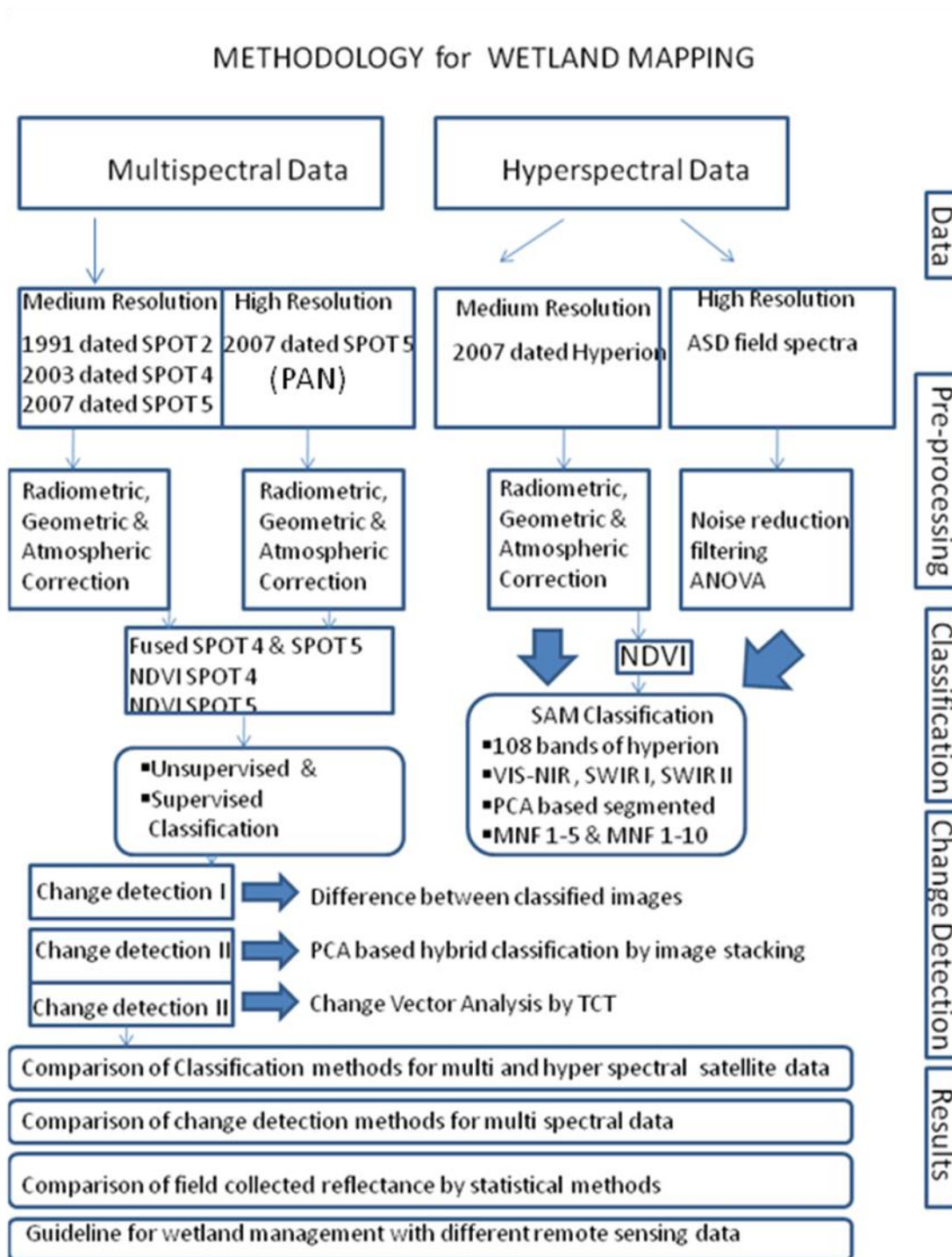
APPENDIX A.1 : Methodology of the study.

APPENDIX A.2 : NDVI images a) 2003 dated SPOT 4 b) 2007 dated SPOT 5
(resampled)

APPENDIX A.3 : Hyperion EO-1 NDVI image (band-30 and band-50)

APPENDIX A.4 : Results of classification and change detection methods

APPENDIX A.1



APPENDIX A.2

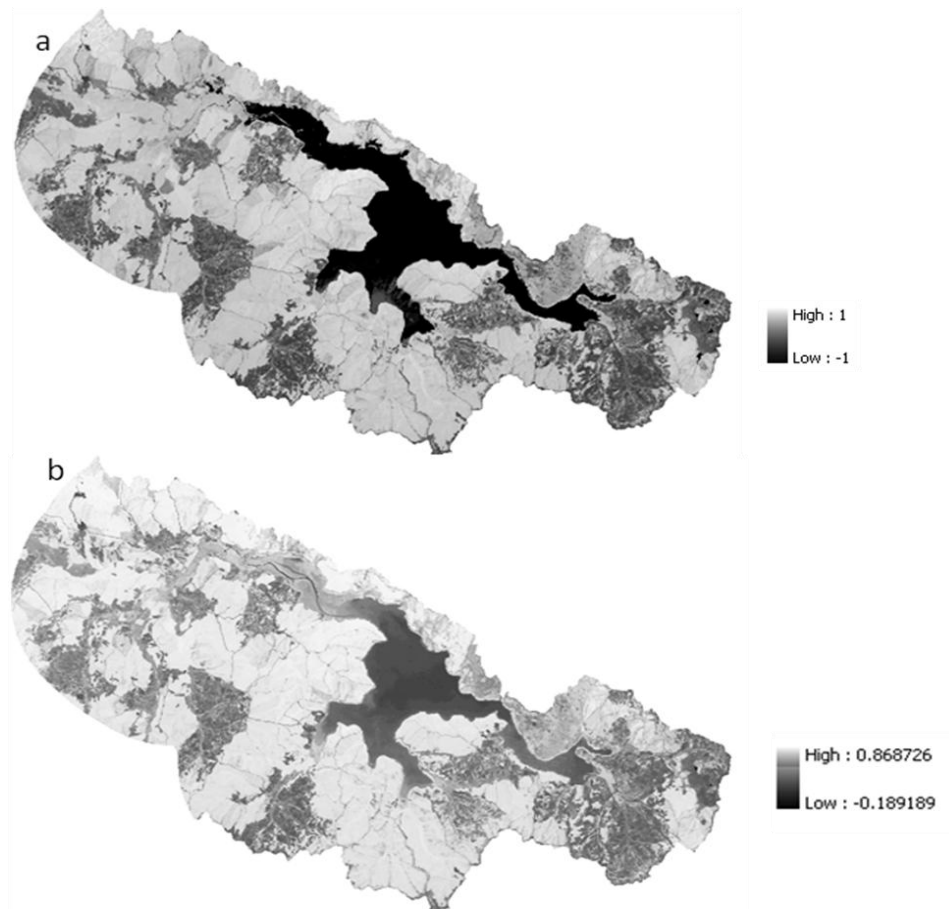


Figure A.2: NDVI images a) 2003 dated SPOT 4 b) 2007 dated SPOT 5.

APPENDIX A.3

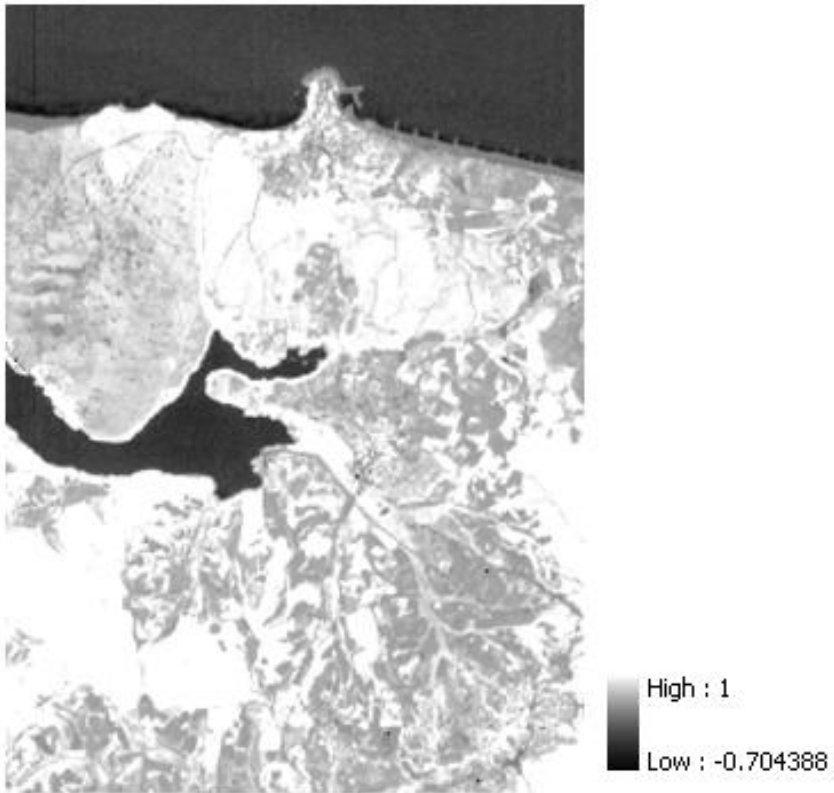


Figure A.3: Hyperion EO-1 NDVI image (band-30 (650 nm) and band-50 (854nm)).

APPENDIX A.4

Table A.1 : Result of classification and change detection methods

Methods	Multispectral Data	Hyperspectral Data
Unsupervised	2003 SPOT 4	
	Mixing problem in land cover categories between natural grassland, forest and wetland. Urban and road categories are mixing with each other.	
Unsupervised	2007 SPOT 5	
	Mixing problem in land cover categories between natural grassland, forest and wetland. Urban and road categories are mixing with each other.	
Classification	Supervised	2003 SPOT 4
		Mixing problem in land cover categories between natural grassland, forest and wetland. Urban and road categories are mixing with each other.
		(VIS) Mixed class problem
		(NIR) Mixed class problem between road and agriculture, sand and agriculture. Wetland mapping possible.
		(SWIR I) Better results for wetland mapping. Mixed class problem between road and agriculture, sand and agriculture

Table A.1 (contd.) : Result of classification and change detection methods

		2007 SPOT 5	(SWIR II)
		Mixing problem in land cover categories between natural grassland, forest and wetland. Urban and road categories are mixing with each other.	Better results for wetland mapping. Mixed class problem between road and agriculture, sand and agriculture. Green areas mixed with forest and sparsely vegetated area.
		Separation is better than unsupervised classification in the complex natural areas, but enough training areas are required.	(PCA) Better discrimination in land cover categories.
			(MNF) Mixing problem between land cover classes especially agriculture, open space, urban and road.
	Hybrid	Better than individual unsupervised and supervised classification.	
	SAM		SAM accuracy is highly sensitive to the choice of reference spectra. It has ability to discriminate wetlands than other green and forest areas. Detailed field work. PCA based gave better results.
Change Detection	PCA	Better than CVA method, it is easier to apply from-to change detection.	
	CVA	It is difficult to decide the threshold value, but it has ability to derive accurate unchanged class. It needs detailed field data.	

CURRICULUM VITA



Candidate's full name: Filiz Bektaş Balçık

Place and date of birth: İstanbul and 26/08/1977

Permanent Address: İTÜ Civil Engineering Faculty

Universities and

Colleges attended: (1995-2000) Yıldız Technical University Geodesy and Photogrammetry Engineering Department, Graduate Program.

Publications:

International Articles

- Göksel Ç., Mercan D.E., Kapdaşlı S., **Bektaş F.**, Şeker D. Z., 2004: Definition of Sensitive Areas In a Lake Shore by Using Remote Sensing and GIS. *Fresenius Environmental Bulletin*. Vol .13, No. 9, pp. 860-864
- **Bektas Balçık, F.**, Goksel, C., 2005: Remote Sensing And GIS Integration For Land Cover Analysis, A Case Study: Bozcaada Island. *Water Science and Technology*. Vol: 51, No: 11, pp. 239-244
- Dogru A. O., **Bektaş Balçık, F.**, Goksel C., Ulugtekin N., 2006: Monitoring Coastal Dunes by Using Remote Sensing and GIS Integration in North West Part of Turkey: A Case Study of Kilyos Dunes. *Fresenius Environmental Bulletin*. Vol. 15, no. 9b, pp. 1216-1220.
- Balik Sanli F., **Bektaş Balçık F.** and Goksel C., 2007: Defining temporal spatial patterns of mega city Istanbul to see the impacts of increasing population. *Environmental Monitoring and Assessment*. Vol. **146**, no. 1-3, pp. 267-275.
- Dogru A. O., **Bektaş Balçık F.**, Balik Sanli F., Goksel C., Ulugtekin N., 2008: Izmir Bird Paradise Change Detection Analysis: Remote Sensing and GIS Integration. *Fresenius Environmental Bulletin*. Vol. 18, no. 1, pp. 51-56.
- Skidmore A. K., Ferwerda J., Mutanga O., Van Wieren S, Prins H. H. T, **Bektas Balcik F.**, Venus V., 2010: Forage quality of savannas - simultaneously mapping foliar protein and polyphenols for trees and grass using hyperspectral imagery. *Remote Sensing of Environment*. Vol. 114, no. 1, pp. 64-72.

- Ulugtekin N., **Bektaş Balcık, F.**, Doğru A. O., Goksel C., Aslan Alaton I., Orhon D., 2009: The Use of Remote Sensing and GIS Technologies for Evaluation of Turkish River Basins: A Case Study of Marmara River Basin and Istanbul. *International Journal of Environment and Health*. Part A. Vol. 44, No. 1, pp. 388-396.

National Articles

- **Bektas Balcik F.**, Goksel C. 2009: SPOT 5 ve Farklı Görüntü Birleştirme Algoritmaları. HKM Jeodezi, Jeoinformasyon Arazi Yönetimi Dergisi, No. 3, pp. 45-50

International Papers

- **Bektas Balcik F.**, Goksel C., Dogru A. Ö., 2009: Land Cover Change Detection Based on PCA and Classification. *INTERCARTO-INTERGIS on Sustainable Development of Territories: GIS Theory and Practice*, 3-6 Temmuz 2009, Belçika/Ghent.
- Abdikan S., Balik Sanli F., **Bektas Balcik F.**, Goksel C., 2008: Fusion of SAR Images (PALSAR and RADARSAT-1) with Multispectral SPOT image: A Comparative Analysis of Resulting Images. *The XXI Congress The International Society for Photogrammetry and Remote Sensing*, 3-11 July 2008 Beijing, China (**En iyi poster ödülü**)
- Dogru A. O., **Bektas Balcik F.**, Balik Sanli F., Goksel C., and Ulugtekin N., 2007: Izmir Bird Paradise Change Detection Analysis: Remote Sensing and Geographic Information System Integration. *14 th International Symposium on Environmental Pollution and Its Impact on Life in the Mediterranean Region*, October 10-14, 2007, Seville, Spain.
- Ulugtekin N., **Bektas Balcik F.**, Dogru A. O., Goksel C., Aslan Alaton I., Orhon D., 2007: The Use of Remote Sensing and GIS Technologies for Evaluation of Turkish River Basins: A Case Study of Marmara River Basin and Istanbul. *International Conference of Environment: Survival and Sustainability*, 19-24 Subat 2007, Kıbrıs
- **Bektas Balcik F.**, Sertel E., 2007: Wavelet-based image fusion of Landsat ETM images: A case study for different landscape categories of Istanbul. *ISPRS COMMISSION VII Conference on Information Extraction from SAR and Optical Data, with Emphasis on Developing Countries*, 16-18 May 2007, İstanbul
- Karakacan A., Goksel C., Ipbuker C., **Bektas Balcik F.**, 2006: Multiquadric Overlay Of Maps And Images. *Remote Sensing: From Pixels to Processes ISPRS Mid-term Symposium*, 8-11 May Enschede, the Netherlands,
- **Bektas Balcik F.**, Saroglu E., Goksel C., & Musaoglu N., 2005: High Resolution Mapping Land Cover Classification of The Elmali Water Basin. *25th EARSeL Symposium and Workshops*, 6 - 11 June, PORTO, Portugal
- **Bektas Balcik F.**, Goksel C., 2005: Analysing and Mapping of Bozcaada Island Land Cover by Means of Remote Sensing and GIS Integration. *25th EARSeL Symposium and Workshops*, 6 - 11 June, PORTO, Portugal
- Musaoglu N., Saroglu E., **Bektas Balcik F.**, Goksel C., & Kaya, S., 2005: Assesment of Forest Degradation by Means of Remotely Sensed Data. *25th EARSeL Symposium and Workshops*, 6 - 11 June PORTO, Portugal

- Dogru A.O, **Bektas Balcik F.**, Goksel C, and Ulugtekin N., 2005: Monitoring Coastal Dunes by Using Remote Sensing and GIS Integration in North West Part of Turkey: A Case Study of Kilyos Dunes. *13. Mediterranean Scientific Association of Environmental Protection (MESAEP) Symposium*, 8-12 October, Thessaloniki – Greece.
- Ulugtekin N., **Bektas Balcik F.**, Dogru, A.O., Goksel C., Aslan Alaton I, Orhon D., 2005: The Use of Remote Sensing and GIS Technologies for Comprehensive Wastewater Management. *31. International Symposium on Remote Sensing of Environment, Global Monitoring for Sustainability and Security*, 20-24 June, Saint Petersburg, Russia. (CD)
- Saroglu E., **Bektas Balcik F.**, Dogru A. O., Musaoglu N., Kaya S., Ormeci C., .2005: Environmental Impact Analyses of Quarries Located On The Asian Side of Istanbul Using Remotely Sensed Data. *International Cartographic Conference*, 9-16 July, A Coruna , Spain-(CD)
- Musaoglu N., Goksel C., Saroglu .E., **Bektas Balcik F.**, 2005: Evaluating Urban Expansion In Asian Part Of Istanbul By Using Multitemporal Satellite Image Data. *3. International Conference on Ecological Protection of the Planet Earth*, abstract book, p62.
- **Bektas F.**, Goksel Ç., 2004. Remote Sensing and GIS Integration For Land Cover Analysis, A Case Study: Gokceada Island. *XXth Congress of the International Society for Photogrammetry and Remote Sensing (ISPRS)*, 12-25 July, Istanbul, Turkey, 711-714
- Saroğlu E., **Bektas F.**, Musaoğlu N., Goksel Ç. 2004: Fusion of Multisensor Remote Sensing Data: Assessing The Quality of Resulting Images. *XXth Congress of the International Society for Photogrammetry and Remote Sensing (ISPRS)*, 12-25 July, Istanbul, Turkey, 575-579
- Kaya Ş. **Bektas F.**, Saroğlu E., Goksel Ç., 2004: Analyses of Izmit Earthquake by Means of Remotely Sensed Data: A case Study, Yalova City. *Proceedings of the 5th European Conference on Product and Process Modeling and Construction Industry ECPPM*, 8-10 September, Istanbul, 603-608
- Musaoglu N., **Bektas F.**, Saroglu E., Kaya Ş., and Göksel Ç., 2004: Use of Corona, Landsat TM, Spot 5 Images To Assess 40 Years Of Land Use/Cover Changes in Cavusbasi. *24. EARSeL Symposium 25-27 May 2004*, Dubrovnik, Croita, 2004.

National Papers

- Coşkun, M., **Bektaş F.**, Saroğlu E., 2004: Landsat 7 ETM Görüntüsünün Fuzzy K Means ve ISODATA Algoritmaları Kullanılarak Sınıflandırılması. *Akıllı Sistemlerde Yenilikler ve Uygulamaları Sempozyumu*, 23-25 Haziran, İstanbul. p.p. 183-186.
- **Bektas Balcik F.**, Göksel Ç., 2005: Uzaktan Algılama ve Coğrafi Bilgi Sistemi Entegrasyonu Gökçeada ve Bozcaada Örneği. *10. Türkiye Harita Bilimsel ve Teknik Kurultayı*, 28 Mart-1 Nisan, Ankara.
- Musaoğlu, N., Göksel Ç., Kaya, Ş., Saroğlu E., **Bektas Balcik F.**, 2005: İstanbul Anadolu Yakası 2B Alanlarının Uydu Görüntüleri ile Analizi. *10. Türkiye Harita Bilimsel ve Teknik Kurultayı*, 28 Mart-1 Nisan, Ankara.

- **Bektas Balcik F.**, Doğru A. Ö., Göksel Ç., Uluğtekin N., 2006: Kilyos Kıyı Kumullarının Uzaktan Algılama ve Coğrafi Bilgi Sistemleri Kullanılarak İzlenmesi. *Türkiye Kıyıları 06, Kıyı ve Deniz Alanları VI. Ulusal Konferansı*, Muğla.
- Doğru A. Ö., **Bektas Balcik F.**, Uluğtekin, N., Göksel Ç., . Aslan Alaton İ., and Orhon D., 2007: Türkiye Su Havzalarının CBS ve Uzaktan Algılama Teknolojileri İle Yönetimi İçin Bir Yaklaşım. *11. Türkiye Harita Bilimsel ve Teknik Kurultayı*. 2 Nisan-6 Nisan, Ankara.
- **Bektas Balcik F.**, Göksel, Ç., 2009: SPOT 5 ve Farklı Görüntü Birleştirme Algoritmaları. *12. Türkiye Harita Bilimsel ve Teknik Kurultayı*. 11 Mayıs- 15 Mayıs, Ankara.
- **Bektas Balcik F.**, Skidmore A. K., Knox N., Schlerf M., 2009: BIOFRAG PROJESİ, Güney Afrika Örneği. *12. Türkiye Harita Bilimsel ve Teknik Kurultayı*. 11 Mayıs- 15 Mayıs, Ankara.
- **Bektas Balcik F.**, Doğru, A.Ö., Köktuna, M., Teksoy, S., Göksel, Ç., Sözen, S., Uluğtekin, N. 2009: Karadeniz Havzası'nda Sürdürülebilir Kalkınmayı Destekleyici Gözleme ve Değerlendirme Sisteminin Oluşturulması, *TMMOB Coğrafi Bilgi Sistemleri Kongresi*, 2-6 Kasım, İzmir.